COMPUTER SIMULATION AND EXPERIMENTAL ANALYSIS
OF TRANSPORT PHENOMENA DURING THE THERMAL
PROCESSING OF MEAT EMULSION PRODUCTS

by

MARTIN SCHAEFER

A dissertation submitted in partial fulfillment
of the requirements for the degree of

Doctor of Philosophy
(Chemical Engineering)

at the
UNIVERSITY OF WISCONSIN—MADISON
1995

A laboratory apparatus was built to provide a means of processing small and medium diameter cylindrical meat emulsion products by generating an air flow of controlled temperature, humidity and velocity. Different relative humidities in the test section of the apparatus were obtained by saturating an air stream at temperatures below the desired processing dry bulb temperature followed by a sensible heat input. This apparatus was used to measure the thermal response and moisture loss of meat emulsion products during processing. Full-fat and no-fat emulsions were contained in small diameter moisture-permeable cellulose casings. The medium diameter products consisted of full-fat meat emulsions stuffed in moisture-permeable fibrous casings and moisture-impermeable polyamide casings. The experiments were conducted at different relative humidities and dry bulb temperatures of approximately 78°C. Thermocouples were used to record the surface and center temperatures of the products during processing. Values of the moisture concentration of processed products at different radial positions were measured with invasive methods on large and small diameter samples. The use of magnetic resonance imaging methods for the determination of moisture profiles was not successful. Low signal to noise ratios prevented the extraction of useful information from the experiments.

A nonlinear parameter estimation program, in conjunction with the simulation model, was used to compute the effective moisture diffusion coefficients that provided the best fit of measured and simulated data. In addition to the dependent variables measured in this study, the effective moisture diffusion coefficient was estimated from reported temperature data for the processing of bologna products. The computed coefficients varied between $D_{eff} = 0.91 \times 10^{-10}$ m^2/s and $D_{eff} = 5.1 \times 10^{-10}$ m^2/s. The effective moisture diffusion coefficients estimated for the no-fat emulsions were larger than those obtained for the full-fat products. This difference was attributed to the higher moisture content of the no-fat emulsions.

Acknowledgements

I would like to thank my advisors, Professors Sanford A. Klein, William A. Beckman and John W. Mitchell for their guidance during the course of this research. Their encouragement and constructive criticism made the completion of this study possible. I am also thankful to Professors Warren E. Stewart and Edwin N. Lightfoot for their suggestions and helpful discussions and to Professors Kevin L. Bray and Richard W. Hartel for serving on my thesis committee.

For the financial support I am indebted to the Oscar Mayer Foods Division of Kraft General Foods. Without their generosity, it would not have been possible for me to continue my graduate studies in Madison. Many experiments were conducted at the Oscar Mayer facilities. The theoretical insight and practical help of the researchers at Oscar Mayer, in particular Jerry Marra and Scott Brackebusch, was greatly appreciated.

Mark Anderson from the Department of Biochemistry helped with the Magnetic Resonance experiments and Patricia Gabarra from the Department of Food Science assisted with the Karl Fischer Titration method. A special thanks goes to Barrett Flake for his continuous help with software and hardware problems.

Finally, I want to thank my parents and my sister for their continuous support during my education.

Contents

List of Tables

List of Figures

Chapter 1

Introduction

Various aspects of the processing of meat emulsion products are discussed in this chapter. First, the processing steps in a commercial manufacturing operation are summarized. This part is followed by an overview of the challenges encountered when trying to incorporate energy and time efficient processing operations. Finally, the research objectives for this study are outlined in Section 1.2.

1.1 Background

The meat industry produces a wide variety of processed meat products. Rust [1976] classifies these according to the manner of processing into fresh sausages, uncooked smoked sausages, cooked smoked sausages, other cooked sausages, dry sausages, luncheon meats, jellied products, cooked hams and canned meats. Hanson [1988] distinguishes between whole-muscle products, for example ham and bacon, and ground or comminuted products. The latter are commonly referred to as sausages. They can be further classified into coarsely ground sausages, for example salami, and the so called meat emulsion products, also referred to as fine-cut sausages, for example frankfurters and bologna.

The heating, or cooking, of meat products increases their shelf life by destroying

pathogenic and food spoilage microorganisms. In addition, cooking enhances and stabilizes various characteristics of meat such as appearance, texture, tenderness, and flavor. Other means of preserving meat products include salting, drying and smoking. The techniques of preserving meat date back thousands of years and they developed gradually in many societies as a means of preserving those portions that could not be consumed at once. The improvement of existing preserving methods was based on past experience and trial-and-error searches and was regarded as an art. The application of engineering principles to the processes of preserving meat is a relatively new discipline. It is driven by the need for a better understanding of the physical and chemical changes occurring during meat processing.

1.1.1 Meat Emulsion Products

Emulsion type meat products make up a significant share of processed meats. Approximately 2 billion pounds were produced in 1990 (Agricultural Statistics). The two most common meat emulsion products are frankfurters and bologna, representing about 25 and 20 per cent of all sausage sold in the United States [Rust, 1976]. Meat emulsion products consist of either beef or a combination of beef, pork and poultry with added water, salt, preservatives, non-meat proteins, spices and curing agents. The beef, pork and poultry cuts can contain lean and fat components. As a result of consumer demands, the market share of reduced-fat and fat-free products has increased over the last years. A typical processed high-fat product contains about 50% moisture, 35% fat and 10% protein. Fat-free products can have moisture contents as high as 85% before and 80% after processing.

An emulsion is defined as a heterogeneous mixture of liquids which under normal circumstances do not dissolve into each other, for example oil and water. Small amounts of substances acting as emulsifiers are used to hold the two liquids suspended

into each other. One of the liquids will form a discontinuous phase in the form of small droplets that are completely surrounded by the other, continuous phase. Milk and mayonnaise are the two best known food examples of an emulsion. The proteins casein and egg yolk act as the emulsifiers for the discontinuous lipid phase. The physical structure of a meat emulsion resembles a classical liquid in liquid emulsion. The animal fat forms the discontinuous phase that is encapsulated by a continuous matrix of water and protein and the term emulsion is applied, even though the fat phase does not behave like a liquid. The contractile or binding proteins from the meat act as the emulsifying agent. The salt in the emulsion formula aids in solubilizing these contractile proteins from the muscle fiber.

1.1.2 The Processing Operations

The manufacturing of meat emulsion products consists of several operations. These are grinding, chopping, vacuumization, stuffing, linking, spraying, smoking, cooking, chilling and peeling. The individual processing steps are described in detail in the following paragraphs. A summary of these processing steps is given in Table 1.1.

In the grinding operation, the meat trimmings are ground through 1/8 to 3/8 inch plates. The lean meats are usually ground to a finer consistency than the fat meats. The ground meats are then chopped with salt and curing ingredients to a temperature of 5 to 7°C (42 to 45°F). At this point, the remaining ingredients are added and the chopping process is ended when the mixture reaches a specified temperature, usually 16 to 18°C (61 to 64°F). Entrained air is removed in order to achieve a uniform product by using vacuum choppers or stuffing machines with vacuumizing capabilities. The stuffing process injects the prepared emulsion into a casing for further processing. The individual links of small diameter products are usually formed by twisting the filled casing. They are then hung on a stick for further processing. Commercial

equipment is available that combines the stuffing and linking process. The links of large diameter products are obtained by closing the casing with metal clamps. These products are then placed on horizontal racks for further processing in order to prevent shape distortion which could result from the weight of hanging.

Manufactured casings are used for most processed meats. The term "manufactured" is used to distinguish it from animal casings, also called natural casings, that were used before the modern manufactured casings were available. The natural casings were made from the stomachs, intestines and bladders of cattle, hogs and sheep. They provided a strong elastic container which shrank with the meat as its moisture content changed gradually. Manufactured casings can be classified into cellulose and collagen types. The latter are made from the corium layer of split beef hides. Manufactured cellulose casings are used for the production of frankfurters. For easier handling, these casings are pleated and compressed after their production. It is possible to compress more than 15 meter (50 feet) of casing into a piece less than 30 cm (1 foot) long. For large diameter products, for example bologna, casings manufactured from a special paper base impregnated with additional cellulose are used. These types are also referred to as fibrous casings and they have a greater strength than the small diameter cellulose casings in order to support the larger weight of the meat emulsion after stuffing. Both cellulose and fibrous casings are permeable to moisture and smoke when moist. However, the degree of permeability decreases with the moisture content of the casing. Moisture impermeable casings are available in many sizes and are made from many materials, e.g. polyamides. Large diameter moisture impermeable casings are also made from surface treated fibrous casings in order to utilize their strength.

In the next operating step, the stuffed and linked casings are sprayed with cold water to wash off any adhering emulsion on the outer surface. The following operations,

preparation of meat emulsion in grinding and chopping operat.

stuffing machine injects meat emulsion into casings

stick hung with stuffed and linked casings

smokehouse with a vertical loop configuration and 5 processing zones

chill zone   second cook zone   first cook zone   smoke zone   water spray

removal of casing, packaging
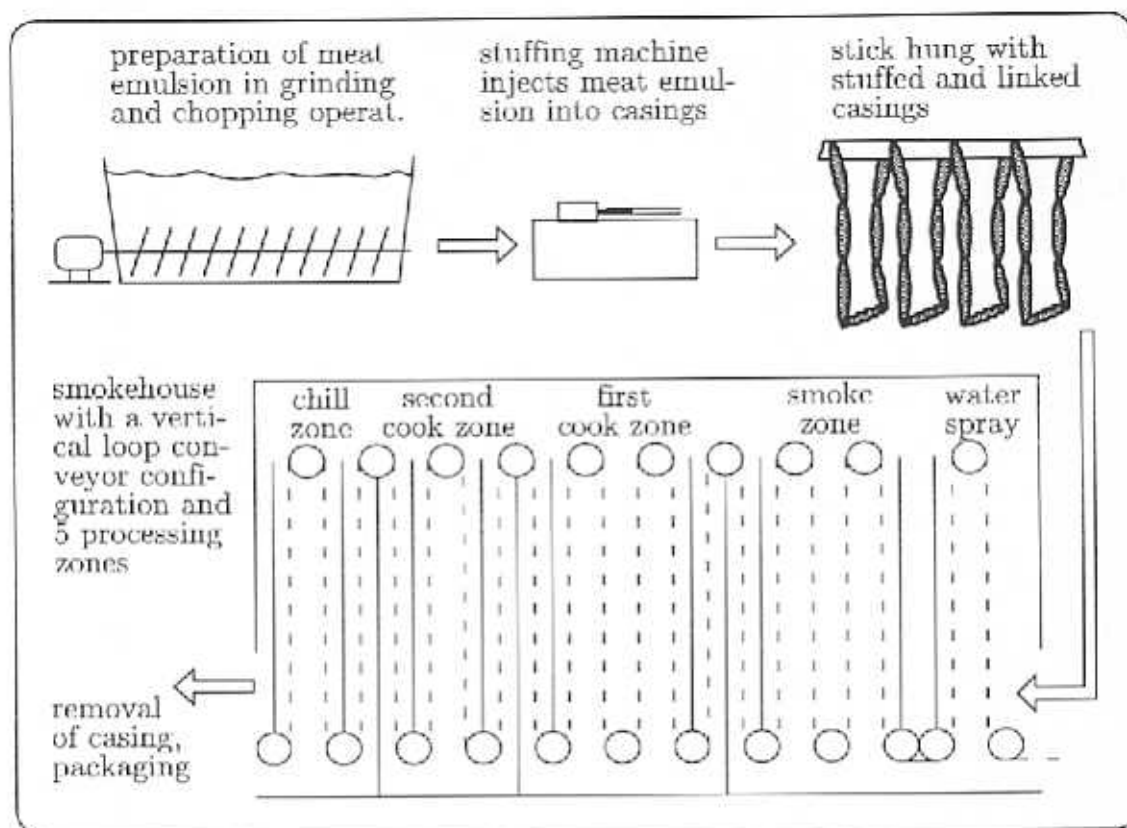
Figure 1.1: Schematic of the manufacturing of small diameter cylindrical meat emulsion products in a continuous smokehouse with a vertical loop conveyor system. The individual parts of the processing equipment are not drawn to scale.

smoking, cooking and chilling are commonly referred to as the thermal processing. These operations take place in large, forced-convection ovens, typically referred to as *smokehouses*. Both batch type processes and continuous operations are used. In a batch system, the product is manually loaded into the oven, cooked, and manually unloaded as a single batch. In continuous systems, the sticks bearing the products are connected to a conveyor chain which carries them through one or more processing zones. The conveyor systems can be designed in a straight-line, a horizontal-loop, or a vertical-loop configuration. Continuous ovens have capacities as high as 12,000 lb/hr. Typical processing times range from 30 minutes for small diameter products (20 to

Table 1.1: Summary of the processing steps in the production of meat emulsion products, Rust [1976]. The smoking, cooking and chilling operations are referred to as the thermal processing.

Operation	Procedure and purpose
1) emulsion preparation	
grinding	the meat trimmings are ground through 1/8 to 3/8 inch plates
chopping	the ground meat is combined with the other ingredients
vacuumization	removes entrained air in order to obtain a uniform product
2) preparation of products	
stuffing	injects the meat emulsion through a stuffing horn into the casing
linking	produces products of uniform length, e.g. by twisting the filled casings
spraying	removes adhering particles of meat on the outside of the casing
3) thermal processing	
smoking	adds flavor, acts as preservative and assists in forming a skin on the product
cooking	changes the product texture and destroys pathogenic microorganisms
chilling	plumps the product and prepares it for the peeling and packaging operations
4) final processing steps	
peeling	removes the casing, usually with high-speed mechanical peelers
packaging	package protects the products and is seen by consumers in the retail display

25 mm (0.8 to 1 inch)) to several hours for large diameter products (10 to 11 cm (3.9 to 4.3 inch)).

The purpose of the smoking operation is to enhance the flavor and the color of the product. In addition, the phenols contained in the smoke are bacteriostats and antioxidants, and hence act as preservatives. During the smoking and cooking processes, the meat proteins at the product surface coagulate, resulting in the formation of a skin on the product surface under the casing. Organic acids contained in the smoke enhance the protein coagulation. When the casing is removed from the products after the thermal processing, the skin remains intact and has the appearance of a casing. The smoke is usually generated by burning wood or sawdust. Unwanted smoke components include polycyclic hydrocarbons, which are suspected carcinogens. Because of the presence of these components, some manufacturers have in recent years

Table 1.2: Typical processing conditions during the thermal processing of small and large diameter meat emulsion products, adapted from Rust [1976] and Hanson [1988].

Time spent in zone [minutes]	Dry bulb temperature [°C] ([°F])	Relative humidity [%]	Wet bulb temperature [°C] ([°F])	Dew point temperature [°C] ([°F])
small diameter products, $D_{pr} \approx 20 - 25$ mm (0.8 – 1.0 inch)				
15 - 30	60 (140)	38.5	43 (110)	41 (106)
15 - 30	82 (180)	37.5	63 (145)	59 (138)
large diameter products, $D_{pr} \approx 10 - 11$ cm (3.9 – 4.3 inch)				
90	66 (150)	23.9	41 (105)	37 (98)
90	88 (190)	17.7	52 (125)	48 (119)
90	93 (200)	19.6	57 (135)	55 (131)

replaced natural smoke with artificial smoke flavorings.

The cooking operation destroys pathogenic and food spoilage microorganisms and enhances the appearance, texture and tenderness of the product. The temperatures and humidities in the smoking and cooking operations vary considerably from manufacturer to manufacturer and are often regarded as proprietary. A common feature of all processes is that the time taken for cooking should be sufficient to bring the temperature of the entire product at least up to 68°C (155°F). The cooking section in the smokehouse can consist of several distinct zones, each with different setpoints for the processing conditions, e.g. temperature, relative humidity and air velocity. A set of processing conditions in several processing zones is sometimes referred to as a thermal schedule. Typical processing conditions for small diameter products (e.g. frankfurters) and large diameter products (e.g. bologna) are summarized in Table 1.2. After cooking, the products are chilled by spraying or submerging in a brine solution. The brine concentrations are controlled to maintain a balance with the salt concentrations in the cooked product.

Chemical reactions taking place during the various processing steps play a crucial

role in obtaining desired meat characteristics such as color and firmness. Of special importance in this context are the so called cured meat reaction and the water holding capacity. The cured meat reaction describes the formation of a red pigment when nitric oxide and myoglobin combine. The nitric oxide is introduced as nitrite salts that rapidly change to nitric oxide in the meat. The water holding capacity of meat, or a meat emulsion, is an important economic factor. Muscle proteins are composed of highly charged amino acids, resulting in the attraction of many water molecules. With increasing times of storage after slaughtering, the acidity of the muscle increases, leading to the release of water molecules. It is desirable for the manufacturer to obtain a high process yield, i.e. to lose as little moisture as possible. Accordingly, the water holding capacity is carefully monitored during the processing operations.

1.1.3 Statement of the Problem

Many aspects of the thermal processing of meat emulsion products can be described as a transient, simultaneous transfer of heat and mass with continuously changing transport properties. The change of these transport properties during thermal processing is caused by the moisture loss, the rather large temperature increase and the structural change of emulsion components, for example the denaturation of meat proteins.

The details of the simultaneous heat and mass transfer are not yet well understood. A systematic investigation of these transport phenomena is hindered by the large number of variables involved in the thermal processing. These variables include product parameters and processing conditions. A summary of those variables believed to be of importance is given in Table 1.3. Opposed to these difficulties is the desire of the manufacturers to incorporate time and energy efficient thermal processing operations in order to gain a cost advantage in a competitive market. Even though the meat

Table 1.3: Variables involved in the processing of meat emulsion products.

Variable	Effect on processing
1) *product parameters*	
diameter	larger diameter products take more time to heat and lose less moisture since the ratio of surface area to volume is smaller
casing type	determines whether mass transfer from the product can occur; the degree of mass permeability can be a function of the moisture content
composition	for example the moisture content or the fat to protein ratio; affects the heat and mass transfer properties, e.g. mass diffusivity
stuffing pressure	affects the density of the product and hence the thermal properties
2) *processing variables*	
dry bulb temperature	potential for heat transfer; high temperatures can cause an emulsion breakdown when the fat particles are no longer encapsulated
wet bulb temperature	together with the dry bulb temperature and the pressure, it determines the relative humidity and the dew point temperature
air velocity	determines the magnitude of the heat and mass transfer coefficients; there can be a variation of the velocities over the oven cross section
orientation of stick	determines the main flow patterns of the processing air over the product, e.g. perpendicular to the long axis of the product
products on stick	if too many products are hung on a stick, they might shield each other, leading to different processing conditions for the products

ingredients represent the highest cost factor in the manufacturing of meat emulsion products. a decrease in the energy costs associated with the production, for example resulting from a reduced cooking time, would provide significant savings. Given the large number of variables involved in the thermal processing, combined with the limited knowledge available concerning the underlying heat and mass transfer processes, it is unlikely that current thermal processing schedules operate at optimum conditions. In the following paragraphs, the need for an increased understanding of the transport phenomena during the processing of meat emulsion products is shown with four specific examples.

In recent years, many reduced-fat and fat-free meat emulsion products have been

developed in response to a strong demand by the consumer. These products have a significantly different composition and hence different heat and mass transfer properties, for example thermal conductivities and moisture diffusivities. Existing thermal processing schedules could not be applied to these new products. The new set of processing conditions was determined in lengthy trial-and-error searches. An improved knowledge of the involved heat and mass transfer principles would have reduced the time needed for the development of these new products.

Periodically, parts of the processing equipment fail, e.g. the conveyor chain or fans maintaining the air flow. Such failure will result in a temporary halt of the conveyor chain or a significant deviation from the desired temperature, relative humidity or air velocity within a processing zone. Under rare circumstances, such equipment failure is not detected immediately and products may be packaged and shipped to the consumer. Currently, no process simulation model is available that could assist in determining whether products processed under those faulty processing conditions are safe for the consumer or should be recalled. The large costs and the negative image associated with recall operations clearly show the need for an accurate process model. Such a model could be used to simulate the processing operation with the erroneous conditions to determine whether the products were cooked to a sufficient temperature.

During the processing of small diameter products, the presence of the sticks hung with products in batch or continuously operated smokehouses can results in uneven flow patterns of the processing air, with larger airflows through open cross sections, for example the regions near the walls of the oven. Attempts to increase the production rate in existing processing equipment may further increase the uneven flow distribution. This channeling of the processing air is similar to the undesired effect in packed distillation columns. Consequently, a distribution of the process parameters

such as air velocity and temperature will result and products located in the middle of the batch smokehouse or in the middle of a processing zone of a continuous oven will be subjected to different processing conditions compared to those products located near the walls of the smokehouse. A similar effect is given by the arrangement of the products on the holding stick. As an example, a so called 3-down 1-across 3-up configuration is shown in Figure 1.1. The product at the bottom (the one "across") will be subjected to different air flows than the products at the side of the stick. A process simulation model could be used to reveal whether the different air flows would result in significantly different processing times or product moisture losses. This knowledge could then be used to change the arrangement of the products on the stick in order to produce uniformly processed products.

The moisture loss during the processing of small diameter emulsion products amounts to about 5 to 8% of the initial mass, depending on the processing time and the process conditions. The manufacturers have to meet product specifications with regard to the final weight of the packaged product, as required by food product labeling laws. Hence, the manufacturers closely monitor the moisture loss, also called process shrink, in order to fall within the narrow limits of the mandatory product weight specifications. This monitoring is often accomplished by measuring the mass of a stick hung with products before and after the thermal processing operations. Deviations from the setpoint are corrected by manually adjusting the amount of emulsion injected into the casings. Alternatively, a precise weight control could be obtained by adjusting other process parameters, for example the relative humidity of the processing air. The use of an on-line process model could accomplish this task and save the labor costs associated with the manual adjusting of the stuffing operation.

1.2   Research Objectives

The goal of this research is to investigate the transport phenomena during the thermal processing of cylindrical meat emulsion products. This objective will be accomplished by a combination of computer simulation and experimental analysis. The computer simulation will be based on a process model that accounts for aspects of special importance in meat processing, such as variable boundary conditions and changing heat and mass transfer properties.

The process model will then be used to identify those product parameters and processing conditions that exhibit a strong influence on the thermal processing results, for example the total moisture loss of the product during processing or the minimum processing time. The identified product parameters will be determined experimentally or obtained from published data. The values of processing conditions currently used in commercial production equipment will be compared to the corresponding optimum values computed from the process model. The values of the process parameters that are not controlled or monitored in current processing equipment, but are found to be of importance, will be determined experimentally.

The accuracy of the simulation model will be tested against data reported in the literature. In addition, data will be recorded under carefully controlled laboratory conditions. These measurements will be designed to minimize the number of involved processing variables. An apparatus will be constructed to provide a means of providing different processing conditions.

The improved understanding of the transport phenomena during the processing of meat emulsion products will help to increase product safety, contribute to the design of efficient thermal processes and aid in the development of new products. This insight into the heat and mass transfer principles can be used to develop a user-friendly software package that can be used on-line in the production process.

Chapter 2

Review of Existing Work

A large number of publications are available on the general topic of food processing and food engineering. However, work related to meat emulsion products and their processing is limited. Previous studies that are of interest to the current research are described in this chapter. Contributions that report modeling approaches, experimental techniques or measured data that will be used in the remainder of this study are described in detail. A summary of previous work on meat emulsion and some related products is given in Table 2.1. References that are related to the research presented in this dissertation but are not cited explicitly are summarized in Table 2.4 at the end of this chapter.

2.1 Thermophysical Properties of Meat Emulsion

Previous research concerning the density, specific heat, thermal conductivity and moisture diffusivity of meat emulsion is described in this section. For easy reference, all described values and models of these properties are also summarized in Table 2.2.

Agrawal [1976] measured the density of a meat emulsion having water and fat mass fractions of 0.65 and 0.18, respectively, with a water displacement method and reported a value of 949 kg/m^3 (59.2 lb/ft^3). This value is similar to those given by

Table 2.1: Previous studies listing thermophysical properties, processing conditions and process modeling approaches of meat emulsions and some related products that are of interest to this research.

Author, year	Format[1,2]		Main area of work/Comments
Monagle [1974]	J	X	effect of smokehouse temp., relative humidity and air velocity
Sweat [1975]	P	L	review of models for the thermal conductivity of meat products
Agrawal [1976]	P	T/X	measurement and modeling of temperature and moisture profiles
Igbeka [1982]	J	X	measurement of the equil. moisture content of cooked emulsions
Mittal [1982]	J	T/X	moist. diffusion in emulsions slabs and cylinders of diff. comp.
Callaghan [1983]	J	X	investigation of cheese structure by nuclear magnetic resonance
Mittal [1983]	J	T/X	weight loss of emul. prod. during different process conditions
Mittal [1985]	J	X	equilibrium moisture content of uncooked meat emulsion prod.
Mittal [1987]	J	X	influence of smokehouse processing conditions on final product
Mittal [1989]	J	X	change of thermal properties during the cooking at diff. temps.
Hanson [1988]	M	X	temp. profiles and moisture loss during processing of bologna
Imre [1989]	J	T	modeling and analysis of moisture profiles during salami drying
Spielbauer [1991]	M	T/X	measur. of heat transfer coeff. in a large continuous smokehouse
Schrader [1992]	J	L	application of magnetic resonance imaging in the food industry

[1] J: journal paper, P: PhD-thesis, M: Masters-thesis
[2] L: literature review, T: theoretical, X: experimental

Qashou *et al.* [1970] for ground beef and ground chuck. These researchers reported values of 928 to 968 kg/m^3 (57.9 to 60.4 lb/ft^3) for the ground beef and 953 to 999 kg/m^3 (59.5 to 62.4 lb/ft^3) for the ground chuck.

The specific heat capacity of food products depends to a large extent on the composition. Hallström *et al.* [1988] suggest calculating the specific heat from the ideal solution model

$$c = \sum_{i=1}^{n} \omega_i c_i \tag{2.1}$$

where ω_i and c_i denote the mass fraction and the specific heat of the major food components water, carbohydrate, protein, fat and inorganic materials. The specific heat values of these components are summarized in Table 2.2. Because of the rather large difference between the specific heats of water and the other major food components, the water content strongly affects the average specific heat. Dickerson [1965] gives a

Table 2.2: Summary of thermophysical properties of meat emulsion and related products reported in the literature. If no product is mentioned, the entries refer to meat emulsion.

Value or model	Range[a] and comments	Reference[b]
Density [kg/m^3]		
$\rho = 949$	$\omega_m = 0.65$, $\omega_f = 0.18$	Agrawal [1976]
$\rho = 928$ to 968	for ground beef	Qashou [1970]
$\rho = 953$ to 999	for ground chuck	Qashou [1970]
Specific heat [kJ/kg K]		
$c = 3.6$	$T < 40°C$, $\omega_m = 0.65$, $\omega_f = 0.18$	Agrawal [1976]
$c = \sum_{i=1}^{n} \omega_i c_i$	approximation for all food products[1]	Hallström [1988]
$c = 1.675 + 2.5\,\omega_m$	approximation for all food products	Dickerson [1965]
$c = 1.60 + 2.6\,\omega_m + 0.015\,\omega_f T$	for meat products	Hallström [1988]
Thermal conductivity [W/m K]		
$k = 0.432$	$T = 21°C$, $\omega_m = 0.65$, $\omega_f = 0.18$	Agrawal [1976]
$k = 0.576$	$T = 93°C$, $\omega_m = 0.65$, $\omega_f = 0.18$	Agrawal [1976]
$k = 0.421$	$T = 20°C$, $\omega_m = 0.65$	ASHRAE [1989]
$k = 0.355$ to 0.468	$T < 25°C$, $0.54 < \omega_m < 0.71$	Timbers [1982]
$k = 0.080 + 0.52\,\omega_m$	for all meats, $0.60 < \omega_m < 0.80$	Swear [1975]
Moisture diffusivity [m^2/hr]		
$D_{eff} = 0.3224 \times 10^{-4}\,T \exp(-0.3302\,FP - 3060.37/T)$, $\quad T < 58°C$		Mittal [1982]
$D_{eff} = 0.232\,T \exp(-0.0414\,FP - 6246.6/T)$, $\quad T > 58°C$		Mittal [1982]

[1] $c_w = 4.18$ kJ/kg K, $c_r = 1.42$ kJ/kg K, $c_p = 1.55$ kJ/kg K, $c_f = 1.67$ kJ/kg K

[a] Conversion of ω_m to u: $\omega_m = u/(1 + u)$

[b] name of first author only

formula for the specific heat of foodstuffs that only considers the moisture content. For meat products in particular, Hallström *et al.* [1988] report a formula that considers the effect of temperature on the specific heat. Agrawal [1976] experimentally determined the specific heat for a meat emulsion with a moisture mass fraction of 0.65 at temperatures between 20°C (68°F) and 40°C (104°F) and reported a value of 3.6 kJ/kg K (0.86 BTU/ft °F).

Sweat [1975] compared several existing models for the thermal conductivity of meats with a large number of data reported in the literature. A model containing a linear dependence on the moisture content per wet basis gave the best fit for temper-

atures ranging from 0 to 60°C (32 to 140°F). The differences in thermal conductivity among the various meat products were reported to be small. It is unclear why the influence of the composition was not reported to be significant, especially since fat has a much lower conductivity than protein.

Mittal *et al.* [1989] investigated the change of thermal conductivity, thermal diffusivity and specific heat of meat emulsions with varying moisture contents and fat to protein ratios after heating them to varying temperatures. For this purpose, the emulsion was either uncooked, cooked up to 45°C (113°F), or cooked up to 65°C (149°F). To prevent any moisture loss, the emulsion samples were stuffed into stainless steel tubes and put into a water bath maintained at 75°C (167°F). When the center of the product reached the desired temperature (i.e. 45°C (113°F) or 65°C (149°F)), the sample was removed from the water bath and cooled in another bath at 15°C (59°F). The thermal properties were determined when the sample reached 25°C (77°F). The thermal diffusivity was measured with the Dickerson method [1965], the thermal conductivity with a conductivity probe and the specific heat with a calorimeter. Several functional forms for the thermal properties were investigated. The models giving the best fit to the measured data are summarized in Table 2.3.

Mittal *et al.* [1982] investigated the moisture mobility in meat emulsion during cooking. A slab geometry was used for low temperatures (42°C to 58°C (108°F to 136°F)). The emulsion was placed on an aluminum disc fitted to an aluminum ring. Since experimental difficulties due to uncontrolled moisture losses from the sides of the experimental setup occurred with the slab geometry, an emulsion-filled casing of 2.54 cm (1 inch) diameter and 15.2 cm (6 inch) was employed at experiments involving higher temperatures (58°C to 81°C (136°F to 178°F)). In both cases, relative humidities and fat protein ratios ranged from 41% to 87% and 1.2 to 3.0, respectively. During the experiments, the surface temperature rose continuously and approached

Table 2.3: Changes in the thermal properties of meat emulsions with varying moisture contents and fat to protein ratios after heating to different temperatures, as reported by Mittal et al. [1989].

Model[1] and numerical example

Thermal conductivity [W/m K]

$k = 1.14\,\omega_m + 0.0159\,CS - 0.0019\,FP^2 - 0.734\,\omega_m^2$

- k incr. by 13% (0.395 to 0.447) at $FP = 2$ and $CS = 1$ when ω_m incr. from 0.50 to 0.70
- cooking from $CS = 1$ to $CS = 3$ ($FP = 1$, $\omega_m = 0.6$) causes a 7.4% increase in k

Specific heat [kJ/kg K]

$c = 7.97\,\omega_m + 0.1268\,FP - 0.0726\,CS - 5.09\,\omega_m^2$

- cooking from $CS = 1$ to $CS = 3$ ($FP = 1$, $\omega_m = 0.6$) decreases c by 4.7% (3.0 to 2.86)

Thermal diffusivity [m²/s]

$\alpha = (252.7\,\omega_m - 0.820\,CS - 110\,\omega_m^2 - 5.8\,FP\,\omega_m)\,10^{-9}$ for $26°C < T < 33°C$

$\alpha = (283.8\,\omega_m + 2.115\,CS - 140\,\omega_m^2 - 5.9\,FP\,\omega_m)\,10^{-9}$ for $34°C < T < 40°C$

- cooking from $CS = 1$ to $CS = 3$ increases α by 14% (1.08×10^{-7} to 1.23×10^{-7})

---

[1] CS — cooking stage: $CS = 1, 2, 3$: no cooking; cooked at 45°C; cooked at 65°C

the dry bulb temperature of the air. This led to the conclusion that "there is no constant water removal rate period during cooking of meat emulsion" and that "internal water movement was the controlling mechanism from the beginning of the cooking process". Empirical correlations were given for the moisture diffusivity as a function of the temperature and the fat to protein ratio. These correlations are summarized in Table 2.2.

2.2 Influence of Process Conditions on the Final Product

Monagle et al. [1974] investigated the effect of smokehouse temperature, humidity and air velocity on weight changes and temperature profiles in frankfurters. These parameters were studied in the range from 55°C to 93°C (131°F to 199°F) for the dry bulb temperature, 20% and 80% for the relative humidity and with air flows equivalent to 5 or 10 smokehouse air changes per minute. The products were contained

in moisture-permeable cellulose casings of 20 to 21 mm (0.79 to 0.83 inch) diameter and were linked in 12 cm (4.7 inch) lengths. For constant smokehouse temperature processes, the internal product temperature increased exponentially towards the smokehouse dry bulb temperature. The rate of evaporation was found to be markedly faster in a product subjected to a low humidity process, when compared to that in a high humidity process. An opposite relationship was observed for the rate of heating. It was concluded that the moisture transfer and the accompanying latent heat needed for the evaporation of water played a major role in the rate of heating of meat products in convection smokehouses. Protein coagulation, skin formation and other changes that alter the water immobilizing properties of the material were found to limit evaporation at very low relative humidities. In this case, the surface temperature was higher than the wet bulb temperature of the air. However, at higher relative humidities, the authors explained that the "rate of evaporation was sufficiently slow to allow a balance between heat transfer and evaporative cooling. Thus, the surface temperature follows very closely the wet bulb temperature of the air".

Mittal *et al.* [1983] measured the weight loss in cylindrical meat emulsion products of 25 mm (1 inch) diameter during the thermal processing as a function of the processing temperatures, relative humidities and the product composition. The moisture ratio, $(\bar{u} - u_e)/(u_o - u_e)$ where u, u_e and u_o denote the average, equilibrium and initial sample moisture content, respectively, was determined as a function of time. For a relative humidity of 60% and a fat to protein ratio of 1.9, it took 5 hours to lose 13% of the moisture at 58°C (136°F) and only 1 hour to lose the same amount at 81°C (178°F). An increase in the fat to protein ratio decreased the rate of moisture loss. This effect was associated with the hydrophobic character of fat and the resistance it offers to the diffusion of moisture. The relative humidity had a distinct influence on the moisture ratio. An increase in the moisture loss rate was found with an increase
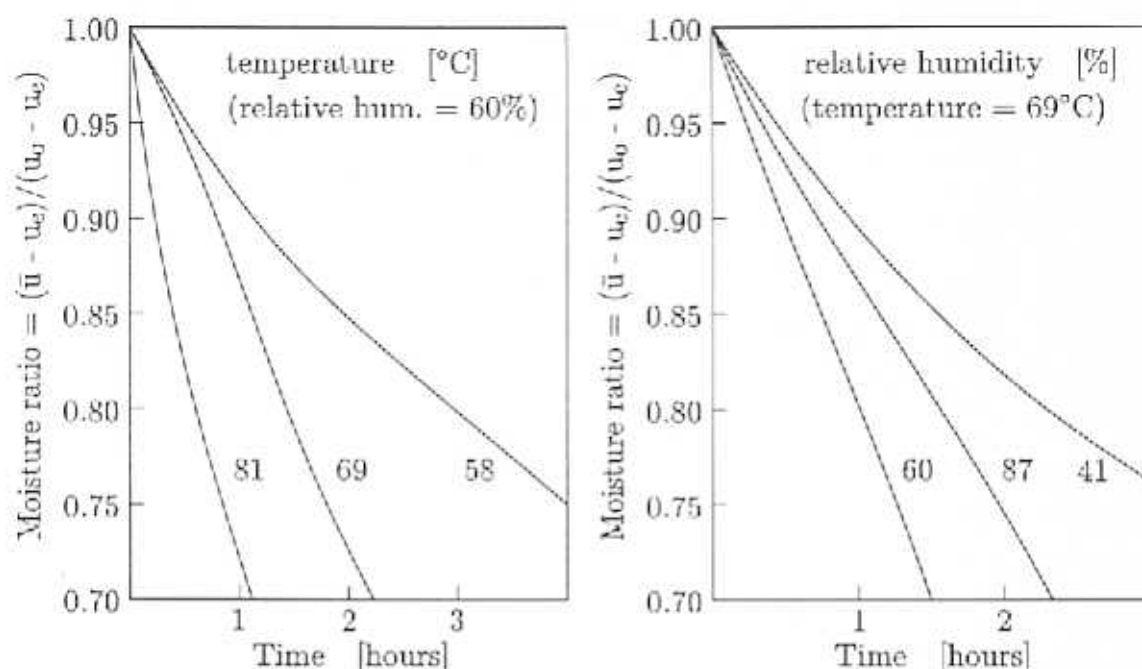
Figure 2.1: Weight loss of cylindrical meat emulsion products of 25 mm (1 inch) diameter during different processing conditions as reported by Mittal *et al.* [1983]. The moisture ratio $\bar{u}$ was calculated from the average moisture content of the samples at various times. The initial moisture mass fraction of the emulsion was reported as 0.55.

in relative humidity from 41% to 60%. A further increase in the relative humidity to 87% resulted in a considerable reduction of the moisture loss rate. The authors explained this phenomena with a skin formation due to protein coagulation at low relative humidities. It was believed that the skin limits evaporation and outweighs the influence of a greater driving force for mass transfer at lower relative humidities. The influence of this diffusional barrier was thought to diminish at higher relative humidities (60% and 87%) because of the stronger dependence on the driving force for mass transfer, which is proportional to the relative humidity. The influence of temperature and relative humidity are shown in Figure 2.1.

Mittal *et al.* [1987] determined the effect of the rate of increase of the smokehouse temperature and the rate of increase of the smokehouse relative humidity on

meat emulsion product qualities. The product qualities were defined as a combination of water holding capacity, emulsion stability, textural parameters and sensory attributes. The sensory evaluation was conducted with a taste panel composed of 9 to 10 untrained judges. A multiresponse optimization program was used to find the optimum thermal process schedule with respect to the described product qualities. It was concluded that a temperature increase of 0.5 to 0.7°C/min (0.9 to 1.3°F/min) and a relative humidity increase of 3.9%/min resulted in an optimum product.

2.3 Average Heat Transfer Coefficients

Spielbauer [1992] measured the heat transfer coefficient in a commercial continuous smokehouse. A cylindrical aluminum probe 23 mm (0.9 inch) in diameter and 15.2 cm (6 inch) in length, resembling a real product, was made. Due to the high thermal conductivity of the aluminum and the magnitude of the expected heat transfer coefficients, the probe was treated as a lumped system with a negligible internal temperature distribution. For the measurements, the aluminum probe was attached to a holding stick (Section 1.1.2) with actual meat emulsion products and allowed to traverse the smokehouse. The orientation of the aluminum probe on the holding stick resembled that of the actual products. The temperature of the probe during the thermal processing was recorded with a temperature data trace, a programmable wireless temperature sensor with an internal memory and clock capable of storing up to 1000 temperatures points at a chosen sampling rate. Since the temperatures were recorded in precise time intervals, accurate plots of temperature versus time were constructed after downloading the recorded data into a spreadsheet program of a personal computer. A second temperature data trace was tied to the holding stick and was used to measure the dry bulb temperature of the processing air. The differential form of the transient energy equation was used to obtain the heat trans

fer coefficient from the measured temperature data. The mass, specific heat, surface area and initial temperature of the aluminum probe were known. The gradient of the probe temperature with respect to time and the difference of the processing air dry bulb temperature and the probe temperature were calculated from the recorded data. The obtained heat transfer coefficients ranged from 5 to 30 W/m^{2}K (1 to 6 BTU/hr ft^2 °F) and confirmed the assumption of a lumped system with Biot numbers ranging from 0.001 to 0.005.

Huang and Mittal [1995] measured the heat transfer coefficient during the cooking of meatballs with a similar technique. A solid aluminum sphere of 4.7 cm (1.85 inch) in diameter, resembling the size of the meat balls, was constructed. Dents, about 0.4 cm (0.16 inch) in diameter and 0.2 cm (0.08 inch) deep, were drilled over the entire sphere surface to simulate the roughness of the meatball surface. A thermocouple was located at the center of the sphere to monitor the temperature changes. The heat transfer coefficients were calculated from the integrated form of the transient energy equation. The obtained heat transfer coefficients for natural convection baking, forced convection baking and boiling in water were 9.0, 23.0 and 4518 W/m^{2}K (1.6, 4.0 and 795 BTU/hr ft^2 °F), respectively.

2.4   Temperature and Moisture Concentration Profiles

Mittal et al. [1981] analysed the moisture and temperature profiles in a meat emulsion slab during processing in order to obtain a value for the moisture diffusivity. The temperatures within the slab were measured with thermocouples at six different locations. Moisture profiles were obtained from a 1.9 cm (0.75 inch) diameter core taken from the center of the slab using a steel cork borer. After removal, the core was quickly frozen by submerging into a solution of acetone and dry ice, maintained at -45°C (-49°F). The frozen core was then sliced into thin sections with the help of a
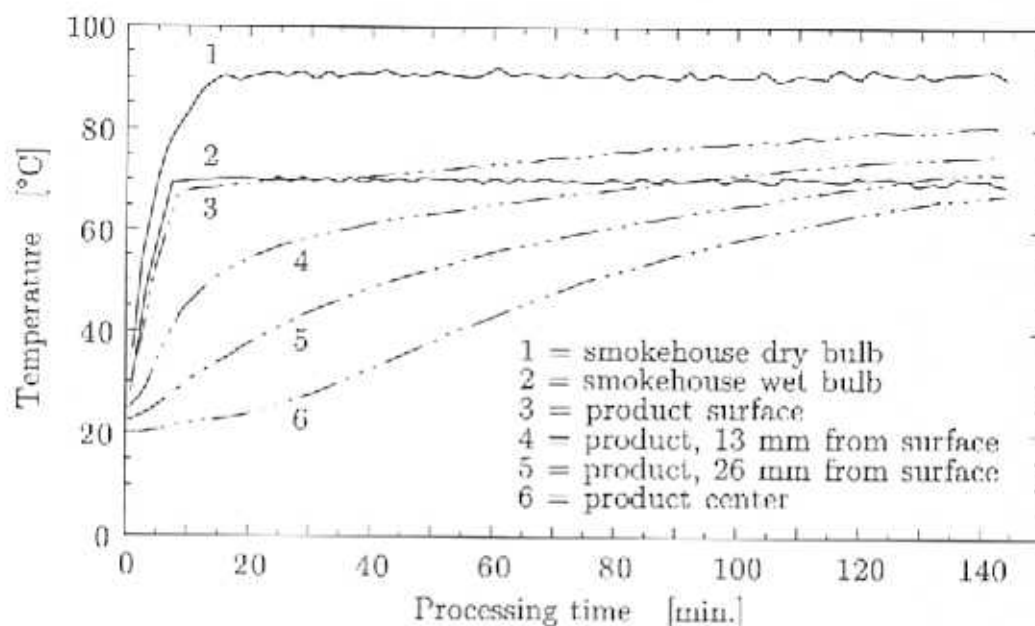
Figure 2.2: Temperature data measured by Hanson [1988] during the thermal processing of fine-cut bologna contained in water-permeable standard fibrous casings.

guillotine device. An oven drying method was used to determine the moisture content of each sample. The moisture profiles were obtained by assigning the mean moisture contents to the mean location on the respective slice. The temperature profiles indicated that the internal temperatures rose quickly to a value above the dew point and wet bulb temperature of the surroundings. Therefore, it was concluded that the moisture transport took place under isothermal conditions. It was observed that after evaporation of water, a protein skin formed on the surface. The authors pointed out that "...the skin formation is believed to be responsible for larger moisture gradients than expected near the surface of the product and reduced gradients in the interior of the product." This skin was thought to be advantageous for "less moisture loss and a better peeling of the casing".

Hanson [1988] conducted a study to determine the effects of various cooking temperatures and relative humidities on heat and mass transfer in fine-cut bologna with

a diameter of 10.4 cm (4.1 inch). Four different processing conditions with dry bulb temperatures and relative humidities ranging from 75 to 91°C (167 to 196°F) and 40% to 80%, respectively, were investigated. Two types of casings were used in this study, moisture-permeable standard fibrous casing and evaporation-resistant fibrous casing. The product temperature at four different locations (surface, 1/4 and 1/2 of the distance to the center and center), the oven dry-bulb and wet-bulb temperatures and the moisture losses were recorded during processing in a batch type smokehouse. Each experiment was conducted with three replications. Three distinct cooking stages in the experiments for both the water-permeable and evaporation-resistant casing were observed: 1) the wet-bulb preheat period where the product surface temperature approaches the oven wet-bulb temperature, 2) the constant rate drying period where the product surface temperature equals the oven wet-bulb temperature and 3) the falling rate drying period where the product surface temperature increases above the oven wet-bulb temperature. The mean product cooking times, defined as the time needed for the center temperature to reach 68°C (154°F), were shorter for the products in evaporation resistant casings. The cooking yield, defined as the total remaining mass after processing, ranged from 91% to 94.2% for the water permeable casing and from 94.3% to 97.5% for the evaporation resistant casing. It is unclear why the cooking yield for the evaporation resistant casings did not equal 100%. Typical results for oven dry and wet bulb temperatures of 91°C (196°F) and 70°C (158°F), respectively, are shown in Figure 2.2.

2.5   Equilibrium Moisture Content of Meat Emulsion

Igbeka and Blaisdell [1982] measured the equilibrium moisture contents, i.e. the isotherms, of a processed meat emulsion product at four different temperatures (5°C, 21°C, 38°C and 55°C (41°F, 70°F, 100°F and 131°F)). The experiments were per-
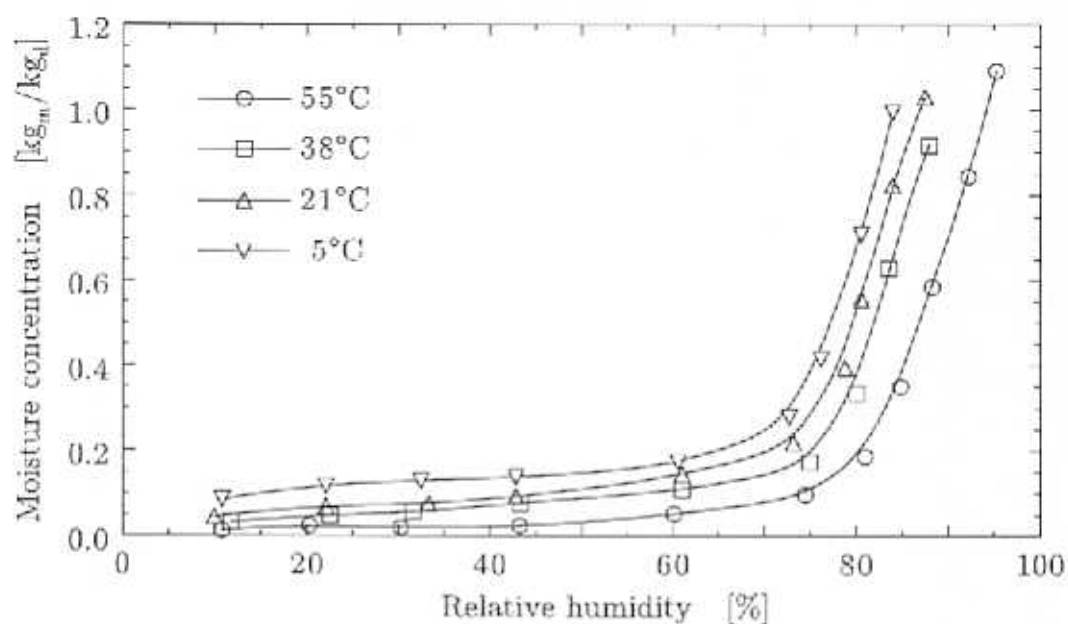
Figure 2.3: Equilibrium moisture content (isotherm) of a meat emulsion for different temperatures as reported by Igbeka and Blaisdell [1982]. The data were obtained after equilibration in closed containers containing saturated salt solutions.

formed at nine relative humidities ranging from 11% to 96%. Saturated salt solutions were used to obtain these relative humidities. The apparatus consisted of an equilibration chamber suspended in a constant temperature bath. The equilibration chamber contained the saturated salt solution, a magnetic stirrer and a sample dish. Core samples of meat, 1.3 to 2.0 mm (0.05 to 0.08 inch) in thickness and 25 mm (1 inch) in diameter, were placed in the sample dish. The sample dish was connected to a weighing balance through a thin wire, allowing a continuous weighing. The moisture content of the sample was assumed to be in equilibrium when the change in mass per 4 hours was less than 0.001 g. The equilibration times ranged from 18 to 48 hours. Two replications of each experiment were made. After equilibration, the samples were dried in a vacuum oven for 8 hours in order to determine the dry weight. The obtained isotherms were sigmoidal in shape. Results are shown in Figure 2.3. The

equilibrium moisture content at low relative humidities (11% to 43%) was almost constant. At higher relative humidities (43% to 80%) the equilibrium moisture content increased exponentially with increasing relative humidity. The isotherms were fitted to an equation of the form

$$1 - RH = \exp(-au^b) \qquad (2.2)$$

where RH is the relative humidity, u the moisture content per dry basis and a and b are constants. Equation (2.2) was rewritten as

$$\ln(-\ln(1 - RH)) = b \ln u + \ln a \qquad (2.3)$$

in order to plot $\ln(-\ln(1 - RH))$ versus $\ln u$. No fit was possible over the entire relative humidity range. A break occurred at relative humidities of about 72% and it was concluded that it indicated a change in the type of water binding. The heat of sorption was determined by using the Clausius Clapeyron equation and found to vary between 10.3 kcal/mole and 17.0 kcal/mole for different moisture contents.

Mittal and Usborne [1985] measured moisture isotherms for uncooked meat emulsions of different compositions. They used four temperatures, (55°C, 65°C, 75°C and 85°C (131°F, 149°F, 167°F and 185°F)), five fat to protein ratios (1.10, 1.30, 1.68, 2.16 and 2.56) and seven relative humidities, ranging from 11.2% to 95%. The reported temperatures are sufficiently high to process (i.e. to cook) the product and hence it is unclear why the meat emulsion was considered to be uncooked. Saturated salt solutions were used for relative humidity control. The meat emulsions were prepared before each experiment using a commercial chopper. The samples were placed in a 2 mm (0.08 inch) thick layer across the bottom of an aluminum foil basket and weighed approximately 3 to 4 grams. This basket was suspended with a wire into a wide mouth jar which was put into a constant temperature cabinet. Approximately 200 mL of solution with excess salt was maintained within the jar. The samples were

weighed occasionally without removal from the humidity control chamber and equilibrium was assumed when the weight change over 3 days was less than 0.1 gram. A period of 5 to 18 days was reported to be sufficient to establish moisture equilibrium. The resulting isotherms were sigmoid in shape. The equilibrium moisture content was almost constant for relative humidities between 11 and 60%, with very little influence of the temperature. Above humidities of 60%, an exponential increase in the equilibrium moisture content with increasing humidity was observed and the influence of the temperature was more pronounced, with higher equilibrium moisture contents for lower temperatures. Isotherms for varying fat to protein ratios were shown for a temperature of 75°C. The fat to protein ratio had very little influence on the equilibrium moisture content below humidities of 60%. For higher humidities, the amount of water adsorbed increased with decreasing fat content and it was explained that fat adsorbs less moisture than protein. The absolute values of the equilibrium moisture content were very similar to the results reported by Igbeka and Blaisdell [1982] for processed meat emulsion products.

2.6   Mathematical Modeling of Thermal Processing

Agrawal [1976] experimentally determined thermophysical properties of meat emulsion (Section 2.1) and developed a simulation model to describe the simultaneous heat and mass transfer in cylindrical meat emulsion products. The temperatures studied ranged from 21°C to 112°C (70°F to 233°F). Three heat and mass transfer models were investigated: 1.) a vapor diffusion model, 2.) a liquid diffusion model in which moisture was assumed to diffuse as a liquid within the product, followed by evaporation at the surface and 3.) a shrink model in which a liquid diffusion was accompanied by a volume reduction. An Arrhenius type equation was used to describe the temperature dependence of the mass diffusivity but it was assumed to be independent of

mass concentration. The driving force for mass transfer at the product surface was assumed to be the difference between the instantaneous moisture concentration and the concentration in equilibrium with the processing air. It was concluded that the measured values for the moisture diffusivity, thermal conductivity, thermal diffusivity and equilibrium moisture content appeared to be reasonable when compared to data for other meat products. However, experimentally determined heat and mass transfer coefficients were substantially higher than those calculated from empirical predictions. The moisture transport was found to have a significant influence on the overall process and Agrawal explained that "predictions made by considering heat transport alone would be inaccurate". The heat and mass transfer model considering internal moisture movement by liquid diffusion was found to be most accurate in predicting the average moisture losses and temperatures of the emulsion products during processing. The values of the effective moisture diffusion coefficient that provided the best fit of the measured data with the simulation model ranged from 0.6×10^{-10} to 1.3×10^{-10} m^2/s. The equilibrium moisture content and the moisture diffusivity were identified as the two key variables future research should focus on in order to make more accurate predictions for the simultaneous heat and moisture transport.

Mittal *et al.* [1982] developed a model to simulate the moisture distribution within a cylindrical product. Since it was found that "after a step rise during the course of the experiment, the temperature increased very little, and plateaued above the wet bulb temperature but below the air dry bulb temperature", the internal temperature gradients were assumed to be small and the moisture distribution was simulated assuming isothermal conditions. Additional assumptions made in the modeling were uniform initial distributions, negligible dimensional shrinkage, concentration independent moisture diffusivity, one-dimensional diffusion (radially outward) and an infinitely high mass transfer coefficient at the boundary. The last assumption was

justified by using relatively high air velocities (1.67 m/s, 330 ft/min) to provide high mass transfer Biot numbers.

Imre [1990] investigated the drying and shrinkage of salami products. The goal of this study was to minimize the time needed for the drying operation by simulating the process with a computer model. The drying process was modeled as a "hygroscopically covered homogeneous and isotropic equivalent colloidal material by interpreting the water concentration as a distributed parameter based on the dry mass". Imre explained that the "sorption equilibrium of the salami was determined by the state of the casing". The moisture transfer was modeled using the Fickian approach, i.e. assuming that the driving force for mass transfer was a moisture concentration gradient. Equations for the equilibrium moisture content and the diffusion coefficient for the meat paste and the casing were given. A contact mass transfer coefficient for the interface between casing and meat paste was introduced. The thermal capacity of the casing was neglected. Imre concluded that the developed model was well suited to describe the drying process. Measured moisture concentration profiles agreed well with predicted results. The maximum rate of drying was limited by the danger of possible deformations and inner fissures within the product.

Mohl [1993] developed a model that combines heat and mass transfer during meat emulsion processing. An isotherm was used to relate the product surface concentration to the vapor pressure above the surface. Two different functional forms for the isotherm were investigated, a linear type and a form derived from the Dubinin-Polanyi adsorption potential theory. It was concluded that the model was capable of predicting the characteristic behavior of the temperature history of the product. The particular functional form of the equilibrium concentration of the meat emulsion (isotherm) and the moisture diffusivity were found to have a strong influence on the thermal response of the product.

Wang and Brennan [1995] modeled the simultaneous heat and moisture transfer during the drying of a potato. The boundary condition for mass transfer was modeled with a sorption isotherm, i.e. the water vapor pressure over the potato surface was related to the instantaneous moisture content of the potato at the interface. The resulting differential equations were solved with a finite difference algorithm. The simulated values of the temperature and moisture concentration profiles were compared with experimental results and reported to be in good agreement. The temperature profiles were obtained with thin thermocouples. A stainless steel cork borer was used to obtain the moisture concentration profiles. For this purpose, samples were removed at various times from the drying environment and cut with the borer. The resulting cylindrical samples were sliced into ten pieces of approximately 1 mm (0.04 inch) thickness, which were then dried in an oven.

2.7 Nuclear Magnetic Resonance Studies

Nuclear Magnetic Resonace (NMR) has contributed greatly to several scientific disciplines in the last decades. It is a powerful nondestructive method for structural identification in analytical chemistry and biochemistry. Magnetic Resonance Imaging (MRI), based on the principles of NMR, is a relatively new method. It is used, for example, in the medical field to obtain images of the human body. The applications of NMR and MRI of interest to this study are described in this section. These are the determination of moisture concentration profiles, temperature profiles and diffusion coefficients in food systems. A thorough discussion of the physics of NMR and MRI can be found in a number of sources, including Abragam [1961], Stilbs [1987], Smith and Ranallo [1989] and Callaghan [1991]. A summary of the applications of MRI in the food industry is given by Schrader et al. [1992].

Ruan et al. [1991] used magnetic resonance imaging to investigate moisture pro-

files and moisture diffusion coefficients in a potato during drying and absorption. Cylindrical samples of 20 mm (0.8 inch) in diameter and 70 mm (2.8 inch) in length were cut from fresh potatos. The two end surfaces were coated with wax in order to obtain mass transfer in the radial direction only. For the drying experiments, the samples were suspended into the center of an imaging probe of 8.8 cm (3.5 inch) internal diameter inside a 4.7 Tesla magnetic resonance imaging machine. For the absorption experiments, the samples were put into a water-filled tube which was placed in the imaging probe. Hot air for the drying experiments was generated with a fan and an electric resistance heater. A dry bulb temperature of 60°C (140°F), a humidity ratio of 0.008 and an air velocity of 1.2 m/s (235 ft/min) were used in the drying measurements. A spin-warp sequence was employed for data aquisition. It took approximately 8 minutes to obtain one image. In addition to the experiments giving the initial moisture distribution, images were taken after 30, 60, 180 and 360 minutes. For the water absorption experiments, the obtained proton density profiles were converted into moisture profiles by scaling the value of the proton density of pure water to 100% moisture. For the drying experiments, the average signal intensity at different drying times was compared with the average moisture content of samples obtained by an oven drying method. In addition, some of the samples were cut after imaging with sharp end pipes into five concentric rings. The moisture content of each ring was determined with the oven drying method and compared with the profiles from the magnetic resonance experiments. The difference between the two methods was reported to be less than 3 percent. The temperature profiles inside the samples were measured with thermocouples outside the imaging system at the same conditions as those used for the imaging experiments. A numerical model of the heat and mass transfer in the samples was developed and solved numerically with a finite difference method. The equilibrium moisture content of the potatoes for the conditions of the

drying air was used as the boundary condition for mass transfer. The relationship between the diffusion coefficient and the moisture content was obtained from determining the former for different average moisture contents of the sample and was modeled as an exponential function of the moisture content. Simulation results from the model indicated that the Fickian diffusion equation did not adequately describe the moisture movement through the samples. These differences were thought to be a result of the method used for obtaining the diffusion coefficient, i.e. from average moisture contents for the entire sample without considering case hardening at the sample surface.

A study similar to that conducted by Ruan *et al.* [1991] was reported by Schrader *et al.* [1992]. Magnetic resonance imaging was used to measure moisture profiles in a model food gel during drying. The model food gel was made from granulated agar, microcrystalline cellulose and distilled water. Gel samples of 40 mm (1.6 inch) in length and 8 mm (0.3 inch) diameter were cut and weighed. In order to obtain samples with different initial moisture contents for the imaging experiments, some of the samples were pre-dried at room temperature for different times. A custom drying apparatus was used to image the gel cylinders while drying in the magnetic resonance apparatus. The samples were placed in a glass tube of larger diameter. Pieces of fishing line were used to prevent the samples from touching the glass tube and to establish uniform flow conditions. The air flow was provided by a compressor. The resulting air velocity in the annulus formed by the gel cylinders and the inner surface of the glass tube was 4 to 5 m/s (800 to 1000 ft/min). It was postulated that this velocity was high enough to provide internally controlled drying conditions. The measurements were conducted at dry bulb temperatures of 80°C (176°F) and 35% relative humidities. Images during the drying were obtained in 10 to 15 minute intervals. The total drying time was 75 minutes. Images were acquired for a two-dimensional slice

at the center of the sample cylinder with a 200 MHz, 4.7 Tesla imaging system. A standard spin-echo sequence was used for the measurements. The time needed for one imaging operation was not specified. The moisture profiles were obtained from the resonance data by imaging calibration samples of known moisture content. The obtained moisture profiles were compared to profiles predicted by a finite difference solution of Fickian radial diffusion in a cylinder. It was postulated that boundary conditions for the model assuming constant surface moisture contents would be inaccurate. Hence, a drying experiment with a thin slice of gel was conducted. The sample weight and the corresponding moisture contents were recorded in one minute intervals. The moisture contents from this drying rate curve were inserted into the finite difference model as the time varying boundary conditions. The moisture content dependent diffusivity of the model equation was adjusted to minimize the error between the model prediction and the measured moisture profiles. The measured moisture profiles were much flatter near the center of the cylinder with steeper moisture content gradients near the edge, as compared to the parabolic shape calculated from the model. It was concluded that the Fickian model was an inaccurate predictor of the interior moisture profiles of the model food gel and that the moisture diffusivity was not a function of the moisture content alone.

Sun et al. [1993] used a magnetic resonance method to measure the temperature distribution in a model food gel during heating and cooling. The molecular pseudo self-diffusion coefficient of water in the gel was used as a temperature indicator and it was obtained from signal attenuation data of spin-echo experiments. This coefficient is a physical constant for a material at a constant temperature and describes the rate of the spatial spreading of molecules undergoing random translational motion. The relation between the relative change of this diffusion coefficient and the absolute temperature was linear. The absolute value at room temperature was given

as 1.26×10^{-9} m^2/s. The model food gel samples were contained in a plastic tube of 25 mm (1 inch) diameter, which was located in the center of the sample holder in the magnetic resonance machine. Water circulating around the plastic tube was used for heating and cooling. For the heating process, the initial temperature of the gel and that of the water was 18°C (64°F) and 35°C (95°F), respectively. The conditions were reversed for the cooling process. The data acquisition time for each temperature mapping experiment was about 30 seconds. Temperature data were also collected under the same conditions with thin thermocouples in a separate experiment outside the magnet. The average variation between the magnetic resonance data and the thermocouple measurements was less than 1.3°C (2.3°F). In a related paper about temperature mapping in a potato, Sun *et al.* [1994] report a refinement in the spin-echo experiment, leading to a reduction in the data acquisition time for one temperature experiment to 10 seconds. In this case, the average variation between the magnetic resonance data and the thermocouple measurements was less than 0.5°C (0.9°F).

Callaghan *et al.* [1983] used a pulsed field-gradient nuclear magnetic resonance method to study the diffusion of fat and water in cheddar and swiss cheeses. In the pulsed field-gradient experiments, the molecules were labeled by the Larmor precession frequencies. These frequencies were made to be spatially dependent by the application of a magnetic field which varied with position. The diffusion coefficients were measured with a technique described by Stejskal and Tanner [1965]. The Fourier transformed one-dimensional spectra showed a clear separation of the water and fat peaks, allowing the assignment of the larger diffusion coefficient to the water phase. The magnitude of the obtained diffusion coefficients was related to the structure of the cheese emulsion. The water diffusion coefficients were about one-sixth that of bulk water at the same temperature. This result was used to postulate that the

water diffusion was confined to surfaces within the protein matrix. The fat diffusion coefficient indicated that the diffusion process was restricted to the inside of the small fat droplets present in the cheese emulsion. The theory of restricted diffusion was extended to allow for a size distribution of the fat droplets and the measured data corresponded to a gaussian distribution of the volume of the fat droplets. The work reported by Callaghan et al. [1983] was extended to different emulsion system by Van Den Enden et al. [1990], Lönnqvist et al. [1991], Balinov et al. [1993] and Fourel et al. [1994].

2.8   Microscopic Structure of Meat Emulsion

Borchert et al. [1967] investigated the structure of a meat emulsion with light and electron microscopes before and after thermal processing. The samples were comminuted to temperatures of approximately 20°C (68°F) and subsequently processed to internal temperatures of approximately 83°C (181°F). The unprocessed emulsion contained a variety of structural materials in the continuous phase with a small group of visible cell organelles that were suspected to be mitochondrial pieces or fragments of the sarcoplasmic reticulum. The thermally processed emulsion showed a number of pores in the membrane surrounding the fat globules. In addition, the continuous phase of the emulsion was highly disrupted with the protein being coagulated into dense, irregular zones. It was noted that "heat processing schedules which differ from the one used in this experiment may give rise to variations in the electron micrographs of the emulsion".

Theno and Schmidt [1978] conducted a microstructural comparison of three commercial meat emulsion products. The products were purchased in a local supermarket and only identified as brands A, B and C. Brand A was made from beef and pork, while brands B and C were all beef products. Light micrographs revealed a coarse

protein matrix structure, including a large single piece of intact muscle and large fat droplets in brand A. A more uniform structure containing only a few large fat droplets was found in brand B. These droplets were covered with a proteinaceous coat and bound into the matrix. Brand C showed a finely structured matrix with a high degree of uniformity. The authors concluded that only brand C possessed "the type of microstructure associated with a true meat emulsion".

Carrol and Lee [1981] examined meat emulsions prepared at 16°C, 21°C and 26°C (61°F, 70°F and 79°F) and after being cooked. The samples were prepared from ground lean beef to which trimming fat was added in order to yield a fat content of approximately 26%. The three different temperatures were obtained by adjusting the temperature of the ingredients. At 16°C (61°F), a homogeneous mixture of liquid droplets surrounded by the protein matrix was observed. The lipid droplets ranged in size from 100 μm down to the resolution of the light microscope. More irregularly shaped fat droplets were found when the processing temperature increased to 21°C (79°F). In addition, some voids or air pockets were observed and the continuous phase was less homogeneous. These voids increased in size at processing temperatures of 26°C (79°F). The lipid droplets tended to coalesce in this case, which the authors explained indicated the fat was beginning to melt.

2.9 Summary of Existing Work

Previous studies on meat emulsion products, their processing techniques and modeling approaches provide a basis for the proposed work of this research. Of particular interest are the results reported by Agrawal [1976], Hanson [1988], Spielbauer [1992] and the various studies of nuclear magnetic resonance techniques with respect to the measurement of moisture profiles and moisture diffusion coefficients (e.g. Callaghan et al. [1983], Ruan et al. [1991] and Schrader et al. [1992]).

Agrawal [1976] made the first attempt to develop a realistic simulation model of the thermal processing of meat emulsion products. The limitations of Agrawal's work were the unrealistic boundary conditions for mass transfer at the interface of product and processing air and the assumption of moisture concentration independent thermophysical properties. Hanson [1988] investigated the effect of four different processing conditions on the temperature at different locations within a large diameter meat emulsion product. Two different types of casing were used in that study. The reported temperature data can be used to compare the output of the simulation model developed in this study with actual data. Spielbauer [1992] developed a method of measuring the heat transfer coefficient in a large, commercial and continuously operated smokehouse. The reported data can be used as a first approximation for the value of the heat transfer coefficient in similar equipment. The developed method of measuring the heat transfer coefficient is directly applicable to a wide array of processing equipment in the food industry and will be used in this study.

Most studies that have compared experimentally determined moisture profiles with data computed from simulation models found that the Fickian approach was well suited to describe the moisture transfer. Some publications, i.e. Ruan *et al.* [1991] and Schrader *et al.* [1992], reported that the Fickian assumption was an inaccurate predictor of the interior moisture profiles of the investigated materials. However, it is possible that the differences between measured and simulated data were caused by limitations of the used simulation model, for example inaccurate boundary conditions and the lack of accounting for moisture concentration and temperature dependent heat and mass transfer properties. Because of these restrictions on the findings of Ruan *et al.* [1991] and Schrader *et al.* [1992], and since the majority of studies reported a good agreement with measured data when using the Fickian mass transfer model, the latter will be used in the simulation model developed for this research.

Table 2.4: References related to the research presented in this dissertation which are not explicitly cited in the text. The entries within each of the four categories are listed in alphabetical order. Only the name of the first author is given.

1) *Heat and mass transfer in food systems*

Aguerre [1992]	Andrieu [1986]	Balaban [1988]	Becker [1959]
Califano [1983]	Chandra [1984]	Chinnan [1984]	Choi [1986]
Christensen [1982]	Chung [1967]	Daudin [1990]	De Baerdemaeker [1977]
Doe [1973]	Fortes [1981]	Gekas [1991]	Gekas [1992]
Gros [1984]	Hallström [1984]	Hallström [1990]	Hamdy [1969]
Hayakawa [1977]	Hayakawa [1988]	Hayakawa [1992]	Husain [1973]
Iglesias [1982]	Karel [1975]	King [1968]	Kostaropoulus [1971]
Laguerre [1991]	Liebenspacher [1989]	Lind [1991]	Loncin [1980]
Lozano [1983]	Miketinac [1992]	Misra [1980]	Motarjemi [1987]
Naveh [1983]	Nicolai [1992]	Parti [1991]	Rao [1986]
Reidy [1971]	Roman [1979]	Roman [1983]	Rossen [1977]
Rotstein [1978]	Saguy [1980]	Saguy [1983]	Sakai [1992]
Savoye [1992]	Singh [1984]	Skjöldebrand [1980]	Toupin [1984]
Vagenas [1993]	White [1981]	Wolf [1985]	

2) *Theoretical aspects of heat and mass transfer*

Ashworth [1972]	Axelsson [1991]	Berger [1973]	Carslaw [1959]
Chu [1968]	Comini [1976]	Crank [1975]	Crapiste [1988]
Dolinski [1991]	Dural [1990]	Fulford [1969]	Furuta [1992]
Gibson [1979]	Hallström [1982]	Harmathy [1969]	Krischer [1978]
Lebedev [1961]	Luikov [1961]	Luikov [1963]	Luikov [1965]
Luikov [1966]	Luikov [1975]	Maroulis [1991]	Mikhailov [1975]
Moyne [1987]	Nasrallah [1988]	Perre [1993]	Plumb [1985]
Prat [1986]	Robbins [1991]	Saito [1977]	Spalding [1963]
Spiess [1983]	Smirnov [1962]	Smolsky [1962]	Sullivan [1990]
Thomas [1980]	Whitney [1968]	Young [1969]	Young [1971]

3) *Chemical aspects of food and food processing*

Berk [1976]	Briskey [1966]	Coenders [1992]	Coultate [1989]
De Man [1976]	Eskin [1990]	Friberg [1976]	Hamm [1962]
Larsson [1990]	Maga [1988]	Price [1971]	Wierbicki [1957]

4) *Processing of meat emulsion products*

Kresse [1979]	Martin [1993]	Rao [1976]	Simon [1969]
Stech [1988]			

Chapter 3

Modeling of Thermal Processing

This chapter will discuss the development of the model for the simulation of heat and mass transfer between the meat emulsion product and the processing air. First, the governing equations from the theory of heat and mass transport are introduced. Next, the simulation model is described. Special emphasis is given to the formulation of the boundary conditions. This model is used in Chapter 4 to determine the sensitivity of simulated data to several input parameters and in Chapter 6 for a comparison of simulated and measured data.

3.1 Governing Equations of Heat and Mass Transfer

The goal of most heat transfer calculations is to obtain information about temperature profiles, average temperatures and energy fluxes. Analogously, mass transfer calculations provide information about the distribution of individual species in two-component or multicomponent systems.

3.1.1 Conservation of Energy and Mass

For simple geometries, e.g. flat plates, long cylinders or spheres, the method of *shell energy balances*, as described by Bird, Stewart and Lightfoot [1960], can be used to

formulate the principles of conservation of energy and mass on the system of interest. Alternatively, the energy and mass balances can be formulated over an arbitrary differential fluid element, accounting for all possible contributions. This approach leads to the *equations of change*, which are tabulated in Bird, Stewart and Lightfoot [1960]. These equations are normally used by discarding those terms that describe physical contributions which are known or suspected to be negligible in the given situation. For example, the application of the energy equation to one-dimensional transient heat transfer in cylindrical coordinates without convection and generation terms results in

$$\rho c \frac{\partial T}{\partial \tau} = -\frac{1}{r}\frac{\partial}{\partial r}(r\, q_r) \tag{3.1}$$

where the radial component q_r of the energy flux vector can be replaced by *Fourier's law of heat conduction*

$$q_r = -k\frac{dT}{dr} \tag{3.2}$$

to yield the so called *conduction equation*

$$\rho c \frac{\partial T}{\partial \tau} = \frac{1}{r}\frac{\partial}{\partial r}\left(r\, k\frac{\partial T}{\partial r}\right). \tag{3.3}$$

Diffusional mass transfer of one component in a binary system consisting of species A and B, or in a multicomponent system, is often considered to be analogous to conductive heat transfer, and a mass diffusivity $D_{AB} = D_{BA}$ (also called the *mutual diffusion coefficient* or simply the *diffusivity*) can be defined analogous to Equation (3.2) as

$$j_{Ax} = -\rho D_{AB}\frac{\partial \omega_A}{\partial x} \tag{3.4}$$

where j_{Ax} is the mass flux relative to a mass average velocity, ρ is the (total) mass density of the binary system and ω_A is the mass fraction of the diffusing species A.

Equation (3.4) is known as *Fick's first law of diffusion*. To demonstrate the analogy between heat and mass transfer, the fluxes of energy and mass are sometimes written as

$$j_{Ax} = -D_{AB}\frac{\partial}{\partial x}(\rho_A) \tag{3.5}$$

$$q_x = -\alpha\frac{\partial}{\partial x}(\rho c T) \tag{3.6}$$

where ρ_A is the mass concentration of the diffusing species A and $\alpha = k/\rho c$ the thermal diffusivity. It has to be noted that Equations (3.4) and (3.5) are not equivalent statements of Fick's first law of diffusion. Only Equation (3.4) is valid in a strict sense. The so-called *hot wall paradox* can be used to explain the difficulties associated with Equation (3.5). A closed system containing the gases A and B with a heated wall at one side will, due to the gas laws, exhibit a gradient in the mass concentrations ρ_A and ρ_B at equilibrium. However, if Equation (3.5) was valid, no gradients in ρ_A and ρ_B could exist at equilibrium. Despite this contradiction, Equation (3.5) is widely used for mass transfer calculations.

Equations (3.4) and (3.5) assume that the driving force for mass transfer is a concentration gradient. This assumption introduces little error in most mass transfer calculations, even though the real driving force for mass transfer is the chemical potential of the transported species. However, when considering mass transfer through different materials, differing affinities to moisture have to be considered and coupling conditions at the interface of the materials have to be introduced. The application of this strategy for the mass transfer processes under investigation in this study is described in Section 3.2.2.

The mass transfer equivalent of the conduction equation (Equation (3.3))

$$\frac{\partial \omega}{\partial \tau} = \frac{1}{r}\frac{\partial}{\partial r}\left(r D_{AB}\frac{\partial \omega}{\partial r}\right) \tag{3.7}$$

Table 3.1: Equivalent forms of the diffusion equation for the case of drying. The equations are based on different expressions for the moisture concentration, the dry-weight moisture concentration u_m, the wet-weight moisture concentration ω_m and the moisture density ρ_m.

Expression for the moisture concentration	Definition	Resulting form of the diffusion equation
dry-weight moisture concentration	$u_m = \rho_m/\rho_d$	$\dfrac{\partial u_m}{\partial \tau} = \dfrac{1}{r}\dfrac{\partial}{\partial r}\left(r\, D_{m,s}\dfrac{\partial u_m}{\partial r}\right)$
wet-weight moisture concentration (mass fraction)	$\omega_m = \rho_m/\rho$	$\dfrac{\partial \omega_m}{\partial \tau} = \dfrac{1}{r}\dfrac{\partial}{\partial r}\left(r\, D_{m,s}\dfrac{\partial \omega_m}{\partial r}\right)$
moisture density	$\rho_m = \rho - \rho_d$	$\dfrac{\partial \rho_m}{\partial \tau} = \dfrac{1}{r}\dfrac{\partial}{\partial r}\left(r\, D_{m,s}\dfrac{\partial \rho_m}{\partial r}\right)$

is called *Fick's second law of diffusion* or the *diffusion equation*. Depending on the choice of concentration units, several mathematically equivalent statements of Equations (3.4) and (3.7) can be used. In the context of drying, Perry *et al.* [1984] suggest using a dry-weight basis, i.e. expressing the moisture in a material as a percentage of the weight of the dry solid, when introducing moisture concentrations. When using a dry-weight basis, the change of moisture is constant for all moisture levels. When the wet-weight basis is used to express moisture contents, Perry *et al.* [1984] explain that "a 2 or 3 percent change at high moisture contents (above 70 percent) actually represents a 15 to 20 percent change in evaporative load." The equations

$$u_m = \frac{\omega_m}{1 - \omega_m}; \quad \omega_m = \frac{u_m}{1 + u_m} \tag{3.8}$$

can be used to convert dry-weight and wet-weight concentrations into each other. The physical processes during the thermal preparation of meat emulsion products, i.e. simultaneous heat and mass transfer, are similar to those encountered during drying operations. Based on Perry's [1984] suggestion, a dry-weight basis for the moisture concentration, called u_m or simply u, is therefore used in the remainder of

this study. Equivalent forms of the diffusion equation are summarized in Table 3.1. The diffusion coefficient of the moisture in the solid, $D_{m,s}$, is identical for all cases in Table 3.1.

3.1.2   The Boundary Conditions for Heat and Mass Transfer

Three different kinds of boundary conditions are frequently used in the mathematical description of heat and mass transfer processes. First, the material temperature or concentration of the diffusing species at the boundary can be specified. Second, it is possible to specify the heat or mass flux at the boundary, hence fixing the temperature gradient or concentration gradient. Finally, the temperature or concentration of the diffusing species at the surface can be related to an external boundary value of temperature or concentration, respectively. The application of these boundary conditions to the simulation model is described in Section 3.2.2.

3.2   The Simulation Model

This section introduces the simulation model for the heat and mass transfer between the product and the processing air. The assumptions made in the model are summarized in Table 3.2 and are described in detail in the following paragraphs. Next, the conservation equations for energy and mass are derived from shell balances. Finally, two options to formulate the boundary conditions at the interface of product and processing air are given.

The simulation model assumes that the moisture diffuses in the radial direction in liquid form from the interior of the product to the surface where it evaporates. The heat of evaporation is provided by the processing air. It is further assumed that the volume of the meat emulsion product remains constant during processing. The moisture can be thought of as the distributed variable in a dry matrix of protein, fat and

Table 3.2: Assumptions made in the simulation model. A more detailed description, including an assessment of the introduced error, is given in this section.

1. The moisture within the product diffuses in liquid form to the surface where it evaporates without causing a change in the volume of the product.

2. The driving force for mass transfer is a moisture concentration gradient and an effective moisture diffusion coefficient (that can depend on the moisture concentration and temperature) can be used as the proportionality factor.

3. The casings do not affect the heat transfer to the product. In addition, the moisture-permeable casings have a negligible resistance to mass transfer.

4. Circumferential dependencies and end effects are negligible and hence the heat and mass transfer within the product occurs in the radial direction only.

5. Latent heats associated with the melting of fats are small compared to the average specific heat of the products and the release of water as a result of protein denaturation is small compared to the initial product moisture content.

6. The exchange of heat and mass between the product and the processing air does not change the temperature and humidity of the processing environment.

7. Flux couplings, i.e. moisture gradients causing energy fluxes (Dufour effect) and temperature gradients causing moisture fluxes (Soret effect), are negligible.

inorganic materials. Typical moisture losses during the processing of meat emulsion products are relatively small, ranging from 3 to 5% for large diameter products to 5 to 8% for small diameter products.

The driving force for mass transfer within the product is assumed to be the gradient of the moisture concentration. The proportionality factor between the mass flux and this driving force is given by an effective moisture diffusivity, D_{eff}, that can be a function of the moisture concentration and the temperature and incorporates other possibly existing modes for mass transfer, for example capillary action. The driving force for mass transfer at the interface of product and processing air is given by the difference in the moisture concentration. Assuming that the processing air behaves like an ideal gas, this concentration difference can be expressed by a vapor pressure difference.

Moisture-permeable and moisture-impermeable casings can be used during the

processing of cylindrical meat emulsion products. Both casing types are very thin and their effect on the heat transfer between the product and the processing air is small. It is further assumed that the resistance of the moisture-permeable casings to mass transfer is negligible. This assumption is verified by moisture loss experiments of products consisting of different emulsion types stuffed into identical moisture-permeable cellulose casings and by moisture loss measurements of water-filled cellulose casings (Chapter 5).

The heat and mass transfer within the product is assumed to be a function of the product radius and time only. Hence, possible circumferential effects, caused by heat and mass transfer coefficients that are a function of the circumferential coordinate, are neglected. The error introduced by this assumption is investigated for representative processing conditions and it is shown that the circumferential dependencies are of minor importance (Section 4.2.1).

The fat particles contained in the meat emulsion melt at the temperatures encountered during the thermal processing. Because of the molecular structure and composition of the fats, the melting process occurs over a range of temperatures. It is assumed that the latent heats associated with the melting of fat particles are small compared to the sensible heat that is necessary to raise the temperature of the product. In addition, it is assumed that the release of water as a result of protein denaturation during the thermal processing is small compared to the initial moisture content of the products.

The effects of heat and mass transfer on the processing environment are neglected. In other words, the processing air is assumed to be an infinite source for heat transfer to the product and an infinite sink for mass transfer from the product. This assumption is built into the simulation model in order to focus the investigation on the fundamental processes of the simultaneous heat and mass transfer and its dependence

on such parameters as the heat and mass transfer coefficients or the relative humidity of the processing air. Without this assumption, specific information about the processing equipment, for example the duct sizes, processing air replacements per unit time or the control mechanisms of the processing oven, would be needed in addition to fundamental parameters, such as the velocity of the processing air. However, the model is capable of simulating processing equipment with different processing zones. All input parameters can be set independently in each zone.

No secondary fluxes are considered, i.e. moisture gradients causing energy fluxes and temperature gradients causing moisture fluxes, are neglected.

3.2.1 Conservation Equations from Shell Balances

With the assumptions outlined above, the application of an energy balance on a cylindrical shell of thickness Δr within the emulsion product for the case of simultaneous heat and mass transfer leads to the equation

$$
\bar{\rho}\,\bar{c}\,\frac{\partial}{\partial \tau}\left(r\,\Delta\theta\,\Delta z\,\Delta r\,T\right) = r\,\Delta\theta\,\Delta z\,\left.q_r\right|_r - r\,\Delta\theta\,\Delta z\,\left.q_r\right|_{r+\Delta r}
$$
$$
+\,r\,\Delta\theta\,\Delta z\,c_w\,j_w\,\left.T\right|_r - r\,\Delta\theta\,\Delta z\,c_w\,j_w\,\left.T\right|_{r+\Delta r} \tag{3.9}
$$

where the left hand side describes the change in internal energy. The terms on the right hand side account for the heat fluxes and the mass fluxes in and out of the control volume. Dividing Equation (3.9) by $\Delta\theta\,\Delta z\,\Delta r$, taking the limit as Δr approaches zero and expressing the heat flux q_r by Fourier's law of heat conduction and the mass flux j_w by Fick's first law of diffusion gives, after some rearrangement

$$
\bar{\rho}\,\bar{c}\,\frac{\partial T}{\partial \tau} = \frac{1}{r}\frac{\partial}{\partial r}\left(r\,k\,\frac{\partial T}{\partial r} + r\,c_w\,\rho_d\,T\,D_{\it eff}\,\frac{\partial u}{\partial r}\right) \tag{3.10}
$$

where $u = \rho_w/\rho_d$ and T denote the moisture concentration per dry basis and temperature, respectively. The second term on the right hand side of Equation (3.10) (or the

last two terms in Equation (3.9)) accounts for the enthalpy associated with the diffusing moisture. This term is not negligible since the changes in moisture concentration, especially near the surface of the product, can be relatively large. An investigation of the importance of this enthalpy term for typical meat emulsion processing conditions is given in Section 4.2.3. The mean density ρ and heat capacity $\bar{c}$ in Equation (3.10) are given by

$$\bar{\rho} = \rho_d + \rho_m \tag{3.11}$$

and

$$c = \omega_d\, c_d + \omega_w\, c_w. \tag{3.12}$$

The application of a mass balance on a cylindrical shell of thickness Δr within the emulsion product results in

$$\frac{\partial}{\partial \tau}(r\, \Delta\theta\, \Delta z\, \Delta r\, u) = r\, \Delta\theta\, \Delta z\ j_w|_r - r\, \Delta\theta\, \Delta z\ j_w|_{r+\Delta r} \tag{3.13}$$

where the left hand side describes the change in the moisture concentration. Dividing Equation (3.13) by $\Delta\theta\, \Delta z\, \Delta r$, taking the limit as Δr approaches zero and expressing the mass flux j_w by Fick's first law of diffusion gives after some rearrangement

$$\frac{\partial u}{\partial \tau} = \frac{1}{r}\frac{\partial}{\partial r}\left(r\, D_{\text{eff}}\, \frac{\partial u}{\partial r}\right) \tag{3.14}$$

which is similar to the diffusion equation described in Section 3.1.1. The effective moisture diffusivities D_{eff} in Equations (3.10) and (3.14) can incorporate other possibly existing modes for mass transfer (Section 3.2).

3.2.2 Formulation of the Boundary Conditions

The driving force for mass transfer at the product surface is assumed to be the difference between the moisture concentration directly over the product surface (i.e.

over the casing) and that of the processing air. Assuming that the processing air can be described as an ideal gas, the moisture concentrations can be expressed by the partial vapor pressures $p_{w,s}$ and $p_{w,\infty}$ to yield

$$-D_{eff} \, \rho_d \, \frac{\partial u}{\partial r} = k_p \, (p_{w,s} - p_{w,\infty}) \tag{3.15}$$

where k_p is the mass transfer coefficient. Since the meat emulsion and the processing air have different affinities to moisture, a coupling condition is used to relate the moisture concentration in the meat emulsion, u, to the water vapor pressure over the product surface, $p_{w,s}$. This coupling condition is given by the equilibrium relationship (isotherm) between the moisture concentration of the meat emulsion and the relative humidity of the air in contact with the product,

$$u = \mathcal{F}(p_{w,s}, T). \tag{3.16}$$

Hence, local equilibrium is assumed at the interface of product and processing air, even though the overall process is transient in nature. Isotherms for meat emulsions were reported by Igbeka and Blaisdell [1982] (Chapter 2). If the resistance of the cellulose casing to mass transfer is negligible, the differing affinities to moisture between the meat emulsion and the casing material can be neglected and the water vapor pressure over the casing material can be obtained from the isotherm of the meat emulsion.

If mass is transferred from the product to the processing air, the latent heat needed to evaporate the moisture at the product surface is supplied by the processing air and the boundary condition for heat transfer can be written as

$$k \frac{\partial T}{\partial r} = h \, (T_\infty - T_s) - \Delta \hat{H}_v \, k_p \, (p_{w,s} - p_{w,\infty}) \tag{3.17}$$

where h and $\Delta \hat{H}_v$ are the overall heat transfer coefficient and the latent heat of evaporation of water, respectively. The sign of the third term in Equation (3.17) shows
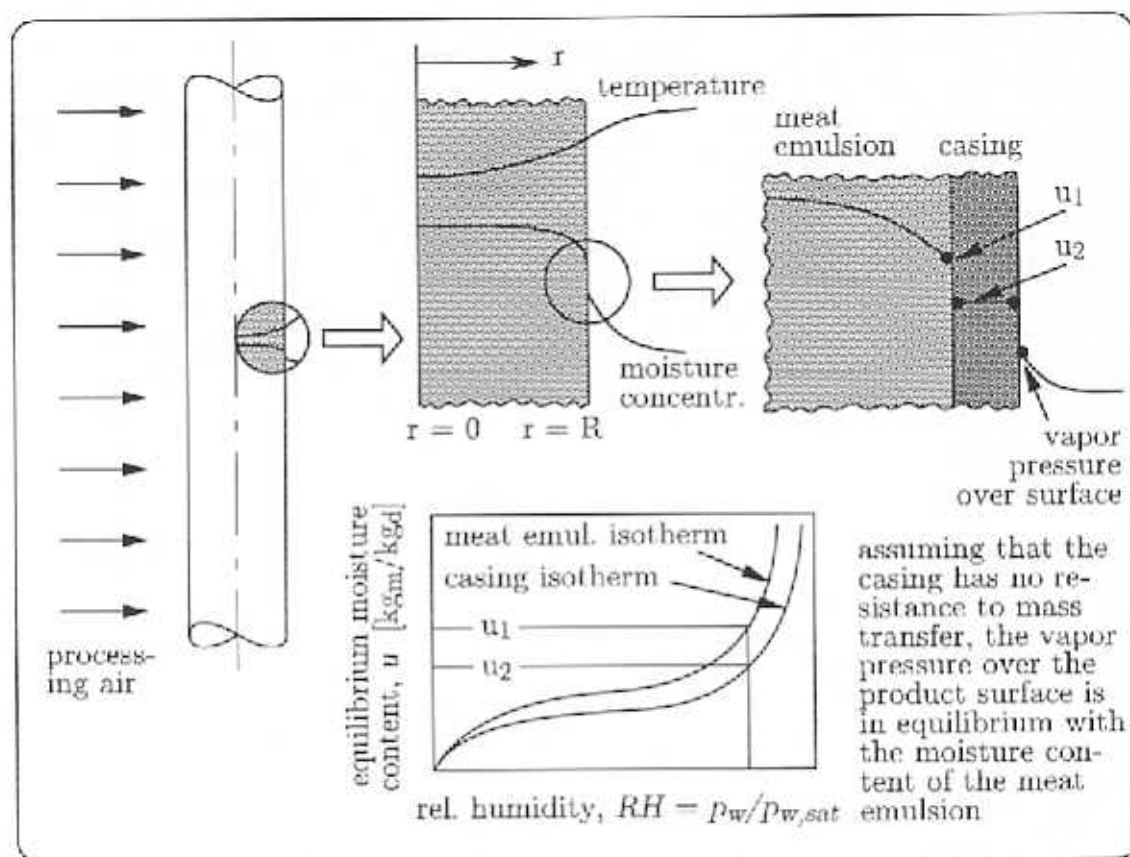
Figure 3.1: Temperature and moisture concentration profiles within the meat emulsion product and the boundary layer. The relation between the moisture concentration in the meat emulsion at the surface and the water vapor pressure over the surface is given by the meat emulsion isotherm.

that the energy needed to evaporate the moisture at the product surface reduces the energy that can be conducted into the product. If the third term in Equation (3.17) were larger than the second term, some of the energy needed for the evaporation of the water would be provided by the product itself and an *evaporative cooling* situation would arise. The second term in Equation (3.17) includes energy transfer by means of radiation. The details of this contribution are described in Section 5.4. A sketch of the temperature and moisture concentration profiles within the meat emulsion product and the boundary layer is given in Figure 3.1. An illustration of the relation between the moisture concentration in the meat emulsion and the resulting

water vapor pressure over the product surface, for the case of negligible mass transfer resistance in the casing, is also given in Figure 3.1.

Condensation of water vapor from the humid processing air on the product will occur if the product surface temperature T_s is below the dew point temperature T_{dp} of the processing air. Assuming an initial product temperature of 6°C and a processing air dry bulb temperature of 80°C, all relative humidities of the processing air above 2% will result in some initial condensation.

The heat and mass transfer processes during the initial condensation period can be simulated in two different ways. First, it is possible to allow mass transfer to the product when the water vapor pressure over the product surface is smaller than the water vapor pressure in the processing air. In this case, the released latent heat of the condensing moisture is assumed to raise the surface temperature of the product until the surface vapor pressure exceeds that of the processing air and mass transfer from the product to the processing air begins. During the initial condensation period, it is assumed that the condensing moisture remains at the product surface. The possibility that some or all of the water drips off the product due to gravity is neglected. In theory, it would be possible to introduce a factor accounting for the ratio of remaining and dripped off water. However, the magnitude of this ratio could only be obtained from guessing. The increase of the surface moisture concentration during the condensation period can be modeled with an adsorption isotherm.

An alternative for the boundary condition considers mass transfer from the product to the processing air only. The mass transfer coefficient is set to zero if the water vapor pressure over the product surface is smaller than the value in the processing air. The heat transfer coefficient in the case of condensation is usually found to be very high. Since the ratio of internal to external resistance to heat transfer (i.e. the Biot number) for high heat transfer coefficients is then very high, it is reasonable to

Table 3.3: Summary of equations for the simulation model. For the case of surface boundary conditions that allow mass transfer to the product, only the last three equations of the entry for $\xi = 1$ are needed.

Conservation equations

$$\frac{\partial u}{\partial \tau} = \frac{1}{r}\frac{\partial}{\partial r}\left(r\, D_{\mathit{eff}}\,\frac{\partial u}{\partial r}\right)$$

$$\rho c \frac{\partial T}{\partial \tau} = \frac{1}{r}\frac{\partial}{\partial r}\left(r\,k\,\frac{\partial T}{\partial r} + r\,c_w\,\rho_d\,T\,D_{\mathit{eff}}\,\frac{\partial u}{\partial r}\right)$$

$$\rho = \rho_d + \rho_w$$

$$\bar{c} = \omega_d\, c_d + \omega_w\, c_w$$

Boundary conditions at $\xi = 1$ $(r = R)$

$$\left.\begin{array}{l} T_s = T_{dp} \\[4pt] k_p = 0 \end{array}\right\} \quad \text{for } h\,(T_\infty - T_s) < -k\left.\frac{\partial T}{\partial r}\right|_s$$

$$\left.\begin{array}{l} k\dfrac{\partial T}{\partial r} = h\,(T_\infty - T_s) \\[8pt] k_p = 0 \end{array}\right\} \quad \text{for } T_s > T_{dp} \text{ and } p_{w,s} < p_{w,\infty}$$

$$\left.\begin{array}{l} u = \mathcal{F}(p_{w,s}, T) \\[8pt] -D_{\mathit{eff}}\,\rho_d\,\dfrac{\partial u}{\partial r} = k_p\,(p_{w,s} - p_{w,\infty}) \\[8pt] k\dfrac{\partial T}{\partial r} = h\,(T_\infty - T_s) - \Delta\tilde{H}_v\,k_p\,(p_{w,s} - p_{w,\infty}) \end{array}\right\} \quad \begin{array}{l} \text{for } T_s > T_{dp} \\ \text{and } \left.p_w\right|_s > p_{w,\infty} \\ \text{or for the case} \\ \text{where mass transfer} \\ \text{to the product} \\ \text{is allowed} \end{array}$$

Boundary conditions at $\xi = 0$ $(r = 0)$

$$\frac{\partial u}{\partial r} = \frac{\partial T}{\partial r} = 0$$

---

assume that the product surface temperature T_s equals the dew point temperature T_{dp}. This assumption simplifies the calculation.

When the surface temperature during condensation is set equal to the dew point temperature, the existing positive temperature difference between the processing air
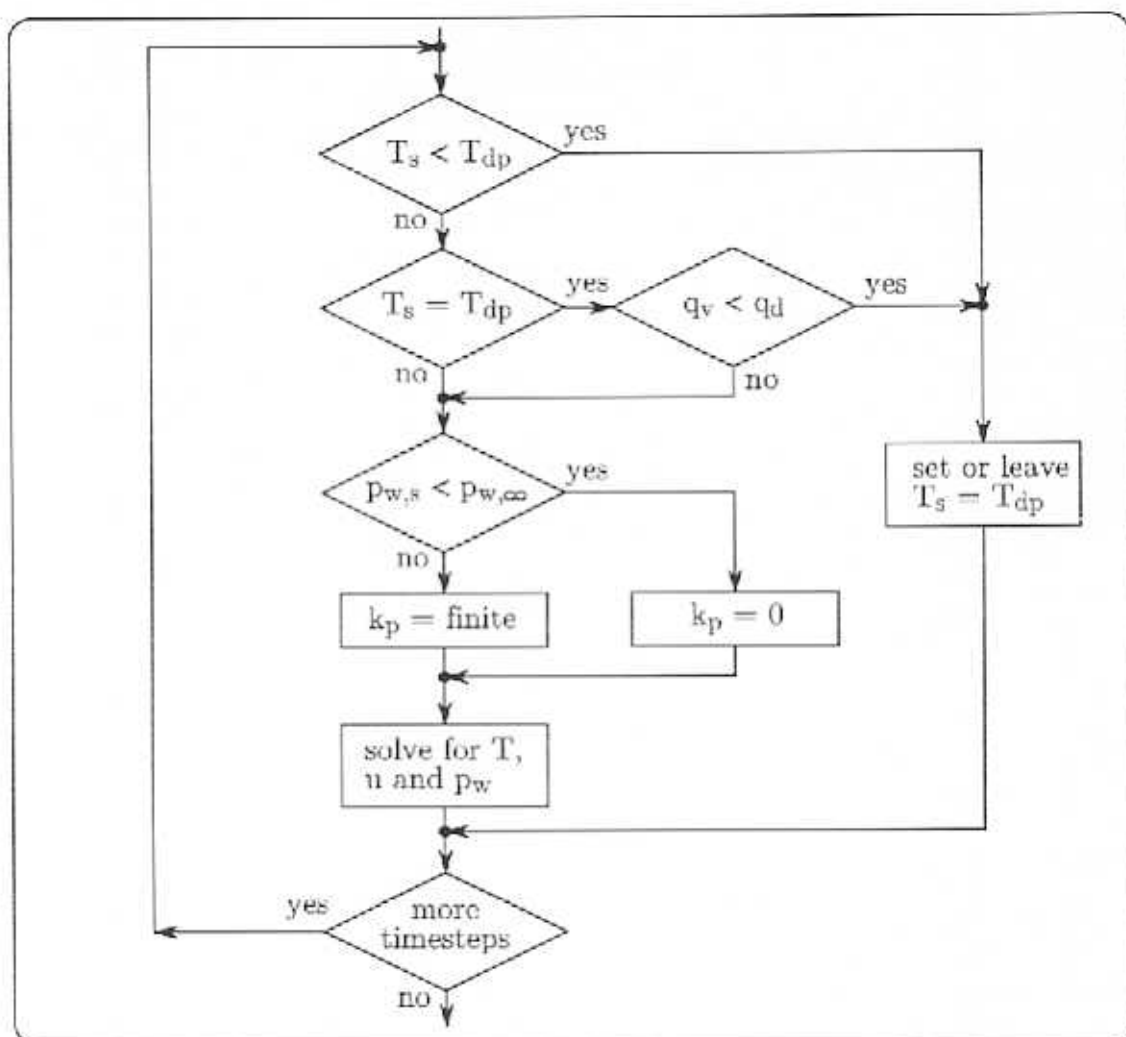
Figure 3.2: Flowchart of the boundary conditions of the simulation model that do not allow mass transfer to the product during the initial condensation period.

and the product surface can only supply additional convective energy (i.e. raising the surface temperature above the dew point temperature) when the convective heat flux is greater than the conductive heat flux towards the center of the product. Otherwise, the existing steep temperature gradient in the product near the surface would "try to relax" not only by conducting energy to the interior but also by lowering the surface temperature (possibly below the dew point temperature). This would in turn cause

the model to set the surface temperature equal to the dew point temperature, leading to a numerical "back and forth" bouncing. In reality, this effect doesn't occur due to the gradual decrease in the heat transfer coefficient caused by a decreasing potential for condensation. Hence, it will take some time for the steep temperature gradient within the product to relax by means of conducting heat to the inner product. The surface temperature is therefore held at the dew point temperature T_{dp} until the convective heat flux to the product is greater than the conductive heat flux at the product surface. Mass transfer away from the surface begins when the vapor pressure at the surface is larger than the vapor pressure of the water in the processing air.

The assumption that the temperature and moisture concentration within the product are only a function of time and the radial coordinate implies that the gradients of temperature and moisture concentration at the geometric center of the product are zero,

$$\frac{\partial u}{\partial r} = \frac{\partial T}{\partial r} = 0. \tag{3.18}$$

These equations are sometimes referred to as the *zero flux* boundary conditions.

The complete set of equations of the simulation model is summarized in Table 3.3. For the case of surface boundary conditions that allow mass transfer to the product, only the last three equations of the entry for $\xi = 1$ have to be used. A graphical representation of the surface boundary conditions with the second option during the initial condensation period (i.e. not allowing mass transfer to the product) is shown in the form of a program flow chart in Figure 3.2. Calculated responses of the product temperature and moisture concentration during processing with typical conditions for both options during the initial condensation period are described in Section 4.2.2 and are shown in Figure 4.4.

Chapter 4

Numerical Solution and Sensitivity Analysis

This chapter is divided into two parts. First, the finite difference method is introduced as a numerical technique. It is used to solve the differential equations of the simulation model developed in Chapter 3. Several important aspects of this method are described in the following subsections. The second part of this chapter utilizes the finite difference method to investigate the error associated with various assumptions of the simulation model and to test the sensitivity of computed results to selected input parameters.

4.1 The Finite Difference Method

The concept of the finite difference approach is to discretize the continuous problem domain of the differential equation so that the dependent variables are considered to exist only at discrete points of a finite difference grid or mesh. The derivatives in the differential equations and boundary conditions are then approximated by algebraic differences. Thus, the differential equations are transformed into a system of algebraic equations. The generation of a suitable finite difference grid (also called *mesh*) is
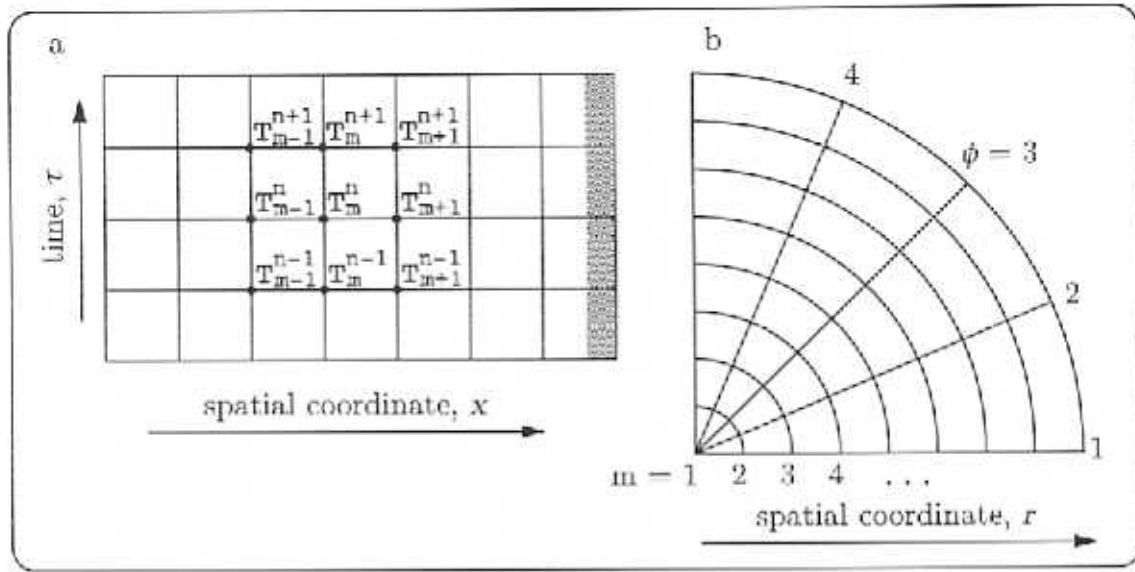
Figure 4.1: Finite difference grids for the one-dimensional conduction equation in rectangular coordinates (Figure a) and two-dimensional problems in cylindrical coordinates (Figure b).

usually the first step in a solution procedure. A finite difference grid for the one-dimensional conduction equation in rectangular coordinates

$$\frac{\partial T}{\partial \tau} = \alpha \frac{\partial^2 T}{\partial x^2} \tag{4.1}$$

is shown in Figure 4.1-a. The indices m and n refer to the grid position for the spatial variable x and the time variable τ, respectively. A two-dimensional finite difference grid in cylindrical coordinates is shown in Figure 4.1-b. The discretization of the time variable τ is not shown but could be imagined to be perpendicular to the plane of the paper. This mesh is used for the computations in Section 4.2.1. The one-dimensional form of Figure 4.1-b (i.e. without discretization of the circumferential variable ϕ) is used in Sections 4.2.3 to 4.2.4 and for the computations in Chapter 6.

Numerous textbooks, e.g. Anderson *et al.* [1984] or Strikwerda [1989], give a detailed account of finite difference techniques and related topics. Aspects of the method that are of special importance to this study are described in the following

subsections.

4.1.1 Discretizing the Spatial and Time Derivatives

Derivatives can be approximated by several finite difference expressions. The definition of the derivative for a function $T(x, y)$ at $x = x_0$ and $y = y_0$

$$\frac{\partial T}{\partial x} = \lim_{\Delta x \to 0} \frac{T(x_0 + \Delta x, y_0) - T(x_0, y_0)}{\Delta x} \qquad (4.2)$$

can be used as a basis for the approximation

$$\frac{\partial T}{\partial x} \approx \frac{T_{m+1,l} - T_{m,l}}{\Delta x} \qquad (4.3)$$

where the subscripts m and l indicate the x and y position on a finite difference grid. The difference approximation can be put on a more formal basis through the use of a Taylor series expansion for the right hand side of Equation 4.2. It is then possible to estimate the order of the truncation error, i.e. the difference between the partial derivative and its finite difference approximation, and Expression (4.3) can be transformed into the equation

$$\frac{\partial T}{\partial x} = \frac{T_{m-1,l} - T_{m,l}}{\Delta x} + O(\Delta x) \qquad (4.4)$$

where $O(\Delta x)$ indicates that the order of the truncation error is Δx raised to the power of one, the largest power which is common to all terms in the representation of the truncation error. Equation (4.4) is called a forward difference approximation. A more accurate representation of the derivative in Equation (4.2) is given by the central difference approximation

$$\frac{\partial T}{\partial x} = \frac{T_{m+1,l} - T_{m-1,l}}{2\Delta x} + O(\Delta x)^2 \qquad (4.5)$$

that involves the two grid points adjacent to the one where the derivative is evaluated. Second order derivatives can be approximated by the three point formula

$$\frac{\partial^2 T}{\partial x^2} = \frac{T_{m+1,t} - 2T_{m,t} + T_{m-1,t}}{(\Delta x)^2} + O(\Delta x)^2. \tag{4.6}$$

Of special importance to this study is a finite difference approximation for the differential expressions on the right hand side of the conservation equations for mass and energy (Equations (3.14) and (3.10). The transport coefficients D_{eff} and k in these expressions can depend on the moisture concentration and temperature and they are within the differential operator. A one-dimensional finite difference approximation for these terms is given by

$$\frac{\partial}{\partial r}\left(r k \frac{\partial T}{\partial r}\right) \approx \frac{\left(r_{m+0.5}\, k_{m+0.5}\, \frac{T_{m+1}-T_m}{\Delta r}\right) - \left(r_{m-0.5}\, k_{m-0.5}\, \frac{T_m-T_{m-1}}{\Delta r}\right)}{\Delta r} \tag{4.7}$$

and an analogous form for the derivative involving D_{eff}. Derivatives with respect to time can be discretized with a forward time approximation of the form

$$\frac{\partial T}{\partial \tau} \approx \frac{T_m^{n+1} - T_m^n}{\Delta \tau} \tag{4.8}$$

which is similar to Equation 4.4. Equation 4.8 provides the basis for the marching-type solution strategy where the solution at the new time step $n+1$ is based on the corresponding values at the previous time step.

4.1.2 Implicit and Explicit Finite Difference Schemes

The terms *explicit* and *implicit* refer to the solution strategy of the resulting algebraic equations in the case of a single partial differential equation. An explicit scheme has only one unknown in the difference equation so that a direct evaluation in terms of known quantities is possible. For example, if the derivative term on the right hand side of the conduction equation (Equation (4.1)) is approximated at the old time

level n, the only unknown at each spatial grid point at the new time level is T_m^{n+1}. However, if the second derivative term is approximated at the new time level $n+1$, the three unknowns T_{m-1}^{n+1}, T_m^{n+1} and T_{m+1}^{n+1} would appear in the algebraic equations at each spatial grid point at the new time step. Hence, all equations at the new time level must be solved simultaneously. This is generally possible because the number of equations equals the number of unknowns (the number of spatial grid points) at each time level. A procedure of this kind is known as implicit.

A different situation can arise when a system of differential equations has to be solved. The word *system* in this context refers to some degree of coupling, i.e. dependent variables that exist in more than one of the equations. In this case, it might be necessary to employ solution schemes that simultaneously solve for the dependent variables in all equations at each time step, even when the so called explicit solution strategies are used to discretize the derivatives of the individual equations.

4.1.3 Grid Clustering with Transformation Functions

In many finite difference calculations, the general nature of the solution is known beforehand. If steep gradients of the dependent variables are expected near a particular region of the investigated domain, for example the moisture concentration near the surface during the processing of meat emulsion products, a finite difference grid with grid points clustered in the region of largest gradients can be used. This strategy would focus computer time on the region of interest to the investigator. To achieve this grid clustering, one could simply design a convenient grid layout and incorporate the nonuniform grid spacing by an appropriate change of the finite difference approximation at each spatial position within the grid. However, this method turns out to be cumbersome and not very well suited to a general treatment with an inbuilt capacity for dealing with different degrees of clustering. A similar but more elegant method is

to apply an algebraic transformation function to the differential equations (including the boundary conditions) which have to be solved to obtain a non uniformly spaced physical grid that corresponds to a uniformly spaced computational grid. A suitable transformation function for a one-dimensional cylindrical problem with boundaries at $r = 0$ and $r = R$ is given by Anderson et al. [1984],

$$\bar{r} = \frac{\ln\left[(\beta + r/R)/(\beta - r/R)\right]}{\ln\left[(\beta + 1)/(\beta - 1)\right]}, \quad 1 < \beta < \infty \tag{4.9}$$

where β is the so called *stretching parameter*. For values of β near 1.0, more grid points are clustered near $r = R$, whereas no clustering is performed when β approaches infinity. A comparison of a clustered grid with a clustering parameter of $\beta = 1.05$ and a uniformly spaced grid is shown in Figure 4.2. The spatial coordinates r and $\bar{r}$ in Equation (4.9) refer to the physical and computational radial position, respectively. In order to apply this transformation to the governing equations, the partial derivatives

$$\frac{\partial}{\partial r} = \left(\frac{\partial \bar{r}}{\partial r}\right) \frac{\partial}{\partial \bar{r}} \tag{4.10}$$

are formed where the gradient $\partial r/\partial r$ is called the *metric* of the transformation. For the transformation function in Equation (4.9), the metric is given by

$$\frac{\partial \bar{r}}{\partial r} = \frac{2\beta}{R \ln\left[(\beta + 1)/(\beta - 1)\right]\left[\beta^2 - (r/R)^2\right]}. \tag{4.11}$$

This derivative contains r, so that an expression for r as a function of $\bar{r}$ is needed. This is referred to as the *inverse of the transformation* and is, in this case, given by

$$r = R\frac{\beta\left[(\beta + 1)/(\beta - 1)\right]^{\bar{r}} - \beta}{1 + \beta\left[(\beta + 1)/(\beta - 1)\right]^{\bar{r}}}. \tag{4.12}$$

Using this method, results for the dependent variables will be obtained on the uniformly spaced computational grid. Equation (4.12) can then be used to transform the results to the physical domain with the clustered grid spacing.
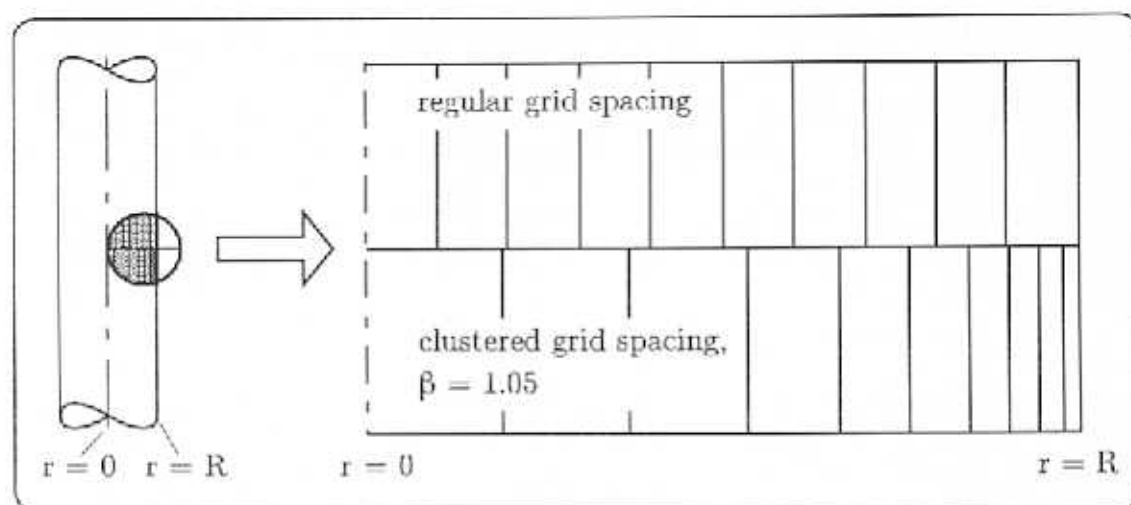
Figure 4.2: Comparison of the grid spacing for a regular and a clustered grid.

4.1.4 Different Discretization Methods

Two distinctly different approaches are possible when using the finite difference method to solve differential equations. In the first case, the differential equation is taken as the correct and appropriate form of the investigated process. Algebraic expressions are then introduced to approximate the derivatives, followed by some mathematical tools to solve the resulting equations. Physical reasoning had been used previously in deriving the differential equations but then put aside. This is the method introduced in Subsection 4.1.1 and the one most often described in textbooks on the subject, e.g. Strikwerda [1989].

The second method, called the *control volume approach*, doesn't start with the governing differential equation but rather with the discrete finite difference mesh on which physical principles are translated into mathematical statements. This method is similar to the procedure of deriving differential equations from shell balances (Bird, Stewart and Lightfoot [1960]), except that the difference equation is not transformed into a differential equation by taking limits. Some textbooks on the subject deal exclusively with the control volume approach e.g. Incropera and De Witt [1990].

Only very few monographs, e.g. Anderson *et al.* [1984] attempt to describe the subtle differences between the two methods.

Both approaches usually yield identical algebraic equations in the interior of a physical region of interest. However, the processes taking place at the surface (the boundary) of a region are in most cases of crucial importance, e.g. in the thermal processing of meat products investigated in this study, and it is at these surfaces where the two finite difference methods yield different results. Since the control volume method keeps the discrete nature of the solution method in view at all times, it leads to more accurate approximations of the physical process. Anderson *et al.* [1984] use the example of convective boundary conditions for the transfer of heat within a two-dimensional rectangular domain and steady state conditions to show the different nature of both methods. Of more interest to this study is the case of heat transfer in a one-dimensional domain under transient conditions. For a rectangular region (Figure 4.1-a) the discretization of the boundary condition

$$k \frac{\partial T}{\partial x} = h \left(T_\infty - T_s \right) \tag{4.13}$$

with a forward difference method for the first described discretization approach would yield

$$k \frac{T_m^n - T_{m-1}^n}{\Delta x} = h \left(T_\infty - T_s \right) \tag{4.14}$$

whereas the control volume approach would not start with Equation (4.13) but with a different form of an energy balance at the surface. Taking the material associated with the boundary point into account (the shaded half node in Figure 4.1-a) results in

$$k \frac{T_m^n - T_{m-1}^n}{\Delta x} = h \left(T_\infty - T_s \right) - \rho c \frac{\Delta x}{2} \frac{T_m^{n+1} - T_m^n}{\Delta \tau} \tag{4.15}$$

showing clearly the difference between the two methods.

Applied to the thermal processing of cylindrical meat emulsion products (i.e. simultaneous heat and mass transfer in cylindrical coordinates), the application of the control volume discretization method for a one-dimensional domain (i.e. the dependent variables temperature and moisture concentration are only a function of the radius and time) yields the boundary conditions

$$V_{hn}\,\rho_d\,\frac{u_m^{n+1} - u_m^n}{\Delta\tau} = -A_{hn}\,D_{eff}\,\rho_d\,\frac{u_m^{n+1} - u_{m-1}^{n+1}}{\Delta r} - A_s\,k_p\,(p_w - p_{w,\infty}) \qquad (4.16)$$

$$V_{hn}\,\rho\,c\,\frac{T_m^{n+1} - T_m^n}{\Delta\tau} =$$
$$- A_{hn}\,k\,\frac{T_m^{n+1} - T_{m-1}^{n+1}}{\Delta r} + A_s\,h\,(T_\infty - T) - A_s\,\Delta\hat{H}_v\,k_p\,(p_w - p_{w,\infty}) \qquad (4.17)$$

at the surface $(r = R)$, where the indices m describe the grid position at the interface of product and processing air, and

$$V_{hn}\,\frac{u_1^{n+1} - u_1^n}{\Delta\tau} = A_{hn}\,D_{eff}\,\frac{u_2^{n+1} - u_1^{n+1}}{\Delta r} \qquad (4.18)$$

$$V_{hn}\,\bar{\rho}\,\bar{c}\,\frac{T_1^{n-1} - T_1^n}{\Delta\tau} = A_{hn}\,k\,\frac{T_2^{n+1} - T_1^{n-1}}{\Delta r} \qquad (4.19)$$

at the geometric center $(r = 0)$. The indices hn in Equations (4.16) to (4.19) refer to the corresponding halfnode. The areas A_{hn} and A_s are those at the interface to the adjacent (internal) node and at the outer surface, respectively. The ratios in the second terms of Equations (4.16) to (4.19) approximate the derivatives at the interface of the corresponding halfnode and the adjacent node. Equations (4.16) to (4.19) can be written in dimensionless form with $\theta = (T_\infty - T)/(T_\infty - T_o)$, $\psi = (u_e - u)/(u_e - u_o)$ and $\xi = r/R$. With expressions for V_{hn}, A_{hn} and A_s and rearranged one obtains

$$\left(\kappa_o - \frac{\kappa_o^2}{2R}\right)\frac{\psi_m^{n-1} - \psi_m^n}{\Delta\tau} = -\frac{R - \kappa_o}{R}\,\frac{D_{eff}}{R}\,\frac{\psi_m^{n+1} - \psi_{m-1}^{n+1}}{\Delta\xi} + \frac{k_p\,(p_w - p_{w,\infty})}{\rho_d\,(u_e - u_o)} \qquad (4.20)$$

$$\left(\kappa_o - \frac{\kappa_o^2}{2R}\right) \frac{R}{k} \rho c \frac{\theta_m^{n-1} - \theta_m^n}{\Delta\tau} =$$
$$-\frac{R - \kappa_o}{R} \frac{\theta_m^{n+1} - \theta_{m-1}^{n+1}}{\Delta\xi} - \frac{hR}{k}\theta + \frac{R}{k} \frac{\Delta\hat{H}_v k_p (p_w - p_{w,\infty})}{(\delta T)_m} \tag{4.21}$$

at the surface $(\xi = 1)$ and

$$\frac{\kappa_i}{2} \frac{\psi_1^{n+1} - \psi_1^n}{\Delta\tau} = D_{\mathit{eff}} \frac{1}{R} \frac{\psi_2^{n+1} - \psi_1^{n+1}}{\Delta\xi} \tag{4.22}$$

$$\frac{\kappa_i}{2} \rho c \frac{\theta_1^{n+1} - \theta_1^n}{\Delta\tau} = k \frac{1}{R} \frac{\theta_2^{n-1} - \theta_1^{n-1}}{\Delta\xi} \tag{4.23}$$

at the geometric center $(\xi = 0)$ where κ_o and κ_i denote the thicknesses of the outer and inner halfnodes, respectively. The finite difference form of the conservation equations of the simulation model (Equations (3.14) and (3.10)) can be obtained from the control volume procedure or directly from the application of Equations (4.7) and (4.8) from Section 4.1.1 to obtain

$$\frac{\psi_m^{n+1} - \psi_m^n}{\Delta\tau} = \frac{1}{R^2} \frac{1}{\xi} \frac{1}{\Delta\xi} \left(\xi|_{m+0.5}^n D_{\mathit{eff}}|_{m+0.5}^n \frac{\psi_{m+1}^n - \psi_m^n}{\Delta\xi} - \right.$$
$$\left. \xi|_{m-0.5}^n D_{\mathit{eff}}|_{m-0.5}^n \frac{\psi_m^n - \psi_{m-1}^n}{\Delta\xi} \right) \tag{4.24}$$

for the diffusion equation and

$$\bar{\rho}\bar{c} \frac{\theta_m^{n-1} - \theta_m^n}{\Delta\tau} = \frac{1}{R^2} \frac{1}{\xi} \frac{1}{\Delta\xi}$$
$$\left[\left(\xi|_{m-0.5}^n k|_{m-0.5}^n \frac{\theta_{m-1}^n - \theta_m^n}{\Delta\xi} - \xi|_{m-0.5}^n k|_{m-0.5}^n \frac{\theta_m^n - \theta_{m-1}^n}{\Delta\xi} \right) \right.$$
$$+ \left(c_w \rho_d (T_\infty - (\delta T)_m \theta) \frac{(\delta u)_m}{(\delta T)_m} \xi|_{m+0.5}^n D_{\mathit{eff}}|_{m+0.5}^n \frac{\psi_{m+1}^n - \psi_m^n}{\Delta\xi} \right.$$
$$\left. \left. - c_w \rho_d (T_\infty - (\delta T)_m \theta) \frac{(\delta u)_m}{(\delta T)_m} \xi|_{m-0.5}^n D_{\mathit{eff}}|_{m-0.5}^n \frac{\psi_m^n - \psi_{m-1}^n}{\Delta\xi} \right) \right] \tag{4.25}$$

for the energy equation.

4.2 Sensitivity of Simulated Data to Model Parameters

This section employs the finite difference equations of the simulation model to investigate the error associated with various assumptions. The sensitivity of computed results to selected input parameters is described in Subsection 4.2.4.

4.2.1 Comparison of 1-D and 2-D Solutions

The flow patterns over a cylinder are a strong function of the Reynolds number and are rather complex. The local values of the heat and mass transfer coefficients vary with the angle ϕ around the cylinder. For highly turbulent flow situations ($Re > 5000$), these coefficients have high values at the stagnation point, $\phi = 0°$, and decrease around the cylinder as the boundary layer thickens. This decrease continues until the boundary layer separates from the wall surface followed by an increase with the remaining distance around the cylinder. For smaller Reynolds numbers, no flow separation occurs but the local heat and mass transfer coefficients still vary around the circumference of the cylinder. This variation at the surface causes the internal transport processes to depend not only on the radius of the cylinder, but also on the circumferential position.

Therefore, the error introduced by the assumption that the thermal processing of cylindrical meat emulsion products can be modeled by one-dimensional transport processes (i.e. temperature and moisture concentration are only a function of the radial position) must be investigated. For this purpose, the temperature response of a cylinder subjected to a heating process with non-uniform convective boundary conditions and uniform initial temperature was calculated. Mass transfer was not considered because it would complicate the calculations considerably. In addition, the ratio of

internal to external resistance to mass transfer is much larger than the corresponding ratio for heat transfer and the local variation of the surface mass transfer coefficient is of little importance to the development of the internal moisture concentration. The equations

$$\frac{\partial T}{\partial \tau} = \alpha \left[\frac{1}{r} \frac{\partial}{\partial r} \left(r \frac{\partial T}{\partial r} \right) + \frac{1}{r^2} \frac{\partial^2 T}{\partial \phi^2} \right] \tag{4.26}$$

$$k \left. \frac{\partial T}{\partial r} \right|_s = h(\phi) (T_\infty - T_s) \tag{4.27}$$

describe the internal temperature during the two-dimensional transient process. In dimensionless form with $\xi = r/R$ and $\theta = (T_\infty - T)/(T_\infty - T_o)$, one obtains

$$\frac{\partial \theta}{\partial \tau} = \alpha \left[\frac{1}{R^2} \frac{1}{\xi} \frac{\partial}{\partial \xi} \left(\xi \frac{\partial \theta}{\partial \xi} \right) + \frac{1}{R^2} \frac{1}{\xi^2} \frac{\partial^2 \theta}{\partial \phi^2} \right] \tag{4.28}$$

$$\left. \frac{\partial \theta}{\partial \xi} \right|_s = - \frac{h(\phi) R}{k} \theta_s = - Bi(\phi) \theta_s . \tag{4.29}$$

The variation of the local heat transfer coefficient $h(\phi)$ with the angular position for high Reynolds numbers ($Re > 70000$) was investigated by Giedt [1949]. His measured values are summarized in Icropera and DeWitt [1990]. The general nature of these results was used to estimate the variation of the local heat transfer coefficient for the smaller Reynolds numbers encountered in this study ($2500 < Re < 50000$). Values for the local heat transfer coefficient used in the present calculations are shown in Figure 4.3-a. The transport properties ρ, c and k were assumed to be constant and a value of $\alpha = k/\rho c = 1 \times 10^{-7}$, similar to values encountered during meat processing, was used in the computations of θ from Equations (4.28) and (4.29). An explicit finite difference method with 50 subdivisions for each spatial dimension and a timestep of 0.005 seconds was used in the calculations. The finite difference representation of the center point in a cylindrical coordinate system for a two-dimensional process is described in Özisik [1968]. At each timestep, an approximation for the temperature

at the origin ($m = 1$) was obtained from the average temperature of all surrounding nodal points ($m = 2$)

$$T_{m=1}^n = \frac{1}{l} \sum_{i=1}^{l} T_{m=2,i}^n . \tag{4.30}$$

Computed temperature profiles after 20 minutes are shown in the form of a contour plot in Figure 4.3-b. The θ contour lines correspond to locations with identical temperature. The higher heat transfer coefficients near the stagnation point ($\phi = 0°$) result in higher temperatures (lower θ values) near the corresponding cylinder region where a contour line of $\theta = 0.325$ can be seen. Lower temperatures are found near the region with smaller heat transfer coefficients ($\phi = 80°$). Overall, the variation of the surface heat transfer coefficient with the angular position ϕ has only a small influence on the development of the internal temperature profile. For a constant heat transfer coefficient, the contour lines would form perfect circles. The relatively small distortions of these contour lines indicate that the assumption of a one-dimensional process without circumferential dependencies is justified.

Most commercial smokehouses are designed to vary the direction of the airflow over the products during processing. The case investigated in this section, i.e. airflow from one direction only, is therefore a worst case scenario and it can be concluded that the circumferential dependencies of the temperature and moisture concentration during commercial processing are even less pronounced than those shown in Figure 4.3-b.

4.2.2 Influence of Boundary Conditions

Two sets of boundary conditions for the simulation model were introduced in Chapter 3. The first set allowed mass transfer to the product when the water vapor pressure over the product surface was smaller than the water vapor pressure in the processing air. In this case, the released latent heat of the condensing moisture was assumed to raise the surface temperature of the product until the surface vapor pressure exceeded
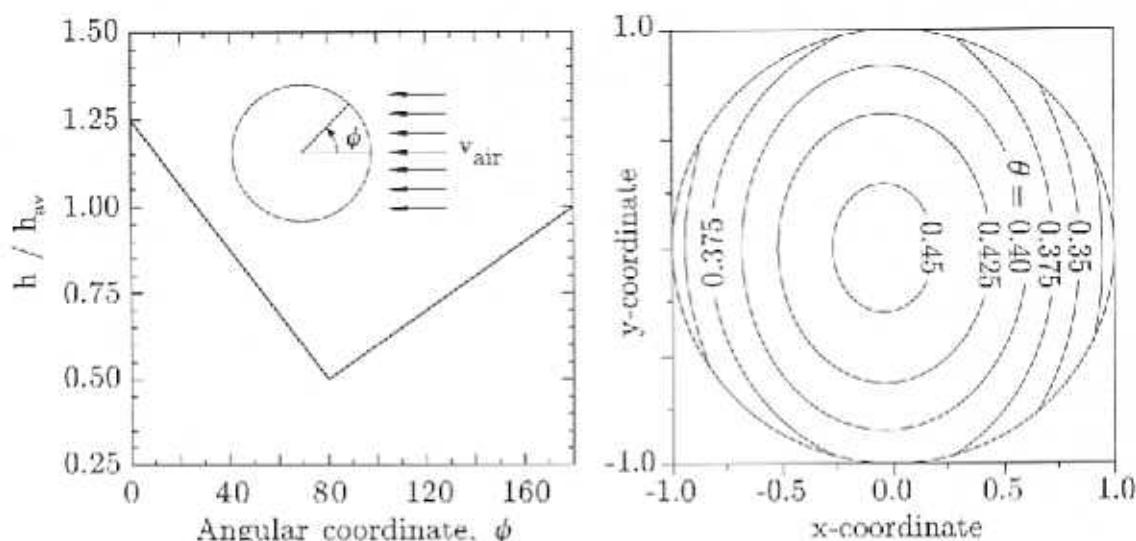
Figure 4.3: Circumferential variation of the local heat transfer coefficient for air-flow normal to a cylinder, adapted from Incropera, DeWitt [1990] for a Reynolds number of 2500 (left plot). The corresponding calculated temperature profiles over the cross section of a cylinder after 20 minutes for a two-dimensional heating process are shown on the right hand side $(\alpha = 1 \times 10^{-7} \text{ m}^2/\text{s}, h_{av} = 25 \text{ W/m}^2\text{K})$.

that of the processing air and mass transfer from the product to the processing air began. The second set of boundary conditions considered mass transfer from the product to the processing air only. The mass transfer coefficient was set to zero if the water vapor pressure over the product surface was smaller than the value in the processing air. The surface temperature during the initial processing stages was set to the dew point temperature of the processing air. It was assumed that the relatively high heat transfer coefficients during the initial condensation period caused a large ratio of internal to external resistance to heat transfer. Consequently, the error introduced by setting the surface temperature equal to the dew point temperature was believed to be small.

Calculated responses of the product temperature and moisture concentration during processing with typical conditions for both sets of boundary conditions are shown
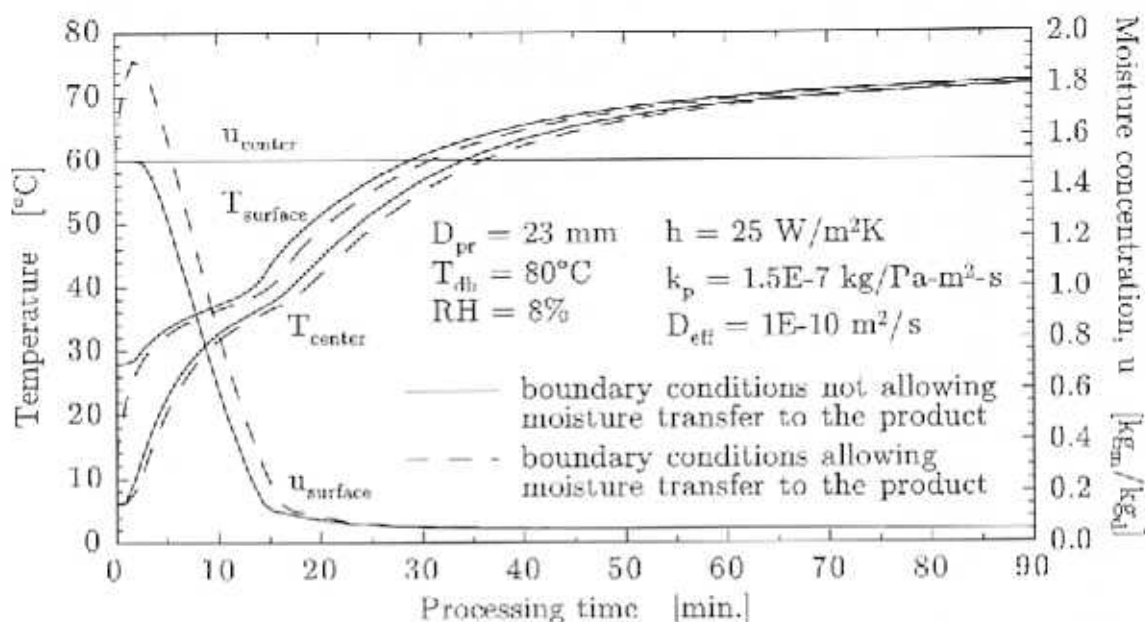
Figure 4.4: Calculated temperatures and moisture concentrations at the product surface and center as a function of time for typical processing conditions and for two different sets of boundary conditions.

in Figure 4.4. The surface moisture concentration for the boundary conditions allowing mass transfer to the product reached a maximum value of approximately 1.9 kg_m/kg_d after a processing time of 2 minutes. The value of the initial uniform moisture concentration was 1.5 kg_m/kg_d. The surface moisture concentration at later processing times for both sets of boundary conditions was in close agreement and reached a steady value of approximately 0.05 kg_m/kg_d after 30 minutes of processing. The surface and center temperatures for both sets of boundary conditions agreed well. A difference of approximately 2°C was calculated for processing times between 15 and 20 minutes. A small difference was computed for later processing times ($t > 50$ minutes). The difference between the two set of boundary conditions with regard to the surface temperature at the beginning of the processing can be seen clearly. One set of boundary conditions sets the surface temperature equal to the dew point temperature of the processing air, whereas the second set applies the released latent heat of

the condensing moisture to raise the surface temperature of the product. However, only a small difference of approximately 1°C for the product surface temperature was observed between the two sets of boundary conditions after a processing time of 5 minutes.

The set of boundary conditions allowing mass transfer to the product assumes that the condensing moisture remains at the product surface and neglects the possibility that some or all of the water drips off the product due to gravity. Water lost by this effect would not be available to raise the surface moisture concentration of this product. In theory, it would be possible to introduce a factor accounting for the ratio of remaining and dripped-off water. However, the magnitude of this ratio could only be obtained from guessing. If some moisture was assumed to remain at the surface, the corresponding increase of the surface moisture concentration had to be modeled with an adsorption isotherm. However, the equilibrium moisture measurements described in the literature (Chapter 2) are performed to yield desorption isotherms and the results of these to types of equilibrium measurements often differ because of a hystereses effect. Because of these two difficulties, it was decided to use the set of boundary conditions that does not allow mass transfer to the product as the basis for the remaining calculations in this chapter and in Chapter 6.

4.2.3 Different Forms of the Energy Equation

The energy equation (Equation (3.10)) contains a term that accounts for the enthalpy of the diffusing moisture. For unknown reasons, many publications dealing with the subject of thermal food processing, e.g. Agrawal [1976], Mallikarjunan and Mittal [1994] and Wang and Brennan [1995], do not include this contribution when proposing simulation models.

The importance of this term was investigated by calculating the temperature

and moisture concentration response of a product for typical processing conditions with and without this term. The calculated temperature and moisture concentration responses for both cases are shown in Figure 4.5. Omitting the enthalpy of the diffusing mass in the energy equation results in a significant error in the calculated temperature response of the product. For the representative processing conditions applied in Figure 4.5, a difference of approximately 5°C between the corresponding temperature values for the two forms of the energy equation was calculated at later processing stages ($t > 30$ minutes) with higher temperatures computed from the energy equation which omits the enthalpy term. This observation is in accordance with the sign of the mass term in Equation (3.10). The surface moisture concentration for the form of the energy equation neglecting the enthalpy of the diffusing mass is lower because the higher temperatures in that case cause a larger water vapor pressure at the surface that translates into a higher driving force for mass transfer. For the processing conditions in Figure 4.5, no mass transfer took place at early processing stages ($t < 10$ minutes) and the calculated temperature responses for both investigated cases were identical.

4.2.4 Sensitivity of Computed Data to Transport Parameters

The simulation model contains many parameters in the form of thermophysical properties, processing and initial conditions. Approximate values for many of these parameters can be obtained from previous work (Chapter 2). However, the results of the models, e.g. the cooking time or process moisture loss, will depend to a varying degree on the several parameters. It is important to quantify the individual dependencies in order to identify the most important parameters. Subsequent experimental work could then focus on the parameters found to exhibit the strongest influence on the simulation results. A straightforward way of achieving this goal consists of obtain-
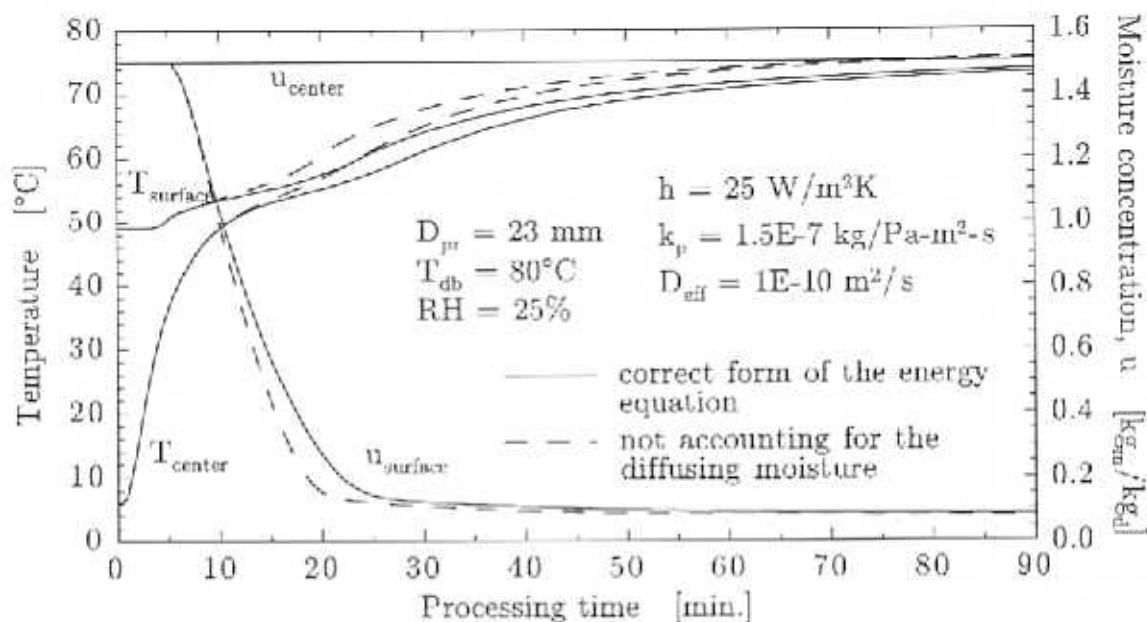
Figure 4.5: Calculated temperatures and concentrations at the product surface and center as a function of time for two forms of the energy equation. The solids lines are based on a form of the energy equation which contains a term accounting for the enthalpy of the diffusing moisture. Omitting this term results in the values plotted with the dashed lines.

ing simulation results for several values or functional forms of the input parameters. The relatively large number of input parameters makes it unfeasable to investigate all combinations of the investigated parameters. However, useful information can still be obtained when one parameter is varied at a time while all others are set to their base values. A summary of the results obtained from this procedure is given in Table 4.1. The first three columns list the investigated input parameter, its units and the chosen values or functional forms, respectively. The underlined entries are the base values, i.e. they are used in the calculations when one of the other input parameters is varied. Hence, the entries for the calculated simulation results (the last four columns) are identical for each underlined base input parameter but are nevertheless reported for clarity.

Mohl [1993] reported an influence of the form of the equilibrium relationship be-

Table 4.1: Sensitivity of computed simulation results to different values of selected transport and boundary condition parameters. The processing conditions and the product parameters that were not varied are given below.[1]

Input parameter	Units	Value or model[2]	Cooking time[3] [min]	Moisture loss[4] [%]	Surface temperature[4] [°C]	Surface concentration[4] [kg_m/kg_d]
EMC	kg_m/kg_d	Fig.4.6	47.5	8.59	69.7	0.10
		Fig.4.7	39.0	5.69	69.6	0.64
k	W/mK	0.3	62.5	10.1	69.6	0.10
		$k = k(u)$[‡]	47.5	8.59	69.7	0.10
		0.4	59.3	9.82	69.3	0.10
D_{eff}	m²/s	5×10^{-11}	32.6	5.01	70.4	0.10
		1×10^{-10}	47.5	8.59	69.7	0.10
		5×10^{-10}	165.1	35.2	70.0	0.10
h[†]	W/m²K	15	102.6	12.9	69.1	0.10
		20	65.5	10.2	69.4	0.10
		25	47.5	8.59	69.7	0.10
		30	37.2	7.56	70.1	0.10
		50	21.1	5.69	71.7	0.09
k_p[†]	kg/Pam²s	1×10^{-8}	59.4	7.96	69.2	0.16
		5×10^{-8}	49.7	8.53	69.7	0.11
		1.5×10^{-7}	47.5	8.59	69.7	0.10
		5×10^{-7}	46.6	8.62	69.7	0.10
		1×10^{-6}	46.5	8.62	69.7	0.10

[1] process conditions: $T_{db} = 80°C$, $RH = 0.25$, $T_o = 6°C$, $u_a = 1.5\ kg_m/kg_d$
product specification: $D_{pr} = 23$ mm, $\rho_d = 400\ kg/m^3$, $c_d = 1580$ J/kgK

[†] the heat and mass transfer coefficients are varied independently in this section even though they are related through the analogy of heat and mass transfer

[2] the underlined values are used when the other input parameters are varied

[‡] the model reported by Sweat [1975] (Table 2.2) was used: $k = 0.080 + 0.52\,u/(1 + u)$

[3] time when the center of product reaches a temperature of 68.3°C (155°F)

[4] values taken at cooking time

tween the moisture content of the meat emulsion and the relative humidity of the surrounding air (isotherm) on the simulation results when using boundary conditions similar to those introduced in Chapter 3. Two differently shaped isotherms (Figure 4.6 and Figure 4.7) were therefore investigated in this preliminary sensitivity analysis with respect to their effect on the simulation results. The nonlinear type isotherm, Figure 4.6, was obtained from a curve fit to the data reported by Igbeka

and Blaisdell [1982] over all four temperatures (Section 2.5). The linear type, Figure 4.7, was chosen to represent a simple model. In order to focus on the influence of the isotherm shape, all temperature dependencies were excluded from the isotherms used in this preliminary sensitivity analysis. The slope of the linear isotherm was adjusted so that the equilibrium moisture content at a relative humidity of 90% was identical with that for the nonlinear isotherm.

The influence of the isotherm shape on product temperatures and moisture concentrations can be seen in Figures 4.6 and 4.7. The cooking time for the reported isotherm is 22% longer than that of the generic linear isotherm. The reason is a higher relative humidity, and hence vapor pressure, at the interface of product and surroundings in the case of the nonlinear type. This causes a higher mass transfer potential which causes a bigger part of the supplied convected heat to be needed for the vaporization of the moisture at the interface. Consequently, less thermal energy is available to raise the temperature of the product, resulting in a longer cooking time.

An increase in the thermal conductivity k of the meat emulsion causes a decrease in the processing time because energy can be conducted faster to the center of the product. The second set of entries in Table 4.1 confirms this behavior. However, the influence of k is rather small. The lower moisture loss in the case of higher values for k is due to the reduced cooking time. The temperature gradient within the product is small for all investigated values of the thermal conductivity. The temperature difference between the surface and the center of the product was calculated to be 1.3°C for $k = 0.3$ W/m K and 1.0°C for $k = 0.4$ W/m K.

The magnitude of the effective diffusion coefficient D_{eff} has a large influence on the cooking time and moisture loss. However, it has to be noted that the investigated values for D_{eff} in Table 4.1 vary in an exponential fashion over one order of magnitude. A comparison of the relative influence of D_{eff} and other parameters, such as k, has
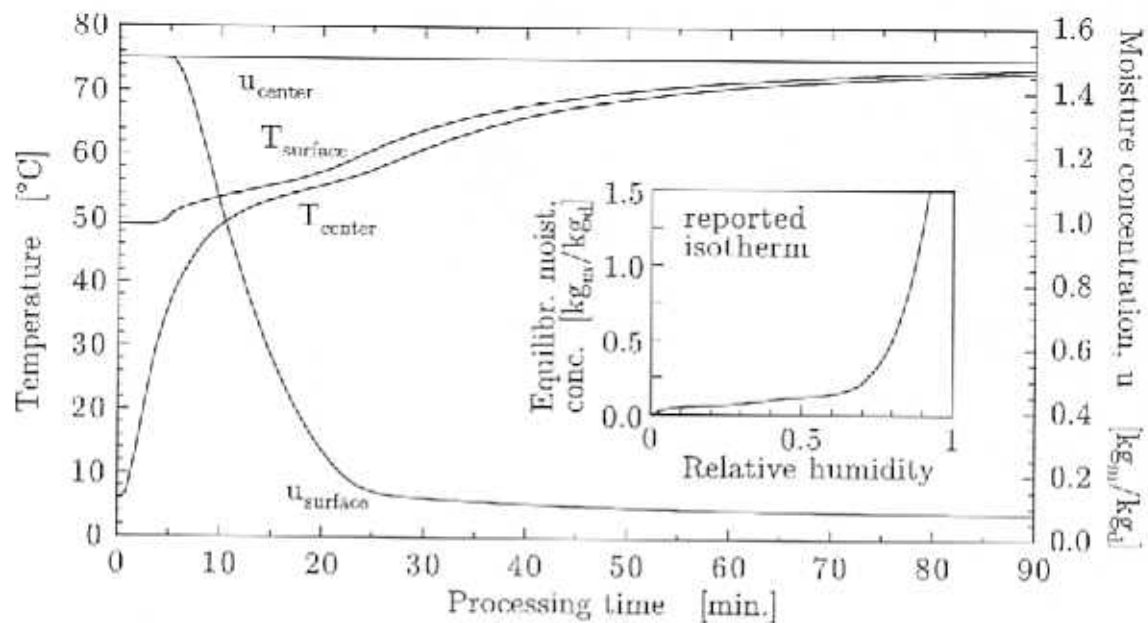
Figure 4.6: Computed temperatures and moisture concentrations for the processing conditions summarized in Table 4.1 and a nonlinear isotherm.
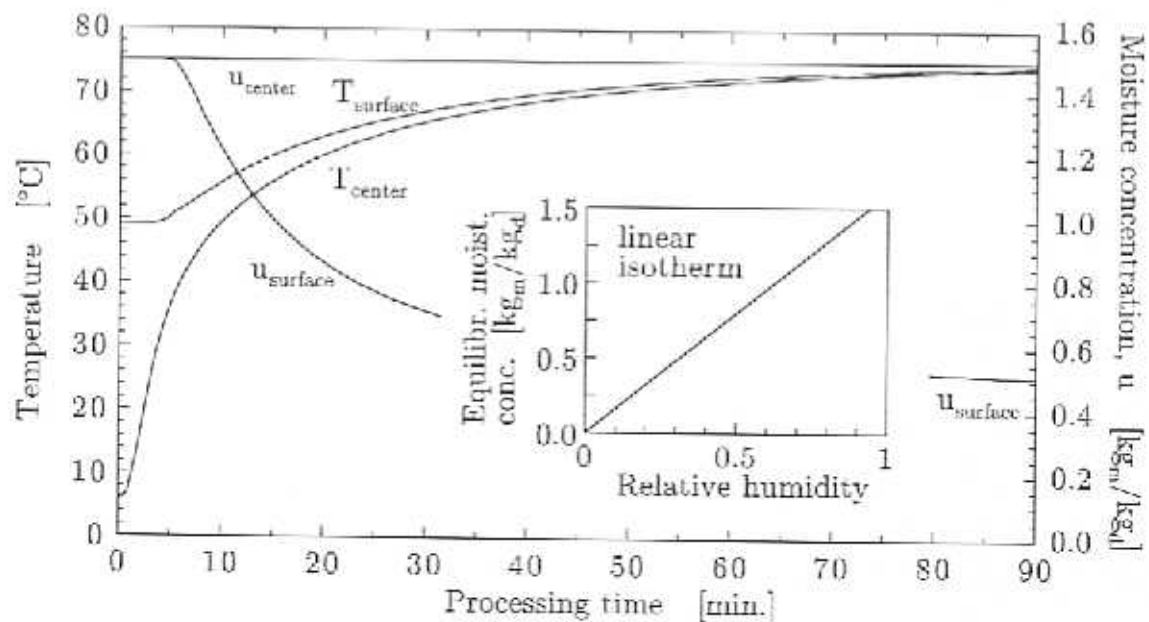
Figure 4.7: Computed temperatures and moisture concentrations for the processing conditions summarized in Table 4.1 and a linear isotherm.

to account for this fact. The larger range of investigated values for D_{eff} was chosen because of the wider range of values reported in the literature (Section 2.1). An increase in D_{eff} increases the cooking time and the moisture loss. The reason for the former effect is the greater amount of moisture diffusing from the inner product to the surface, where a larger amount of the supplied heat is needed for its vaporization.

The influence of the heat transfer coefficient h is listed in the fourth entry section of Table 4.1. The increase of h causes a decrease in the cooking time and moisture loss. A 2.5 fold increase of h from 20 to 50 W/m^2 K results in a 68% reduction of the cooking time.

The mass transfer coefficient k_p is varied in an exponential fashion. There is very little influence of k_p on the cooking time and moisture loss above a critical value of $k_p = 1.5 \times 10^{-7}$. The reason is the limiting behavior of the moisture diffusion coefficient D_{eff} in this regime. Since D_{eff} is rather small, the mass transport can be said to be diffusion limited, resulting in large moisture concentration gradients within the product. The overall decrease in the computed cooking time with an increase in k_p is caused by a rapid loss of moisture at the product surface. After this surface moisture is lost, all supplied convective heat can be used to raise the product temperature. With increasing mass transfer coefficients, the surface moisture is lost at earlier times and the overall cooking time decreases. However, at early processing times when the moisture level near the product surface is still close to its initial value, higher mass transfer coefficients cause the product temperatures to be lower because larger fractions of the supplied convected heat are used to evaporate the moisture at the surface.

Chapter 5

Experimental Investigation

The measurements of temperature and moisture concentration profiles, convective heat and mass transfer coefficients, process moisture losses and selected transport parameters are discussed in this chapter. First, the laboratory apparatus used in some of these experiments is described. Next, a detailed account of the individual measurements is given. The last section of this chapter summarizes the attempts made to utilize Nuclear Magnetic Resonance (NMR) methods to obtain moisture concentration profiles and effective moisture diffusion coefficients.

Most results are reported in graphical form, for example product surface and center temperatures during processing. The original data used to generate the plots can be downloaded. Details about this procedure are given in Appendix C.

5.1   Apparatus for Processing of Meat Emulsion Products

A laboratory apparatus was built to provide a means of processing small and medium diameter cylindrical meat emulsion products by generating an air flow of controlled temperature, humidity and velocity. A schematic of the apparatus is shown in Figure 5.1. Different relative humidities of the processing air in the test section were obtained by saturating an air stream at temperatures below the desired processing
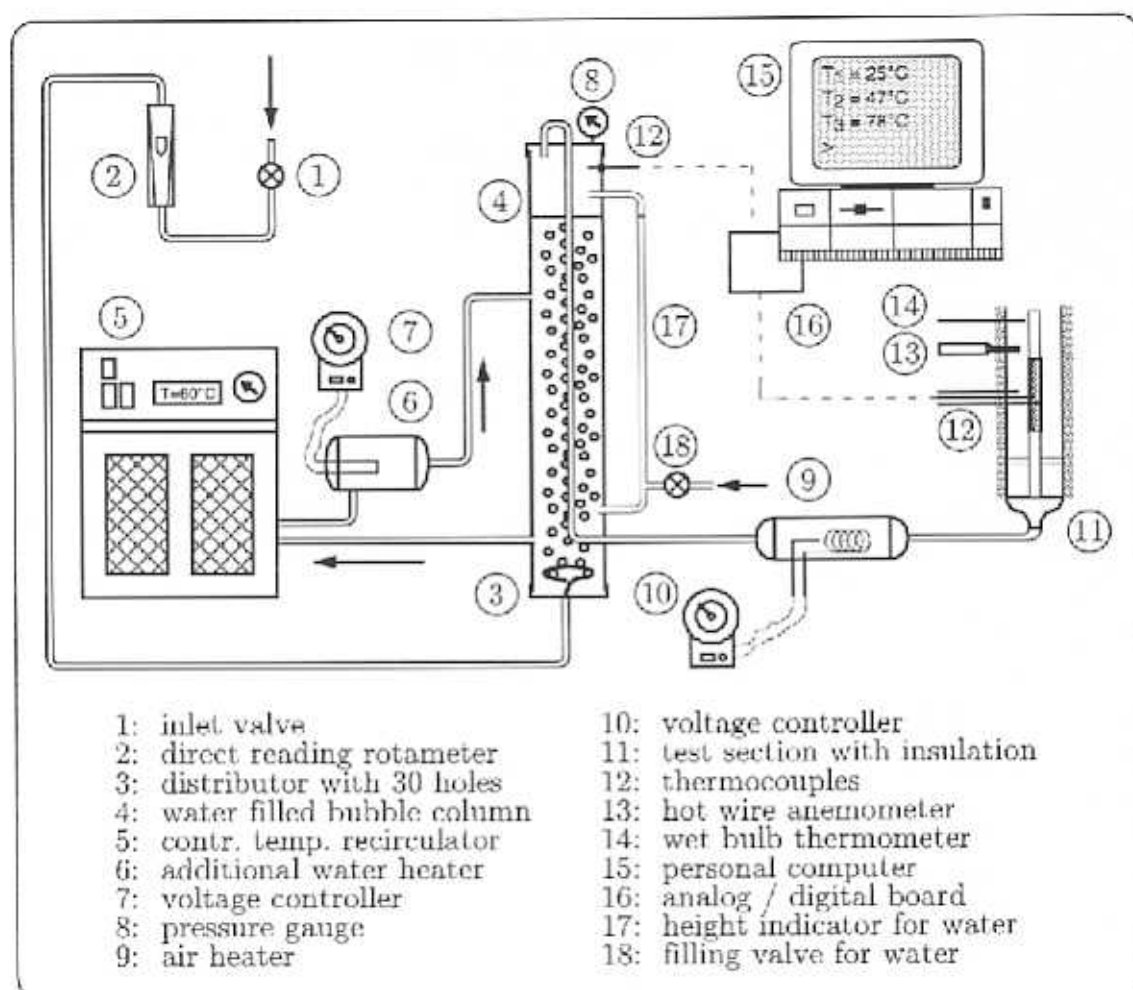
Figure 5.1: Laboratory apparatus for processing of emulsion products. Different humidities in the test section are obtained by saturating an air stream at temperatures below the desired processing dry bulb temperature.

dry bulb temperature followed by a sensible heat input. This design avoided the need for steam injection to generate the moist processing air and enabled the apparatus to be used at different locations.

Compressed air from the University of Wisconsin-Madison Physical Plant (supplied at a nominal pressure of 621 kPa (90 psig) and a relative humidity smaller than 2.0%) was metered with a direct reading rotameter (Cole-Parmer, G-03248-95, maximum flow of 9 l/s (20 scfm)) and introduced through a distributor into a bubble

column filled with water. The distributor was made from 3/8 inch O.D. copper tube bent into a ring of 3 inch diameter. Thirty holes of 1.5 mm diameter, evenly distributed around the circumference, were drilled through the top portion of the ring. The main body of the bubble column was made from a polyvinylchloride tube and measured 10.16 cm (4 inch) in diameter and 183 cm (6 feet) in height. A pressure gauge was located at the upper end cap of the column. The water in the column was heated, recirculated and temperature controlled with a cooling/heating recirculator (Cole-Parmer, G-01283-80), featuring a temperature range of 0 to 80°C (32 to 176°F), proportional temperature control and a heating capacity of 1500 Watts. Additional heating capacity was provided by a custom-made secondary water heater in series with the recirculator consisting of a 1500 Watt water heater element (ACE Hardware, No. 44969) placed inside a short section of a polyvinylchloride tube of 10.16 cm (4 inch) diameter. The heating element of this water heater was connected to a variable voltage controller (Cole-Parmer, G-01575-10).

The air at the top of the bubble column was directed into a 1.27 cm (0.5 inch) O.D. Tygon hose. This hose was then introduced back into the column and exited at the lower end through a compression fitting. This design was chosen to minimize condensation of the humidified air inside the flow system. After exiting from the column, the air was sensibly heated with an air heater consisting of an industrial grade heat gun heating element (Cole-Parmer, G-03026-02) placed inside a steel tube. The heating element was connected with high temperature wires to a variable voltage controller (Cole-Parmer, G-01575-10). The heated moist air was then directed to the test section (Figure 5.2).

The test section was made from a 50 cm (20 inch) long piece of acrylic tube of 5.08 cm (2 inch) internal and 6.35 cm (2.5 inch) external diameter. The meat emulsion products were inserted from the top. A steel tube at the bottom of the test section
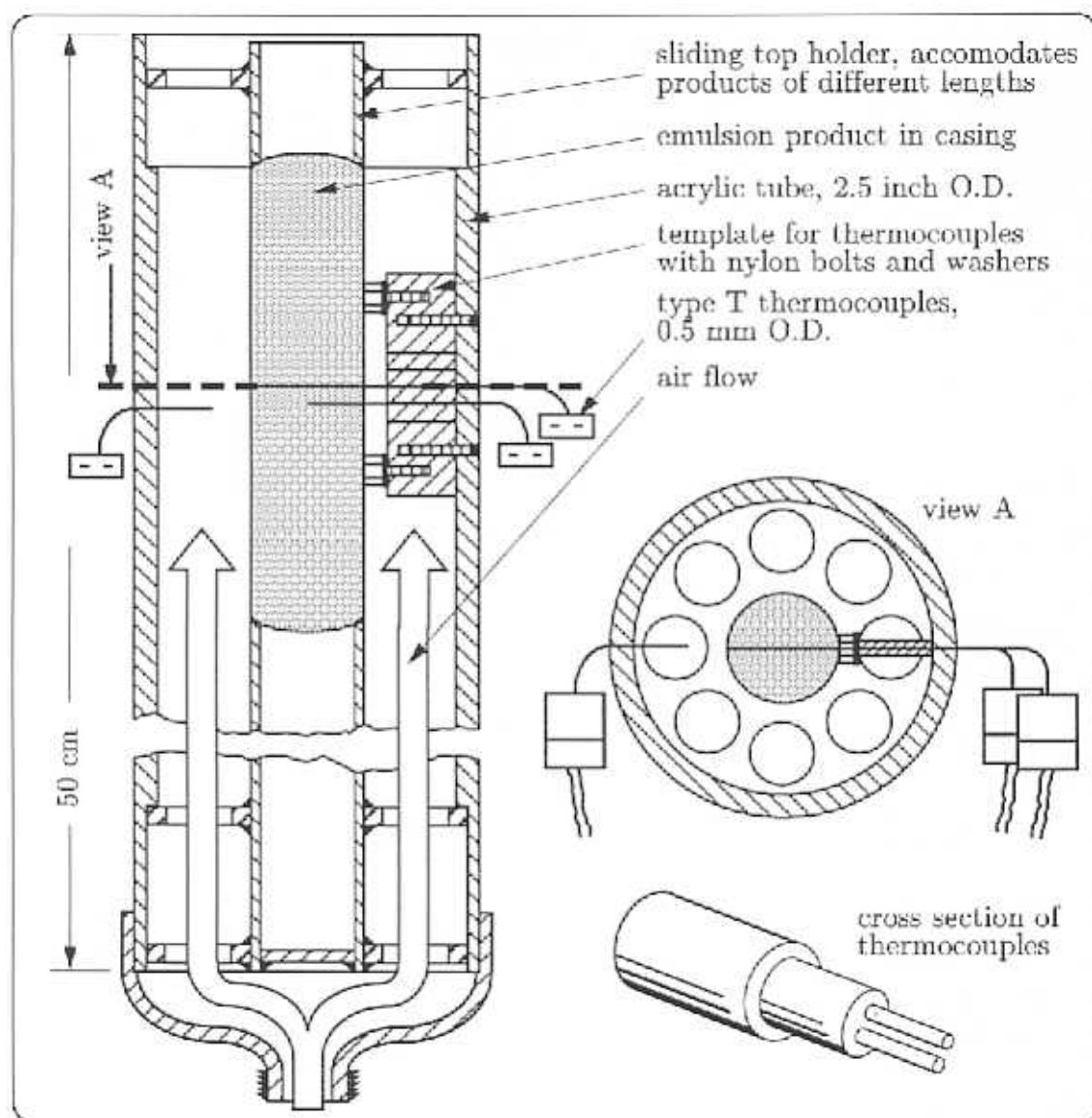
Figure 5.2: Test section of the laboratory apparatus. An air stream of controlled
temperature, humidity and velocity processes the meat emulsion product
in the center.

with a diameter similar to that of an emulsion product centered the product in the
acrylic tube and established uniform flow conditions along the emulsion product. The
processing air moved upwards through the annulus formed by the inner surface of the
acrylic tube and the steel tube and the emulsion product, respectively. A sliding top
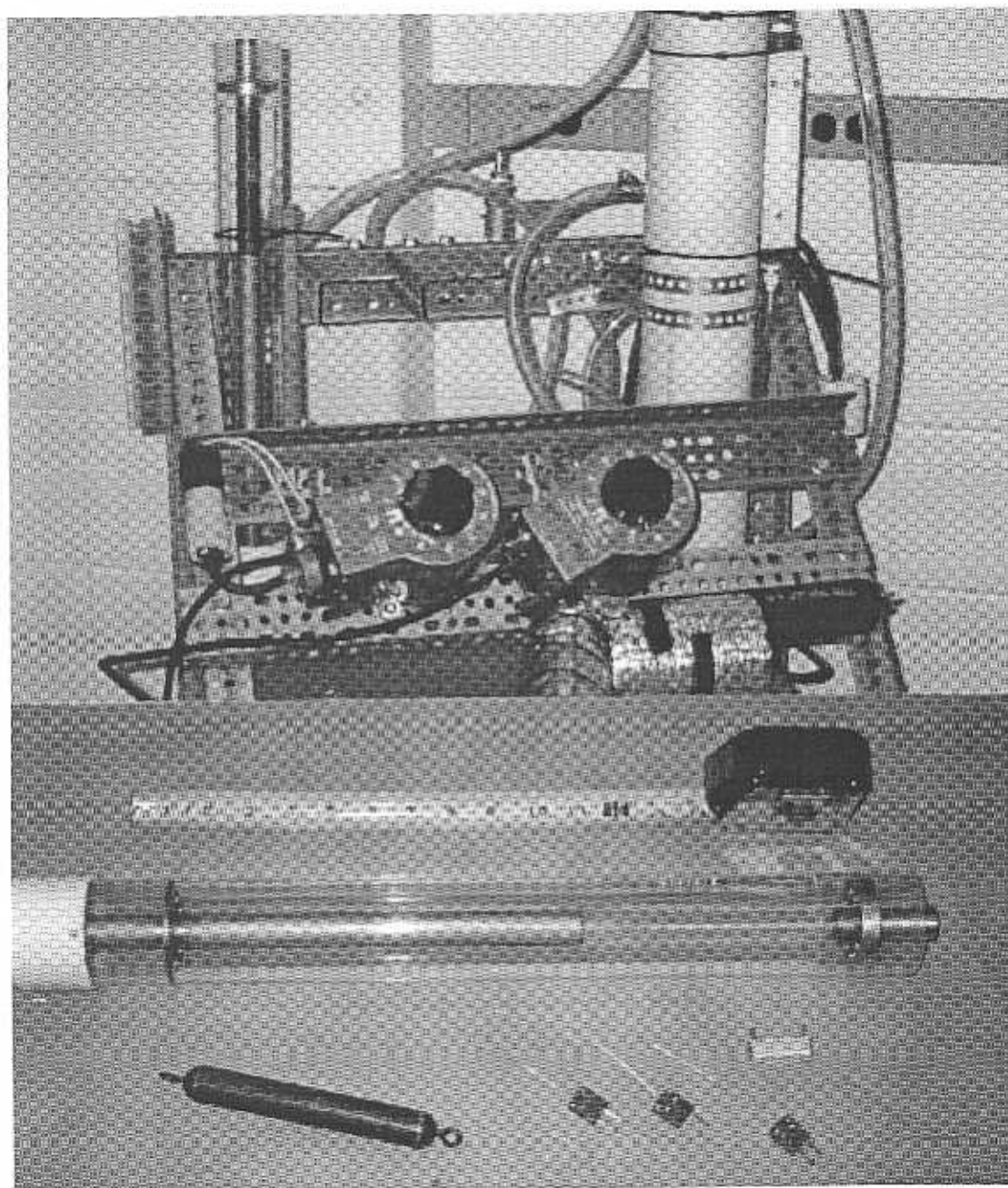
Figure 5.3: Photographs of the laboratory apparatus and some related equipment. The top picture shows a partial front view of the apparatus. The test section, the two voltage controllers and the bubble column can be seen. The photograph at the bottom shows the test section, a solid aluminum probe used for measurements of the heat transfer coefficient and three thermocouples.
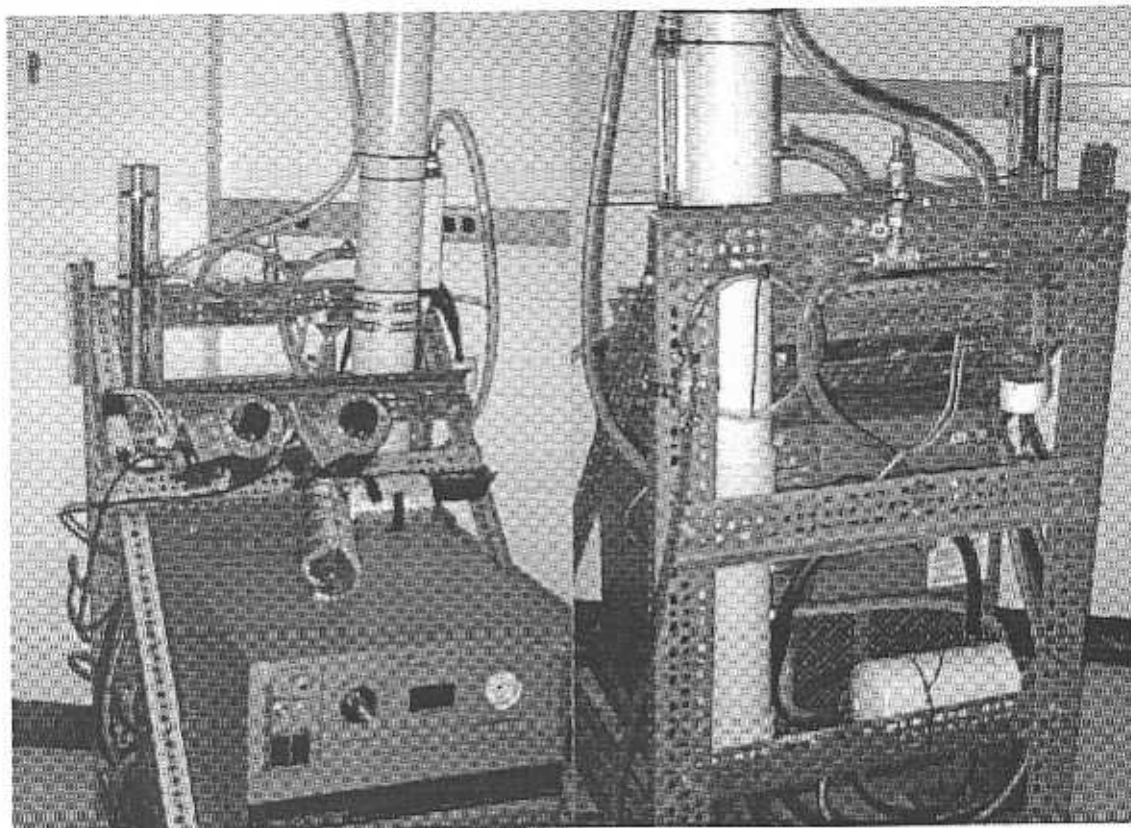
Figure 5.4: Photographs of the laboratory apparatus. The controlled temperature recirculator can be seen in the front of the left picture. The right photograph shows a rear view of the apparatus. The additional water heater is located to the right of the bubble column. The air heater is hidden behind the middle slotted iron.

holder was used to fix the position of the product within the acrylic tube and to accommodate products of different lengths.

Measurements of the temperature response of the emulsion products, of the dry bulb temperature in the test section and of the temperature in the bubble column were performed with preassembled subminiature type T (copper/constantan) thermocouple probes of 0.508 mm (0.02 inch) diameter (Omega, TMQSS-020G-6). The thermocouples used to monitor the temperature response of the emulsion products were inserted through the acrylic tube and a removable template into the product.

The template assured a reproducible position of the thermocouples and prevented their bending when some initial force was necessary to overcome the mechanical resistance of the casing upon inserting the thermocouple into the product. Two small nylon bolts maintained a small distance between the product and the template to minimize the contact area for conduction of heat into the product. Thin nylon washers between the bolts and the template were used to adjust the position of the emulsion product.

The thermocouple used for the measurement of the dry bulb temperature in the test section was inserted through the acrylic tube at a location opposite to those used for the temperature response of the product. The thermocouple at the top portion of the bubble column was inserted into the polyvinylchloride tube through a small hole drilled into a threaded end plug. Since the air in the bubble column was saturated at the temperature of the water inside the column, its dry bulb, wet bulb and dew point temperatures at that location were identical. The mass of water needed for complete saturation of the compressed air bubbling through the column was calculated from psychrometric relations. The height indicator on the column (Figure 5.1) was used to monitor the rate of moisture loss during operation. The observed value agreed with the rate needed for complete saturation. The air temperature measured at the top of the bubble column was identical with the value displayed on the recirculator for the temperature of the recirculated water, indicating that the heat loss through the bubble column was negligible. The analog voltage signals of the thermocouples were logged to a personal computer via an analog to digital (A/D) converter board (Omega, High Resolution Interface Card, Model WB-AAI) featuring sixteen channels with sixteen bit conversion resolution.

The precision of the thermocouples used in this research was investigated by recording their temperatures when subjected to the same environment. For this
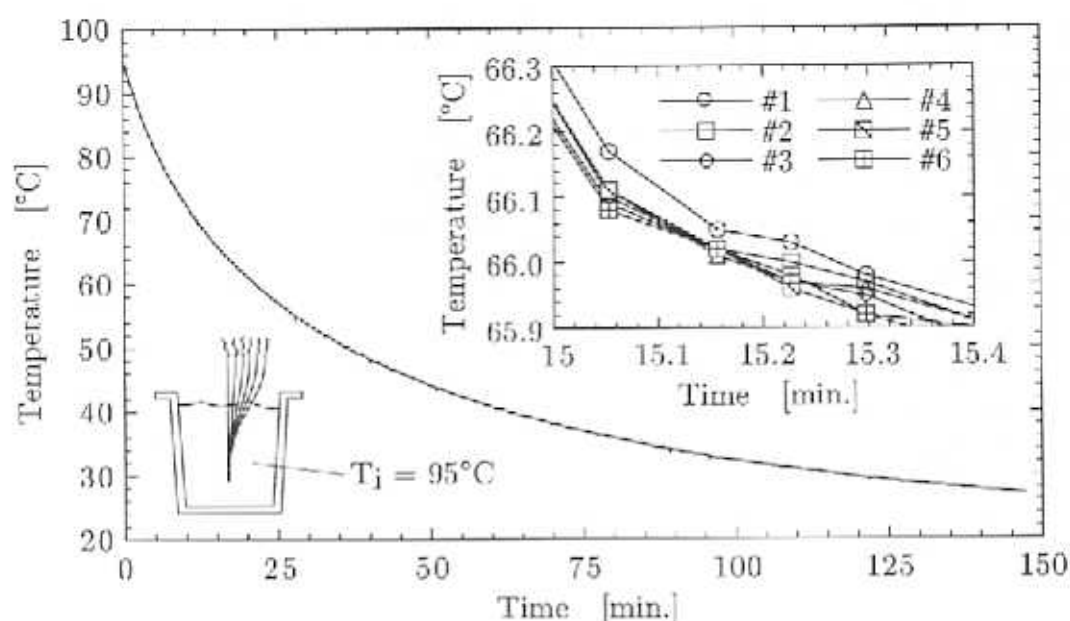
Figure 5.5: Precision of the thermocouples used in this study. The large plot shows the temperature response of all six thermocouples. An enlarged temperature scale is provided in the form of the small plot. The sketch in the lower left corner shows the arrangement of the thermocouple tips in the water filled cup.

purpose, the thermocouples were suspended in an insulated cup filled with hot water that was then allowed to cool. First measurements were affected by the temperature stratification inside the cup. Subsequently, this effect was avoided by using an adhesive tape to fix the position of the thermocouple tips. The measured data are shown in Figure 5.5. Over the whole temperature range, the variations measured with the individual six thermocouples are very small. The smaller plot inside of Figure 5.5 shows an enlarged temperature scale during 24 seconds of the experiment. The maximum deviation between the recorded temperatures is smaller than $0.1°C$ ($0.18°F$). The accuracy of the thermocouples was determined by a baseline calibration in an ice bath. Purified water and ice were used for this experiment and a temperature of $-0.45°C$ ($31.2°F$) was measured. All data subsequently recorded with the thermocouples were corrected for this offset. Similar to the precision at the higher temperatures, the devi-

ations between the data measured with the six thermocouples at this low temperature were smaller than 0.1°C (0.18°F).

The relative humidity, wet bulb and dew point temperatures in the test section were calculated from the measured air temperature in the bubble column, the measured dry bulb temperature in the test section, the measured pressure difference between the air in the bubble column and the test section and the absolute pressure. It should be noted that the pressure loss of the air stream between bubble column and test section had a rather large influence on the wet bulb and dew point temperatures and the relative humidity in the test section. For example, at a pressure loss of 28 kPa (4 psi) and an air temperature in the bubble column of 50°C (122°F), the dew point and wet bulb temperatures and the relative humidity in the test section at a dry bulb temperature of 78°C (172°F) are $T_{dp} = 45.2°C$ (113°F), $T_{wb} = 48.6°C$ (119°F) and $RH = 22.2\%$. Neglecting the pressure loss between bubble column and test section results in calculated values in the test section of $T_{dp} = 50.0°C$ (122°F), $T_{wb} = 52.4°C$ (126°F) and $RH = 28.3\%$, showing that air at lower pressures can accommodate more moisture. These psychrometric calculations were performed with the computer program EES (Engineering Equation Solver, Klein [1990]). The results of these calculations were verified with a wet bulb thermometer inserted into the test section from the top opening. The measured wet bulb temperature agreed with the calculated values for the 28 kPa (4 psi) pressure loss within the reading accuracy of the wet bulb thermometer ($\pm$0.5°C (0.9°F)).

The air velocity in the test section was measured with a hot wire anemometer. The measured values agreed well with the velocities calculated from the volumetric flowrate through the rotameter and the free area for air flow in the test section when corrected for the different temperatures and pressures in the rotameter and test section, respectively. The convective heat transfer coefficient for a product in the test

section was determined from the thermal response of an aluminum probe resembling a real product. Details and results are given in Section 5.4.

5.2 Temperature Profiles

The temperature response of meat emulsion products subjected to a step change in the processing conditions in the test section of the laboratory apparatus was measured with thin thermocouples (Omega, TMQSS-020G-6) located at the product surface (under the casing) and at the geometric center. The details of the used equipment were described in Section 5.1 and were shown in Figure 5.2. Two sets of experiments were performed. The first set consisted of full-fat and no-fat meat emulsions stuffed into identical moisture-permeable cellulose casings of 23 mm (0.91 inch) diameter. In the second set of experiments, a full fat emulsion was stuffed into two different casings, a fibrous moisture-permeable casing of 45 mm (1.77 inch) diameter and a moisture-impermeable polyamide casing of 43 mm (1.69 inch) diameter. These two types of casings were not available in the same diameter. However, the small difference was not considered to be significant. Both sets of experiments were conducted at three different relative humidities. A summary of the experimental conditions is shown in Table 5.1. The flowrates through the laboratory apparatus for the temperature profile experiments were 2.2 l/s (5 scfm) for the small products (D_{pr} = 23 mm) and 1.1 l/s (2.5 scfm) for the larger samples (43 and 45 mm). Pressure losses of 41.1 kPa (6 psi) and 27.6 kPa (4 psi) between the bubble column and the test section were measured for these two flowrates. The corresponding calculated air velocities in the test section were v_{air} = 2.5 m/s, v_{air} = 3.5 m/s and v_{air} = 4.6 m/s for the product diameters of 23 mm, 43 mm and 45 mm, respectively.

The samples used in the experiments were stored in sealed plastic bags in a refrigerator. At the beginning of an experiment, the flowrate through the apparatus was

Table 5.1: Summary of the processing conditions and measured moisture losses of all temperature profile experiments. The last column indicates the figures where the corresponding data are shown.

D [mm]	Casing[1]/ Emuls.[2]	Run/ Reps.	T_{db} [°C]	T_{wb} [°C]	T_{dp} [°C]	RH [%]	m_i [g]	m_f[3] [g]	Δm[3] [%]	Figure(s)/ on page(s)
23	cell./FF	1/1	78.0	34.5	22.3	6.1	73.5	62.1	15.5	5.6/87
23	cell./NF	1/1	78.0	34.5	22.3	6.1	67.6	50.3	25.6	5.6/87
23	cell./FF	1/3	78.0	43.7	38.5	15.6	74.0	61.5	16.9	5.7,5.9/87,88
23	cell./FF	2/3	78.0	43.7	38.5	15.6	71.5	54.8	$-$[4]	5.9/88
23	cell./FF	3/3	78.0	43.7	38.5	15.6	72.2	63.5	12.0	5.9/88
23	cell./NF	1/1	78.0	43.7	38.5	15.6	67.7	50.0	26.1	5.7/87
23	cell./FF	1/1	78.0	54.7	52.8	32.4	72.2	61.8	14.4	5.8/88
23	cell./NF	1/1	78.0	54.7	52.8	32.4	68.0	51.2	24.7	5.8/88
45	fibr./FF	1/1	77.0	35.1	23.9	7.1	276.0	261.1	5.4	5.10/90
43	imp./FF	1/1	77.0	35.1	23.9	7.1	241.5	240.1	0.6	5.10/90
45	fibr./FF	1/1	77.0	44.9	40.4	18.0	258.4	244.4	5.4	5.11/90
43	imp./FF	1/2	77.0	44.9	40.4	18.0	244.6	241.0	1.5	5.11,5.13/90,91
43	imp./FF	2/2	77.0	44.9	40.4	18.0	245.4	242.0	1.4	5.13/91
45	fibr./FF	1/1	77.0	56.4	54.9	37.4	271.6	257.6	5.2	5.12/91
43	imp./FF	1/1	77.0	56.4	54.9	37.4	240.4	239.0	0.6	5.12/91

[1] cell.: moisture-permeable cellulose casing, fibr.: moisture-permeable fibrous casing; imp.: moisture-impermeable polyamide casing
[2] FF: full-fat emulsion, NF: no-fat emulsion
[3] after a processing time of 90 minutes
[4] weight loss after 240 minutes: 23.4%

set to the desired value and the temperature of the water in the bubble column was adjusted with the dials on the controlled temperature recirculator and the voltage controller connected to the additional water heater. The desired air dry bulb temperature in the test section was then obtained by adjusting the dial of the voltage controller connected to the air heater. After the temperatures reached their steady values ($\approx$ 15 minutes), the samples were taken from the refrigerator, weighed, and placed into the test section. The data logging with a sampling interval of 5 seconds began at this time. The two thermocouples used to monitor the temperature response of the product were inserted after approximately 8 minutes. Uncontrolled rupturing of the casings occurred when the thermocouples were inserted at the very beginning

of the experiments.

Two thermocouples were used to monitor the temperature response of the product. One thermocouple was inserted to the center of the product, the other one was inserted to the surface opposite of the point of insertion (Figure 5.2) to a position directly under the casing. The metal tip of this thermocouple could be seen from the outside shining through the thin casing. Because of the stronger texture of the larger diameter casings (43 and 45 mm), it was necessary to pre-pierce the hole for the thermocouples with a steel needle through the template for the thermocouples.

After inserting the thermocouples into the product, the top portion of insulation around the acrylic tube of the test section was mounted. When measuring the thermal response of small diameter products ($D_{pr} = 23$ mm), the dry bulb temperature in the test section was measured with a separate thermocouple as indicated in Figure 5.2. Because of the little remaining space between the inner wall of the acrylic tube and the larger products (43 and 45 mm), the correct setting of the dry bulb temperature of the processing air in the test section was monitored for these cases with a hand held thermocouple, inserted periodically during the experiments from the top opening of the test section.

After the experiment was completed, the two thermocouples were removed and the product was taken from the test section and weighed. A razor blade was then used to cut the product at the location of the thermocouples to verify their correct position. If necessary, the water level in the bubble column was adjusted for the next experiment. The decrease of the mass of water inside the column during one experiment was small compared to its total mass. Results for the small diameter products ($D_{pr} = 23$ mm) are shown in Figures 5.6 to 5.9.

Experiments were conducted for both emulsion types at three different relative humidities, 6.1%, 15.6% and 32.4%. The thermal response of the two emulsion types

Figure 5.6: Air dry bulb, product surface and product center temperatures for a full-fat and a fat-free emulsion in a cellulose casing at humidities of 6.1%.

Figure 5.7: Air dry bulb, product surface and product center temperatures for a full-fat and a fat-free emulsion in a cellulose casing at humidities of 15.6%.
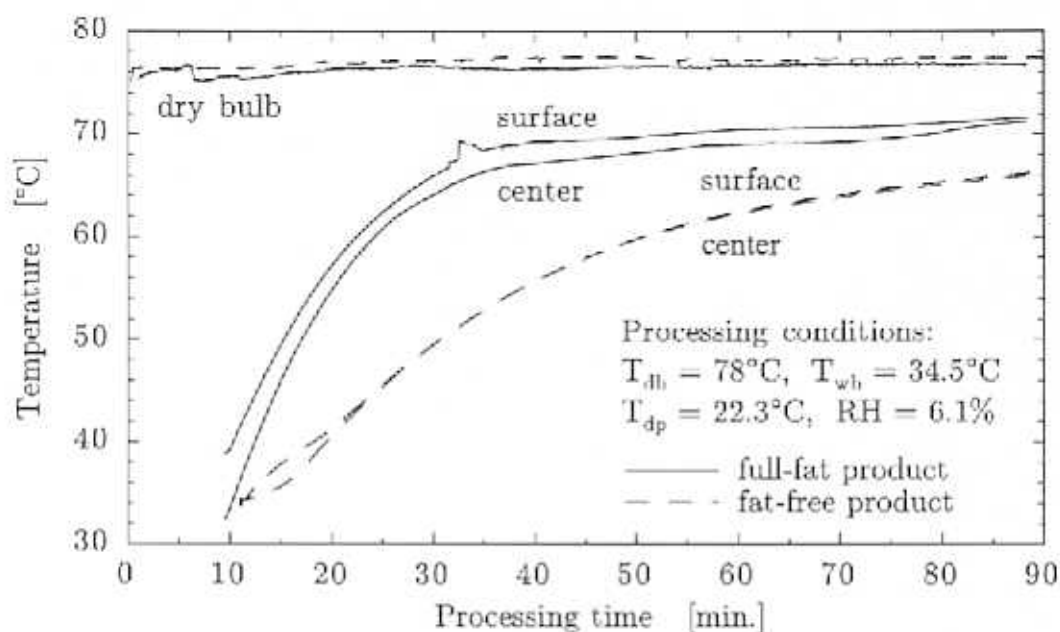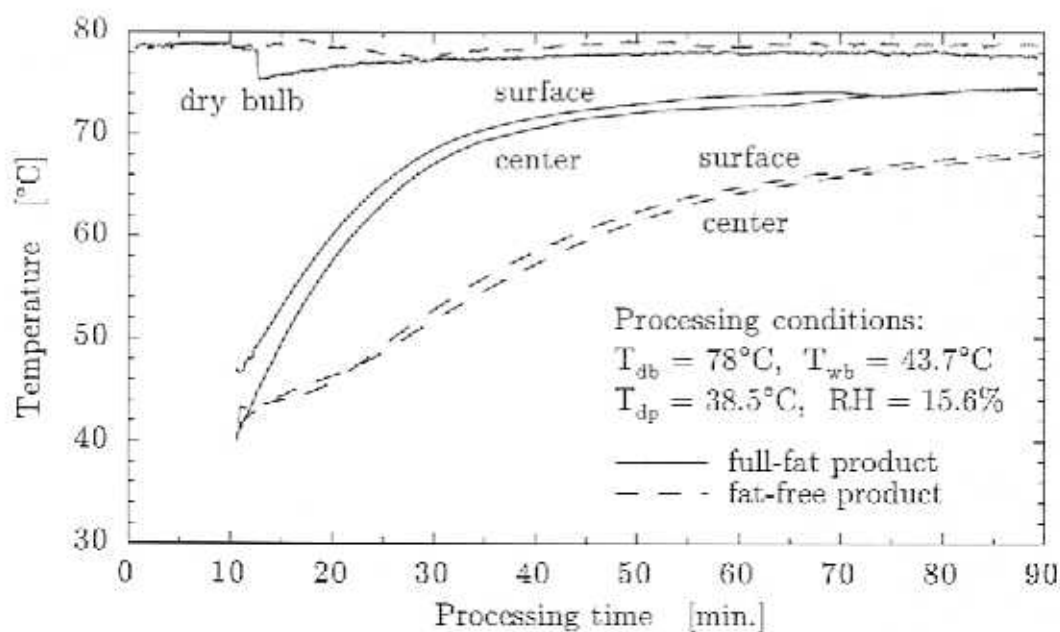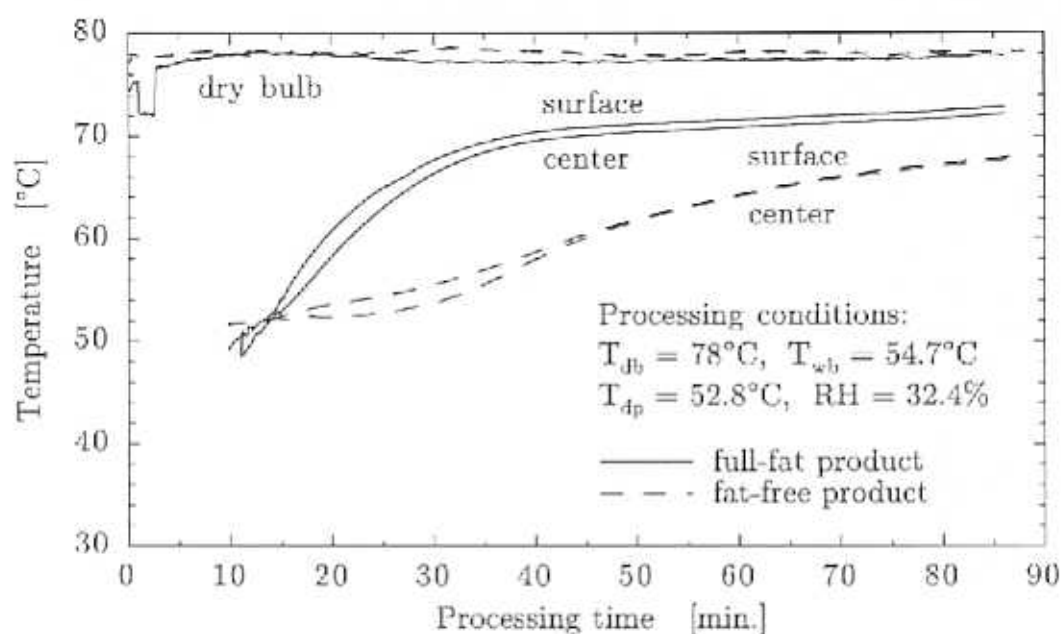
Figure 5.8: Air dry bulb, product surface and product center temperatures for a full-fat and a fat-free emulsion in a cellulose casing at humidities of 32.4%.
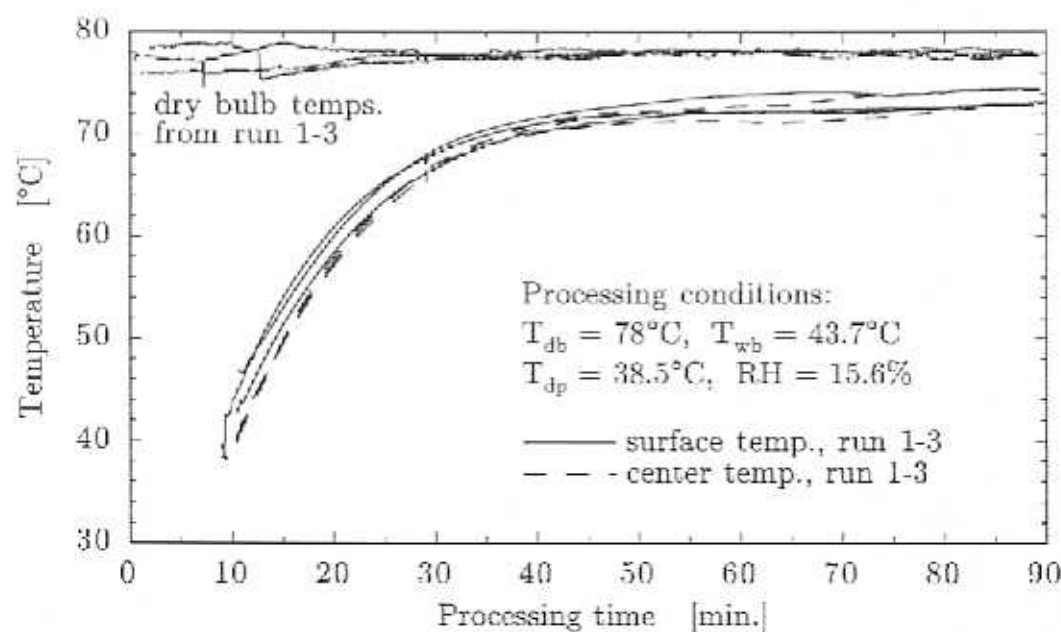
Figure 5.9: Comparison of product surface and product center temperatures of a full-fat emulsion from three successive experiments at humidities of 15.6%.

was significantly different for all three processing conditions. The surface and center temperatures of the no-fat samples showed a slower response to the dry bulb temperature of the processing air. This behavior was attributed to a higher moisture diffusivity of the no-fat emulsion, resulting in a higher moisture flux from the inner part of the product to the surface. A larger part of the supplied convective heat was then needed to evaporate the moisture at the surface, leaving less energy to raise the temperature of the product. The temperature response of the full-fat product was similar for all three relative humidities. In contrast, the temperature of the no-fat emulsion showed an increasing tendency to remain at the wet bulb temperature of the processing air as its relative humidity increased. The temperature gradient within a product was small for all investigated cases. However, a small correction for heat conducted along the length of the thermocouple has to be applied to the measured data. Because of this effect, the measured temperatures are slightly higher than the actual temperatures, affecting the thermocouple in the center of the product more than the one at the surface. Since the exact magnitude of the necessary correction could not be determined, the original measured data is reported. Details of this effect are given later. Three experiments at the intermediate relative humidity level were conducted for the full-fat emulsion in order to test the reproducibility of the experimental technique. Results are shown in Figure 5.9. A maximum difference of approximately 3°C (5.4°F) between the surface and center temperatures of the individual runs was observed. The bump in the measured surface temperature during processing at 6.1% (Figure 5.6) at a processing time of approximately 33 minutes was caused by a temporary dislocation of the corresponding thermocouple.

The measured thermal responses for the two larger casing types (43 and 45 mm) stuffed with a full-fat emulsion are shown in Figures 5.10 to 5.13. These experiments were conducted at approximately the same three levels of the relative humidity as

Figure 5.10: Product surface and center temperatures for a full-fat emulsion in standard fibrous and evaporation-resistant casings at humidities of 7.1%.
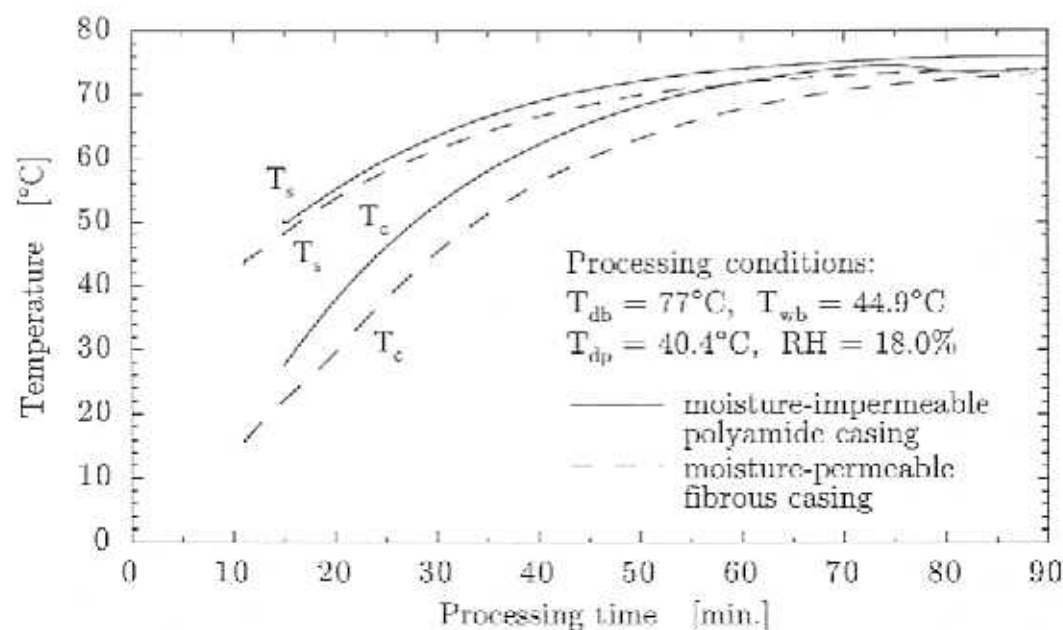
Figure 5.11: Product surface and center temperatures for a full-fat emulsion in standard fibrous and evaporation-resistant casings at humidities of 18.0%.
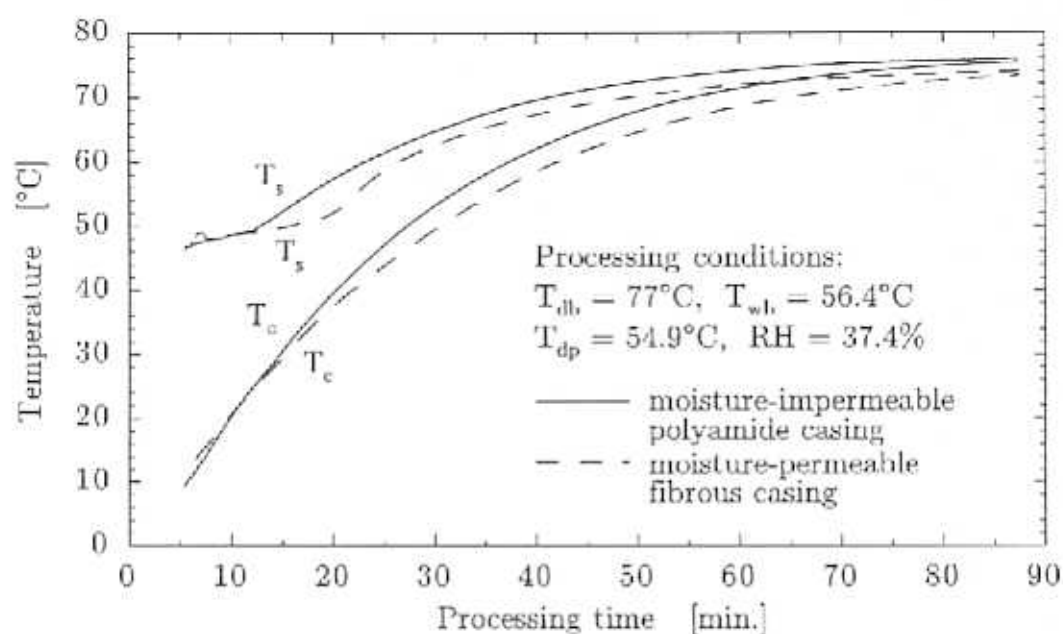
Figure 5.12: Product surface and center temperatures for a full-fat emulsion in standard fibrous and evaporation-resistant casings at humidities of 37.4%.
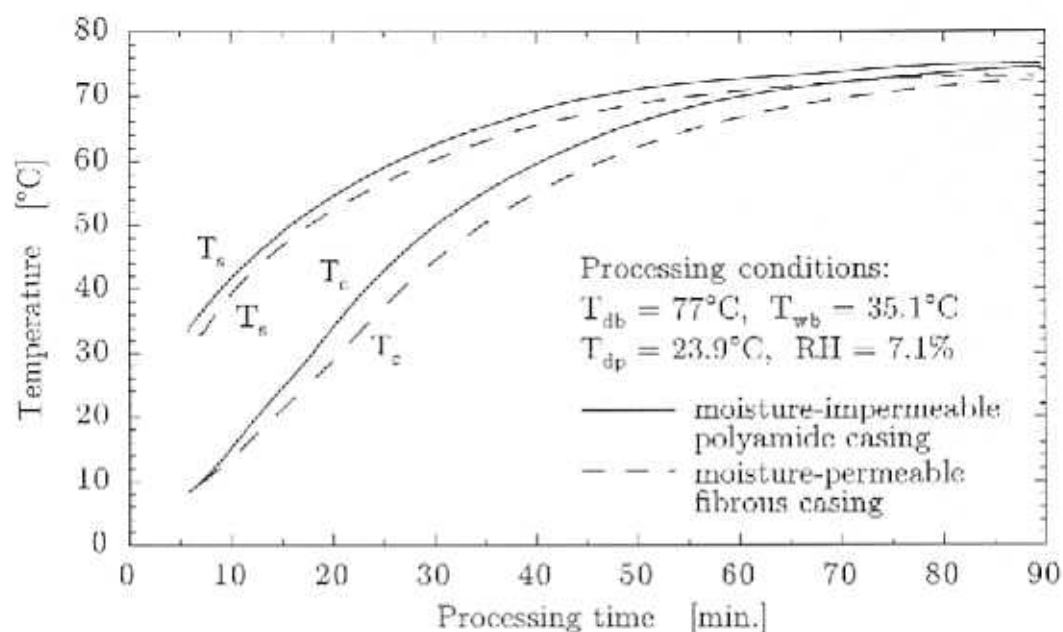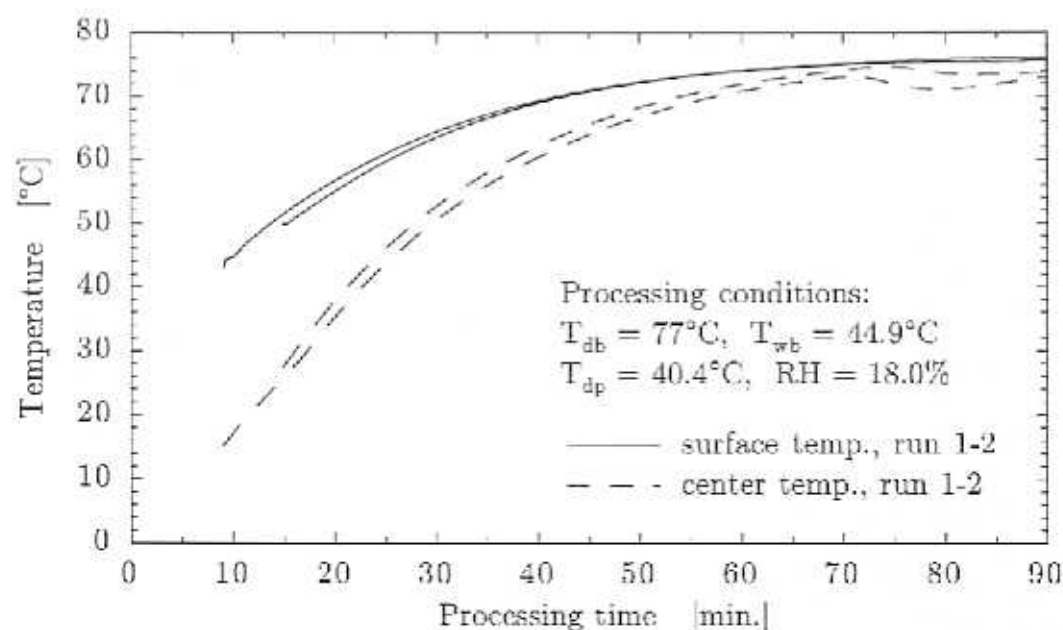

Figure 5.13: Comparison of product surface and center temperatures of a full-fat emulsion in impermeable casing from two successive experiments.

those used for the smaller casings. The products in the moisture-permeable fibrous casings showed a slower response to the dry bulb temperature of the processing air than the products in the moisture-impermeable casings. This behavior is due to the energy needed to evaporate the moisture on the surface of the permeable casings. The magnitude of the temperature gradients within the products at the beginning of the processing was approximately 20°C (36°F) and therefore much larger than the gradients encountered in the products stuffed in the smaller casing type. To test the reproducibility of the experimental technique, two experiments were conducted for the product in the impermeable casing at the intermediate relative humidity level. A maximum difference between the surface and center temperatures of the individual runs of approximately 3°C was measured. The decrease in the measured center temperature towards the end of the experiment (72 to 90 minutes) was attributed to some moisture leaking at those times from the insertion points of the thermocouples. The presence of this liquid on the product surface caused evaporative cooling that effected the center temperature but not the temperature at the opposite surface. The leaking moisture could be seen through the acrylic tube of the test section. No moisture leaked from the thermocouple insertion points in the fibrous casing or the impermeable casing at the low and high humidity levels.

As stated earlier, a small correction had to be applied to the temperatures measured with the thermocouples. Some regions of the stainless steel sheaths are exposed to the hot processing air. The thermal energy gained by the thermocouple (the expression *thermocouple* refers to the whole assembly of stainless steel sheath, the insulating magnesium oxide powder and the copper and constantan wires with the coupling at the tip of the sheath) at this location is then conducted along its length to colder regions, including the tip with the coupling of the copper and the constantan wires, the location where the temperature is measured. Consequently, the temperature mea-
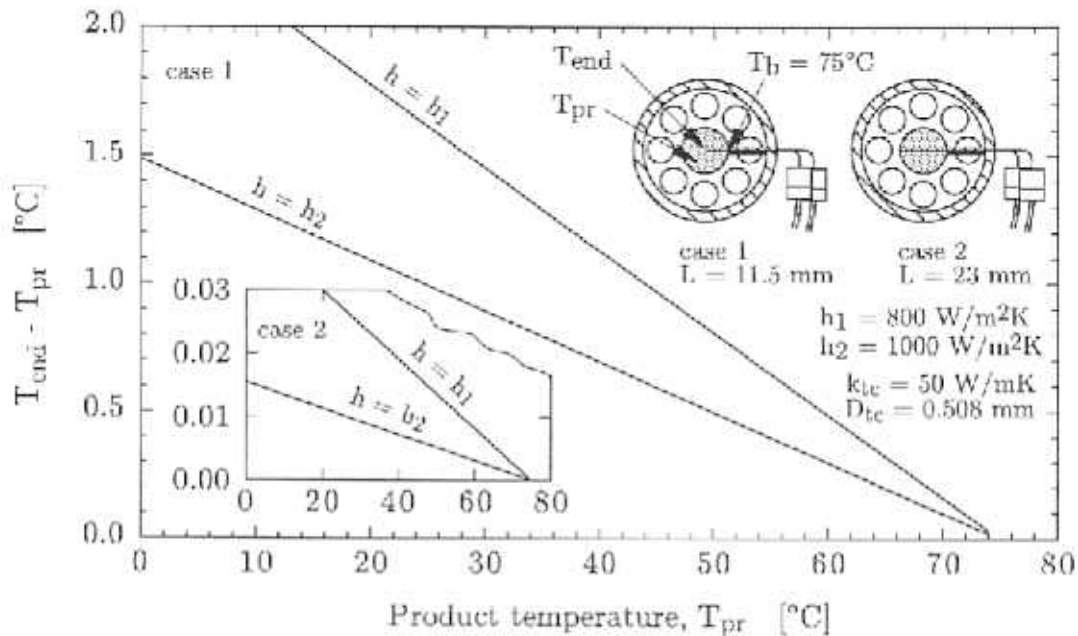
Figure 5.14: Measurement error of thermocouples due to conduction of heat along the length as a function of the surrounding product temperature for two different lengths and heat transfer coefficients.

sured at the tip of the thermocouple is higher than the true temperature, i.e. the temperature at that point if no thermocouple were present. In order to estimate the error associated with this effect with a mathematical analysis, the thermocouples can be viewed as needle fins. The temperature T of the fin at any location x, measured from the base can be obtained from an energy balance resulting in the differential equation

$$\frac{d^2T}{dx^2} - \frac{hP}{kA_c}(T - T_\infty) = 0 \tag{5.1}$$

where h is the heat transfer coefficient between the fin (the thermocouple) and the surrounding meat emulsion, P its perimeter, k its thermal conductivity, A_c its cross section and T_∞ the temperature of the surrounding emulsion.

Analytical solutions to Equation (5.1) can be obtained when T_∞ is considered to be constant (Incropera, DeWitt [1990]). For the case of convective heat transfer at

the tip of the fin, one obtains

$$\frac{T - T_\infty}{T_b - T_\infty} = \frac{\cosh m\,(L - x) + (h/mk)\,\sinh m\,(L - x)}{\cosh m\,L + (h/mk)\,\sinh m\,L} \qquad (5.2)$$

where T_b is the temperature at the base of the fin (corresponding to its temperature at the point of insertion into the emulsion where it is assumed to be at the temperature of the processing air), L its total length and $m^2 = hP/kA_c$. Equation (5.2) can be used to estimate the measurement error due to conduction of heat along the length of the thermocouple. For this purpose, it is necessary to neglect the variation of the product temperature over the cross section. The thermocouples consist of several materials, a copper and a constantan wire insulated from the stainless steel sheath with magnesium oxide powder (Figure 5.2). An average cross sectional conductivity must be defined. The measurement error for an average thermocouple conductivity of 50 W/mK is shown in Figure 5.14 for two different lengths and two different heat transfer coefficients as a function of the product temperature. At the beginning of an experiment, i.e. at low product temperatures, the measurement error for the chosen set of parameters associated with the shorter length, i.e. the thermocouple in the product center for a small diameter product, is approximately 2°C (3.6°F). The error associated with the longer thermocouple at the product surface or both thermocouples in the larger diameter products (43 and 45 mm) is negligible. However, because of the unknown heat transfer coefficient between the meat emulsion and the thermocouples, the exact magnitude of the correction necessary for the small diameter product could not be determined. Hence, the original data is shown in Figures 5.6 to 5.9.

5.3 Moisture Concentration Profiles

Values of the moisture concentration of processed products at different radial positions were measured with invasive methods for large ($D_{pr} = 10.8$ cm (4.25 inch)) and

Table 5.2: Processing conditions within the individual zones of the smokehouses used for the moisture profile experiments on small and large diameter products. The samples were removed after exiting from the last processing zone.

Time spent in zone [minutes]	Dry bulb temperature [°C] ([°F])	Relative humidity [%]	Wet bulb temperature [°C] ([°F])	Dew point temperature [°C] ([°F])
large diameter products (Figure 5.15)				
90	66 (150)	23.9	41 (105)	37 (98)
90	88 (190)	17.7	52 (125)	48 (119)
90	93 (200)	19.6	57 (135)	55 (131)
small diameter products (Figure 5.16)				
12	71 (160)	21.5	43 (110)	39 (102)
18	79 (175)	14.1	43 (110)	38 (100)
12	73 (163)	54.6	60 (140)	59 (139)
18	82 (180)	70.4	74 (165)	74 (165)

small ($D_{pr} = 23$ mm (0.91 inch)) diameter samples. The products were removed from commercial continuously operated smokehouses after exiting from the last processing zone. The processing conditions within the individual smokehouse zones are summarized in Table 5.2. The entries for the large diameter product are identical with the values given in Table 1.2.

A slice of approximately 1 cm thickness was cut in a perpendicular fashion from the center of a large diameter product. After the casing was removed, ten small pieces of 1 cm length and 0.25 cm width were cut with a razor blade and a cutting template from three different circumferential positions. The pieces were immediately placed into preweighed aluminum drying beakers and subjected to the A.O.A.C. [1990] method for the determination of moisture in meat (oven drying, 16 to 18 hours at 100 to 102°C). The results of this analysis and a sketch of the location of the cut pieces are shown in Figure 5.15. The measured moisture contents are constant in the center and decrease towards the surface of the product, indicating that most water is lost from regions close to the surface of the product. The variations in the moisture
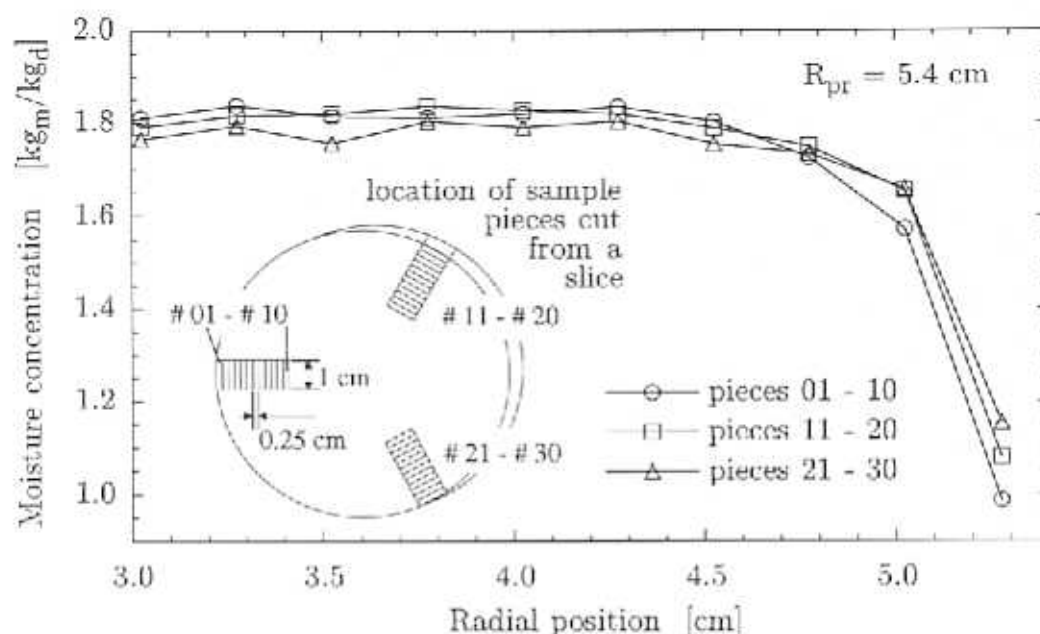
Figure 5.15: Moisture concentration profiles of a processed large diameter product at three circumferential positions. The product was removed from a commercial smokehouse after exiting from the last processing zone. The processing conditions within the individual smokehouse zones are summarized in Table 5.2.

content at different circumferential positions are small.

Concentric cork borers, custom-made from stainless steel, were used to obtain moisture concentration profiles of four small diameter products. Different cutting diameters were used to maintain reasonable sizes of the cut pieces and to obtain moisture concentration values at different radial positions. The cut concentric rings were subjected to the A.O.A.C. [1990] method described above. Typical results of this analysis and a sketch of the concentric cork borers are shown in Figure 5.16. The measured moisture concentrations decrease towards the center of the product. It was thought that the cutting procedure was responsible for the found behavior. The inner rings (and the center core) had a lower surface to volume ratio than the outer rings. Although all sample pieces were relatively small, this difference can affect the results obtained with the A.O.A.C. [1990] method. The center pieces with
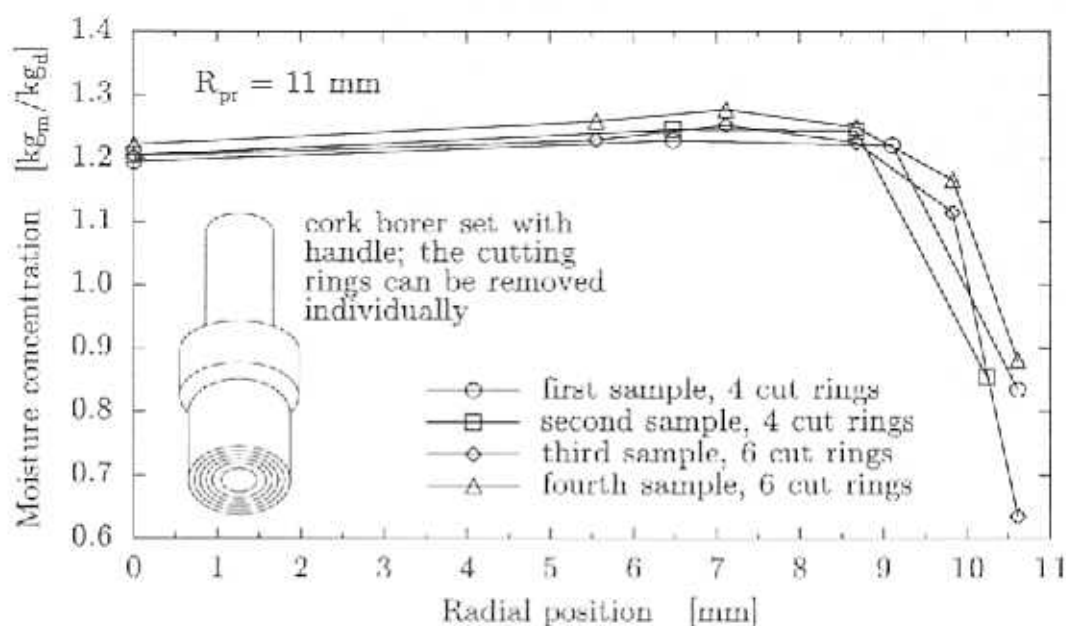
Figure 5.16: Moisture concentration profiles for a small diameter product obtained with concentric cork borers. The product was removed from a commercial smokehouse after exiting from the last processing zone. The processing conditions within the individual smokehouse zones are summarized in Table 5.2.

the lower surface to volume ratio would lose less moisture, which would translate into a smaller moisture concentration of the investigated sample, consistent with the behavior seen in Figure 5.16. In order to investigate the influence of the sample size on the measured moisture concentration, further experiments were conducted. In these tests, the center core and the inner rings were cut into smaller pieces. The results of these measurements suggest that the sample size is of importance. However, the increased number of cutting steps was a source of additional error and no conclusive results could be obtained.

To avoid these problems, it was attempted to use a non-invasive magnetic resonance imaging (MRI) method as a means of obtaining moisture profiles. Experiments were conducted at the National Magnetic Resonance Facility at Madison (NMRFAM) and the laboratory apparatus described in Section 5.1 was moved to that location.

The goal was to process meat emulsion products under the same conditions used in the temperature profile experiments and to subject them to the imaging process. It was planned to remove the samples from the test section at different processing times in order to obtain moisture profile snapshots at different stages of the processing. However, the signal to noise limits of the experiment prevented the extraction of useful information from the measurements. A description of the experimental procedure, together with some obtained data, is given in Section 5.7.2.

The precision of the A.O.A.C. [1990] oven drying method was tested with a different analytical technique, the Karl Fischer method, which is believed to be more accurate. For this purpose, an external extraction solvent was prepared from a one to one mixture (by mass) of methanol and chloroform. The moisture content of this mixture was determined by titrating with a pyridine free Karl Fischer reagent using the automated procedure of a Karl Fischer titrator (Metrohm 701 KF Titrino, Brinkmann Instruments, Inc.). The extraction solvent was then stored in a sealed container to minimize absorption of atmospheric moisture. The titer of the Karl Fischer reagent, determined before the experiments, was 5.237 mg_{H_2O}/ml. A whole cooked small diameter full-fat product (without casing) from a store-bought package was then submersed into the external extraction solvent and chopped with a high speed blender (Pro Scientific Inc., Pro 300D) for three minutes to extract the water. Aliquote portions of approximately 30 mg were removed with a syringe from the solution, immediately injected into the titration vessel of the titrator and titrated. This procedure was then repeated four times. The measured moisture contents are shown in Table 5.3.

A second product from the same package was subjected to the A.O.A.C. [1990] oven drying method described above. Five slices of approximately 5 mm thickness were cut from different locations of the product, placed into preweighed aluminum

Table 5.3: Comparison of the moisture content of a cooked small diameter full-fat meat emulsion product measured with two different experimental techniques, the A.O.A.C. [1990] method and Karl Fischer titration.

Experimental method	No. of samples or titrations	ω_m, mean value $[kg_m/kg_t] \times 100$	ω_m, standard deviation $[kg_m/kg_t] \times 100$
A.O.A.C. [1990] (oven drying)	5	52.7	0.823
Karl Fischer titration	5	54.0	0.857

drying dishes, cut into 6 smaller pieces, weighed and placed in an oven. The results are summarized in Table 5.3.

The moisture contents measured with the Karl Fischer method are slightly higher. These findings are in accordance with results reported in the literature for different food systems and can be attributed to the more efficient nature of moisture removal in the Karl Fischer method.

5.4 Convective Heat and Mass Transfer Coefficients

The convective heat and mass transfer coefficients are determined by the thermal and concentration boundary layers, respectively. Their magnitude depends on the nature of the fluid motion, the surface geometry and thermodynamic and transport properties of the fluid. In principle, these coefficients can be obtained by solving the appropriate boundary layer equation. However, this approach is only feasible for simple flow situations, and in practice the convective heat and mass transfer coefficients for specific flow situations are usually calculated from empirical relations that correlate measured coefficients in dimensionless groups. If the exact nature of the fluid motion is not known, the convective coefficients can be measured directly. This approach is also preferred when a high accuracy is desired. The analogy between heat and mass transfer at low mass transfer rates (Bird, Stewart, Lightfoot [1960]) can be

used to calculate mass transfer coefficients from measured heat transfer coefficients. A distinction has to be made between local heat and mass transfer coefficients and surface averaged values. The latter are usually used in macroscopic energy and mass balances and are used in the remainder of this section.

The convective heat transfer coefficient for a given flow situation can be calculated from the thermal response of a body that is initially at a different temperature than its surrounding fluid. However, the internal resistance to heat transfer within the body complicates the necessary calculations and it is advantageous to construct a system where the only resistance to heat transfer is located in the boundary layer. This can be done by constructing the body from a material with a sufficiently high thermal conductivity k. Such a system is referred to as *lumped* and the solution strategy of transient conduction problems based on this technique is called the *lumped capacitance method*. The Biot number, defined as

$$Bi = hL/k, \tag{5.3}$$

is a measure of the ratio of internal to external resistance to heat transfer. The conductivity k in Equation (5.3) is that of the heated or cooled body and L denotes a characteristic length, for example the radius of an infinitely long cylinder. If the Biot number of a system is smaller than 0.1, the error introduced by the approximation as a lumped system is negligible. An energy balance on a small lumped system in a large enclosure takes the form

$$m c \frac{dT}{dt} = h_c A \left(T_\infty - T\right) + \epsilon \sigma A \left(T_\infty^4 - T^4\right) \tag{5.4}$$

where m, c and A are the mass, the specific heat and surface area of the system. The temperatures T and T_∞ indicate the temperature of the body and the fluid temperature, respectively. The parameters h_c, ϵ and σ are the convective heat transfer coefficient, the surface emissivity and the Stefan-Boltzmann constant. The

left hand side of Equation (5.4) accounts for the rate of change in internal energy. The contributions of convection and radiation are accounted for by the right-hand side. It is assumed that the temperature for radiation exchange, i.e. the temperature of the surrounding matter, is identical with the fluid temperature. Expanding the last term in Equation (5.4) yields

$$m\,c\,\frac{dT}{dt} = h_c\,A\,(T_\infty - T) + \epsilon\,\sigma\,A\,(T_\infty^2 + T^2)\,(T_\infty + T)\,(T_\infty - T). \tag{5.5}$$

The right hand side of Equation (5.5) can be combined to give

$$m\,c\,\frac{dT}{dt} = h\,A\,(T_\infty - T) \tag{5.6}$$

where the heat transfer coefficient h is the sum of convective and radiative contributions

$$h = h_c + h_r \tag{5.7}$$

with

$$h_r = \epsilon\,\sigma\,(T_\infty^2 + T^2)\,(T_\infty + T) \approx \epsilon\,\sigma\,4\left(\frac{T_\infty + T}{2}\right)^3. \tag{5.8}$$

Equation (5.8) can be used to estimate the magnitude of the radiative contribution to Equation (5.6). With $\sigma = 5.67 \times 10^{-8}$ W/m^{2}K^4, $\epsilon = 1$, $T_\infty = 350$K and $T = 300$K one obtains a value of $h_r = 7.8$ W/m^{2}K. Integrating Equation (5.6) yields

$$\frac{T - T_\infty}{T_o - T_\infty} = \exp\left(-\frac{h\,A\,t}{m\,c}\right) \tag{5.9}$$

where T_o is the is the temperature of the body at $t = 0$.

Integration of a more general case of Equation (5.6), where the temperature of the fluid T_∞ is allowed to be a linear function of time

$$m\,c\,\frac{dT}{dt} = h\,A\,((T_{\infty,o} + a\,t) - T), \tag{5.10}$$

yields

$$T = T_{\infty,o} - (T_{\infty,o} - T_o)\exp(-\gamma t) + \frac{a}{\gamma}[(\gamma t - 1) + \exp(-\gamma t)] \tag{5.11}$$

with

$$\gamma = (h\,A)/(m\,c). \tag{5.12}$$

For $a = 0$, i.e. a constant ambient dry bulb temperature, Equation (5.11) reduces to Equation (5.9).

Two fundamentally different approaches are possible to employ the above equations in order to calculate the heat transfer coefficient from the thermal response of a lumped system. In the differential approach, the instantaneous heat transfer coefficient is obtained from the temperature gradient dT/dt and the temperature difference $(T_\infty - T)$ at any given time. The integral approach uses the analytical solution (i.e. the integrated form) of the differential equation (Equation (5.9) or Equation (5.11)) to obtain h from the known initial and final temperatures and it is advantageous when time averaged values of the heat transfer coefficient are sought. A variation of the integral approach is given when the measured temperature response of the lumped system is fitted with a regression analysis to the form of the analytical solution. In this case, the heat transfer coefficient h or the parameter γ (from which h can be calculated directly) are the single curve fit parameter. This technique is employed in the remainder of this section.

In this study, the convective heat transfer coefficient was measured in four different processing environments, a commercial continuously operated smokehouse used for the processing of small diameter products and consisting of several processing zones, a batch operated pilot plant smokehouse, the test section of the laboratory apparatus described in Section 5.1 and a commercial continuous smokehouse consisting of several processing zones used for the processing of large diameter products.

A solid aluminum probe of 15.2 cm length and 2.3 cm diameter was used as the lumped system for the first three processing environments. The size and form of this probe closely resembled a real small diameter meat emulsion product. The Biot number for all expected heat transfer coefficients was sufficiently small to justify the lumped capacitance assumption ($Bi = 0.0065$ for $k = 177$ W/mK and $h = 100$ W/m²K). A brine-filled aluminum vessel was used as the lumped system to measure the heat transfer coefficient in processing environments for large diameter products ($D_{pr} = 4.25$ inch (10.8 cm)). The Biot number of a solid aluminum probe of that diameter would still be small enough to neglect an internal temperature distribution but the probe would be too heavy for easy handling. The relatively low thermal conductivity of water or a salt solution would cause a rather large temperature gradient upon heating but the motion of the liquid inside the brine-filled vessel prevents any significant internal temperature stratification. This assumption was verified before the experiments. Details of the brine-filled vessel are given later in this section. A sketch of the equipment used for the measurement of the heat transfer coefficient is given in Figure 5.17.

The method used for the measurement of the heat transfer coefficient in a commercial continuous smokehouse used for the processing of small diameter products was similar to that reported by Spielbauer [1992]. The dry bulb temperature of the processing air and the temperature response of the solid aluminum probe traversing through the smokehouse were recorded with temperature data traces (Datatrace Micropack, Mesa Laboratories, Wheat Ridge, Colorado). These devices are wireless programmable temperature sensors (thermistors) with an internal memory and clock capable of storing up to 1000 time/temperature observations. Since all electronic components are encapsulated in stainless steel, the temperature traces can be used in many processing environments. Before use, the data traces are inserted into an
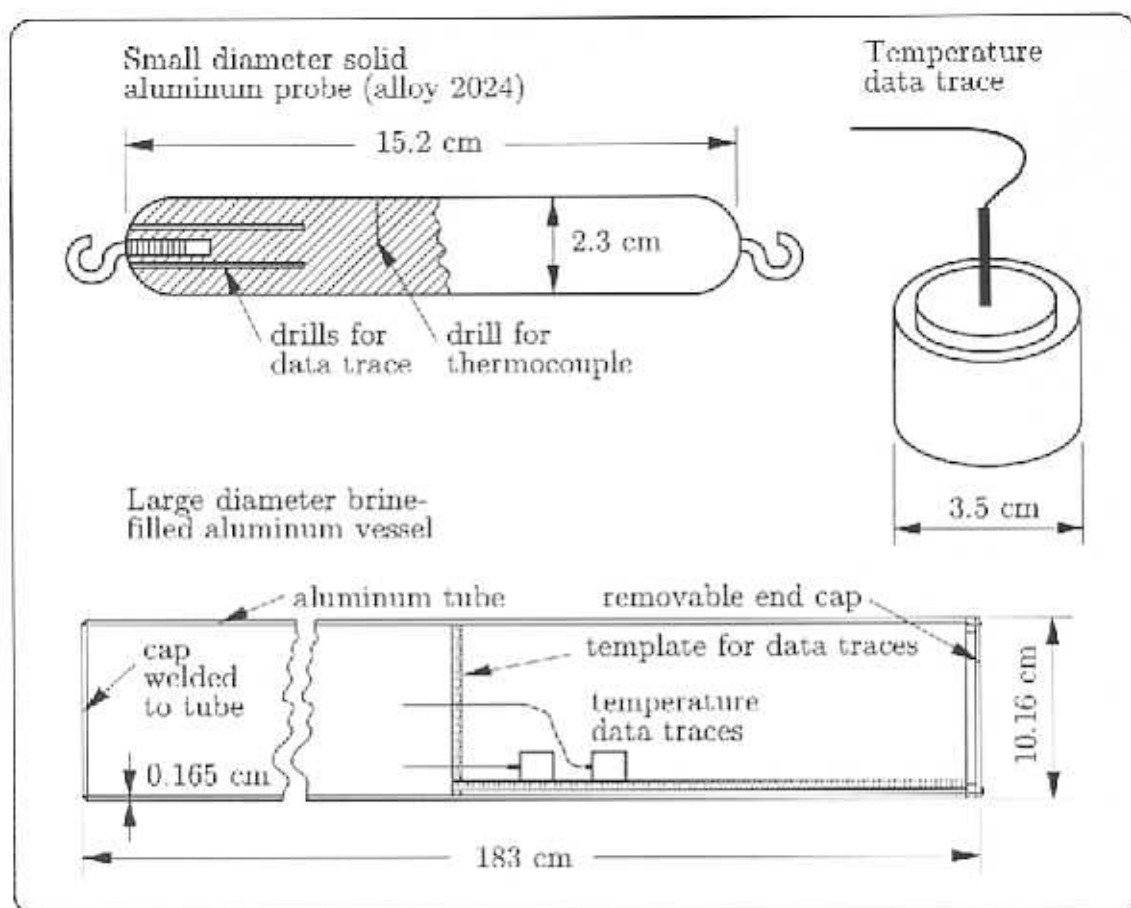
Figure 5.17: Equipment used in the experimental determination of the convective heat transfer coefficient in different processing environments based on the lumped capacitance method.

interface connected to a personal computer, and the time at which the data recording starts and the sampling interval are chosen. The latter can be varied from one second up to 24 hours. After recording, the temperature trace is inserted into the interface and the data is downloaded into a spreadsheet file. The measurement accuracy specified by the manufacturer for the temperature range of 10°C to 150°C (50°F to 302°F) is 0.5°C (0.9°F). Spielbauer [1992] used the same temperature data traces that were employed in this research. He evaluated their measurement precision by submerging them into a water bath and reported a value of 0.56°C (1.0°F).

Table 5.4: Summary of results from the experimental determination of the convective heat transfer coefficient based on the lumped capacitance method in four different processing environments.

Zone or experiment	$\gamma \times 10^5$ [a] [1/s]	A [m²]	m [kg]	c [J/kgK]	a [°C/min]	h [†] [W/m²K]	Figure/ on page
solid aluminum probe (D = 23 mm) in commercial smokehouse							
zone 2	141	0.0108	0.173	875	0.104	19.8	not shown
zone 3	96.7	0.0108	0.173	875	0.110	13.6	5.19/107
solid aluminum probe (D = 23 mm) in pilot plant smokehouse							
1/1	471	0.0108	0.173	875	-0.207	66.0	5.20/108
solid aluminum probe (D = 23 mm) in test section of the laboratory apparatus							
(h-values for product diameters of 43 and 45 mm are obtained from Equation (5.13)) [b]							
1/2	241	0.0108	0.173	875	0.013	33.8	5.21/109
2/2	234	0.0108	0.173	875	0.025	32.8	not shown
brine-filled aluminum vessel (D = 4 inch) in commercial smokehouse							
(the shown h-values are corrected for a product diam. of 4.25 inch using Equation (5.16))							
zone 1 [c]	46.1	0.584	17.9	2983	0.179	41.1	5.22/111
zone 1 [c]	40.9	0.584	17.9	2983	0.149	36.5	5.22/111
zone 2	40.8	0.584	17.9	2983	0.158	36.5	5.22/111
zone 3	27.0	0.584	17.9	2983	0.084	24.1	5.22/111

[a] γ is defined in Equation (5.12). The given values are obtained from a regression analysis of Equation (5.11) to the temperature response of the lumped system.

[†] h in units of W/m² K can be multiplied by 5.68 to get units of BTU/hr ft² °F

[b] based on Equation (5.13), one obtains $h = 39.4$ W/m²K for $D_{pr} = 43$ mm ($v_{air} = 3.5$ m/s) and $h = 45.2$ W/m²K for $D_{pr} = 45$ mm ($v_{air} = 4.6$ m/s).

[c] before and after the production delay in zone 1.

The solid aluminum probe with an inserted temperature data trace was tied to a holding stick (used to support the weight of the meat products and placed with both ends into a conveyor chain, which moved it through the smokehouse) and closely represented the orientation of a typical product. A second temperature data trace was located approximately 5 cm away from the aluminum probe and was used to record the dry bulb temperature of the processing air. The recorded temperatures are shown in Figure 5.18. The dry bulb and aluminum probe temperature for the last processing zone, together with a linear fit to the dry bulb temperature and a fit of

the aluminum probe temperature to Equation (5.11), are shown in Figure 5.19. The resulting curve fit parameters a and γ and the calculated heat transfer coefficients (from Equation (5.12)) for this and the following experiments are summarized in Table 5.4.

The same equipment was used to measure the heat transfer coefficient in a batch type pilot plant smokehouse operated at medium air velocity. The recorded dry bulb temperature and the temperature response of the solid aluminum probe, together with the corresponding curve fits, are shown in Figure 5.20. The slight decrease in the dry bulb temperature of the processing air over the course of the experiment was attributed to an imperfect control mechanism.

The heat transfer coefficient in the test section of the laboratory apparatus described in Section 5.1 was measured in a similar fashion. In this case, the dry bulb and aluminum probe temperatures were recorded with thermocouples and the data logging equipment described in Section 5.1. It was necessary to use an ungrounded thermocouple (Omega, TMQSS-020U-6) to record the temperature of the aluminum probe to avoid problems with static electricity that added to the voltage signal sent from the thermocouple to the analog to digital converter board. Two experiments under the same conditions were conducted. The recorded temperatures and the corresponding curve fits from the first experiment are shown in Figure 5.21. Heat transfer coefficients for the larger diameter samples (43 and 45 mm) were estimated from the measured heat transfer coefficient for the small diameter product ($D_{pr} = 23$ mm) and the known air velocities in the test section (Section 5.2) for the different product and probe diameters. For this purpose, it was assumed that the flow situation could be described by the *flat plate in parallel flow* geometry with the Nusselt correlation

$$\overline{Nu_x} = \frac{h_x x}{k} = 0.664\, Re_x^{1/2}\, Pr^{1/3}. \tag{5.13}$$

Hence, the heat transfer coefficient increased with the square root of the velocity.
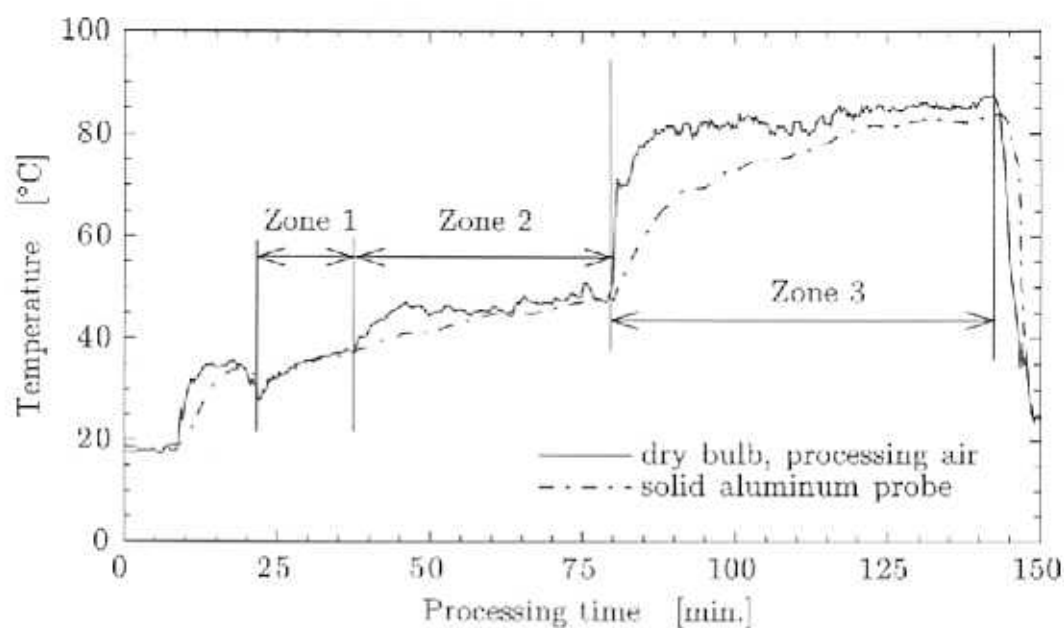
Figure 5.18: Dry bulb temperature and thermal response of a solid aluminum probe traveling through three processing zones of a continuous smokehouse.
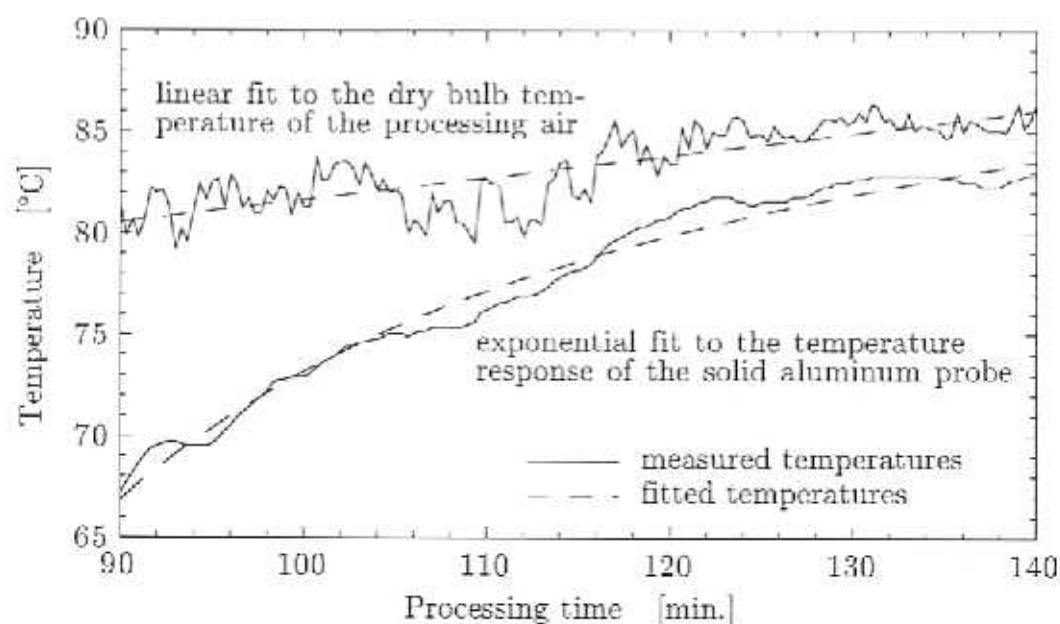
Figure 5.19: Dry bulb temperature and thermal response of a solid aluminum probe traveling through the last processing zones of a continuous smokehouse.
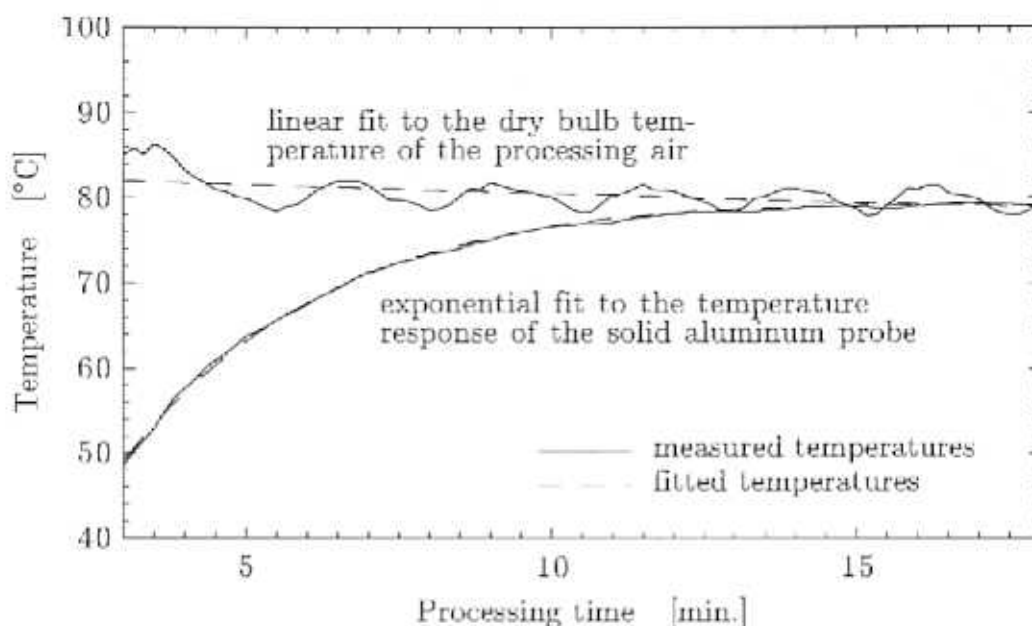
Figure 5.20: Dry bulb temperature and thermal response of a solid aluminum probe located in the center of a batch type smokehouse at medium air velocities.

The brine-filled aluminum vessel described earlier in this section was used to measure the heat transfer coefficient in a commercial continuous smokehouse used for the processing of large diameter products. This vessel was made from an aluminum tube of 6 feet (1.83 m) length, 4 inch (10.16 cm) outer diameter and a wall thickness of 0.065 inch (1.65 mm). A similar tube with a diameter of 4.25 inch (i.e. more closely resembling the real product diameter) was not available at reasonable costs. A correction was applied to the measured heat transfer coefficient to account for the slightly different diameter of the aluminum tube and a real product. Details of this correction are given later in this section. An aluminum disk was welded to one end of the vessel. The other side featured a removable end piece, sealed with a rubber ring. Two temperature data traces of the type described earlier in this section were used to record the temperature of the vessel as it traversed through the smokehouse. A template inside the tube held the temperature data traces in position during the
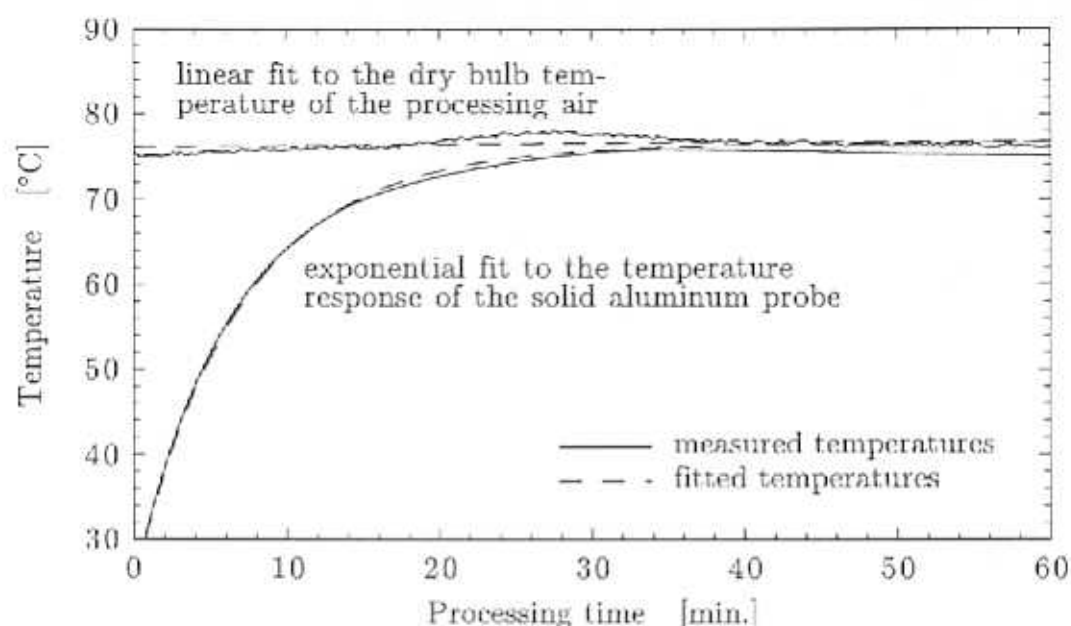
Figure 5.21: Dry bulb temperature and thermal response of a solid aluminum probe located in the test section of the laboratory apparatus described in Section 5.1.

experiments and allowed their insertion to a position approximately in the middle of the length of the vessel. The vessel was filled with a saturated sodium chloride solution. The filling with this brine was necessary to prevent freezing while the device traveled through the chilling zones following the processing zones. It was not possible to remove the vessel from the smokehouse before it entered the chilling zones. The average specific heat of the aluminum vessel and brine was calculated from the equation

$$\bar{c} = \frac{m_b\, c_b + m_{al}\, c_{al}}{m_b + m_{al}} \tag{5.14}$$

where the indices b and al refer to the brine solution and the aluminum, respectively. The masses m_b and m_{al} were obtained by weighing the empty and the brine-filled vessel.

Since the thermal expansion coefficient of water (or of a salt solution) is larger

than that of aluminum, an analysis was performed to estimate the pressure inside the
brine-filled tube when subjected to warm processing air. Based on a heating process
of $\Delta T = 70°C$ and allowing a total final pressure inside the vessel of 2 atmospheres,
approximately 15 cm of air space was left when the vertically standing tube was filled
with the salt solution.

The recorded temperatures from this experiment are shown in Figure 5.22. The
heat transfer coefficient within each zone was obtained from a linear fit to the dry
bulb temperature of the processing air and a fit of the aluminum probe temperature
to Equation (5.11) in the same way that was described earlier in this section. Results
are shown in Table 5.4. It can be seen that the temperatures recorded by the two
data traces inside the aluminum tube are in close agreement, indicating that the
internal motion of the brine was sufficient to prevent temperature gradients and that
the assumption of a lumped system was justified. A production delay occurred while
the aluminum vessel was traversing the first processing one.

Assuming that the air flow in the smokehouse can be described by the *cylinder in
cross flow* situation, the empirical relation

$$\overline{Nu}_D = \frac{hD}{k} = C_1 \, Re_D^n \, Pr^{1/3} \tag{5.15}$$

with $Re_D = \rho \, v_{air} D / \mu$ and C_1 and n being functions of the Reynolds number (Incr-
opera, DeWitt [1990]) can be used to correct the obtained heat transfer coefficient for
the slightly different diameter of a meat product. Rewriting Equation (5.15) yields

$$h = C_2 \, \frac{1}{D^{1-n}}. \tag{5.16}$$

For all Reynolds numbers, the value of n is less than unity (Incropera, DeWitt [1990]).
Hence, the heat transfer coefficient h decreases with increasing diameter. Equa-
tion (5.16) with $n = 0.193$ ($4000 < Re < 40000$) was used to correct the heat transfer
coefficient measured with the brine-filled aluminum tube ($D = 4$ inch (10.16 cm)) for
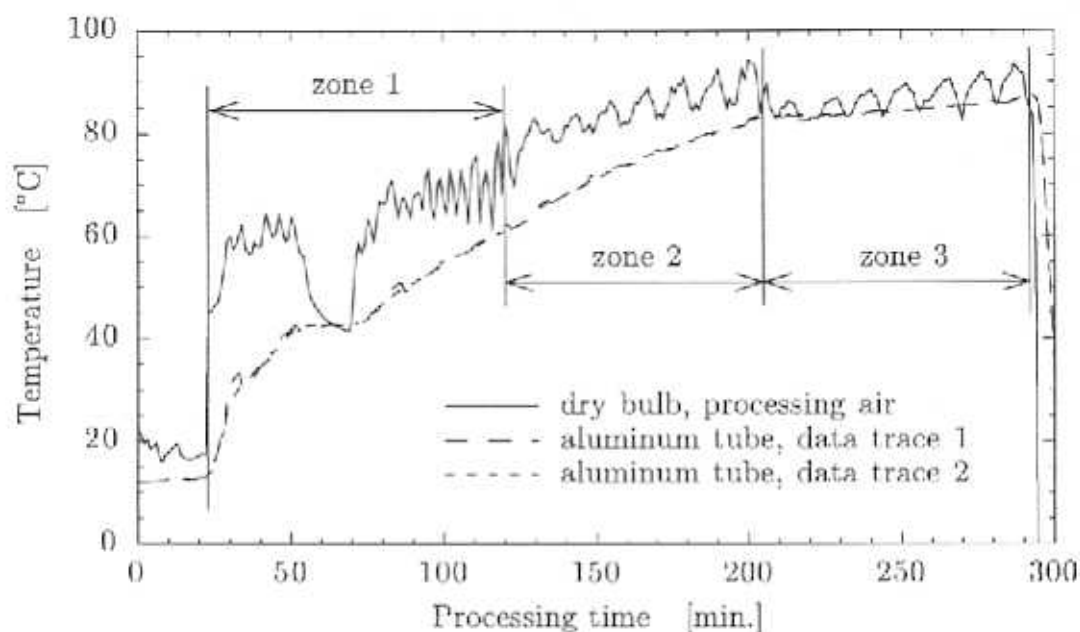
Figure 5.22: Dry bulb temperature and thermal response of a brine-filled aluminum vessel traveling through the processing zones of a commercial continuous smokehouse. A production delay occurred in the first processing zone.

the diameter of the real product ($D_{pr} = 4.25$ inch (10.8 cm)). The corrected values are given in Table 5.4.

The convective mass transfer coefficient can be calculated from the measured heat transfer coefficients by employing the analogy between heat and mass transfer for low mass transfer rates as described in Bird, Stewart and Lightfoot [1960]. The mass transfer rates under investigation in this study were assumed to be small enough to qualify as *low mass transfer rates*. Equating the Chilton-Colburn j-factors for heat and mass transfer yields

$$\frac{h}{k_{x,m}} = \tilde{c}_{p,f} \left(\frac{Sc}{Pr}\right)^{2/3}_f \tag{5.17}$$

where the mass transfer coefficient $k_{x,m}$ is based on a mole fraction driving force. The ratio of the Schmidt and Prandtl numbers in Equation (5.17) is also called the *Lewis*

number and can be written as

$$Le = \frac{\alpha}{D_{AB}} \tag{5.18}$$

where α and D_{AB} are the thermal diffusivity and the binary diffusion coefficient of the moist air, respectively. The diffusion coefficient can be obtained from the relation

$$D_{air,H_2O} \; [\mathrm{m^2/s}] = 0.2810^{-4} \left(\frac{T \; [\mathrm{K}]}{298}\right)^{3/2} \tag{5.19}$$

given by Incropera and DeWitt [1990]. To obtain a mass transfer coefficient based on a vapor pressure driving force k_p, the coefficient $k_{x,m}$ can be converted with the relation

$$k_p = k_{x,m} \frac{M_w}{P_t} \tag{5.20}$$

where M_w and P_t are the molecular weight of water and the total pressure, respectively. Mass transfer coefficients k_p calculated from Equation (5.17) for several values of the relative humidity and one dry bulb temperature are shown in Figure (5.23).

The applicability of the heat and mass transfer analogy was verified with direct measurements of the mass transfer coefficient. These experiments consisted of recording the weight loss of water-filled standard moisture-permeable cellulose casings ($D = 23$ mm) suspended in a stream of unsaturated air. A similar technique was reported by Agrawal [1976]. The filling with water prevented any internal resistance to moisture transfer that would complicate the calculation of k_p. It was assumed that the casing caused no resistance to mass transfer, i.e. the casing surface was assumed to be fully wet. It should be noted that this assumption was realistic under the conditions of the experiment. However, during the thermal processing of a meat emulsion product, the casing dries out and its resistance to mass transfer has to be investigated further.
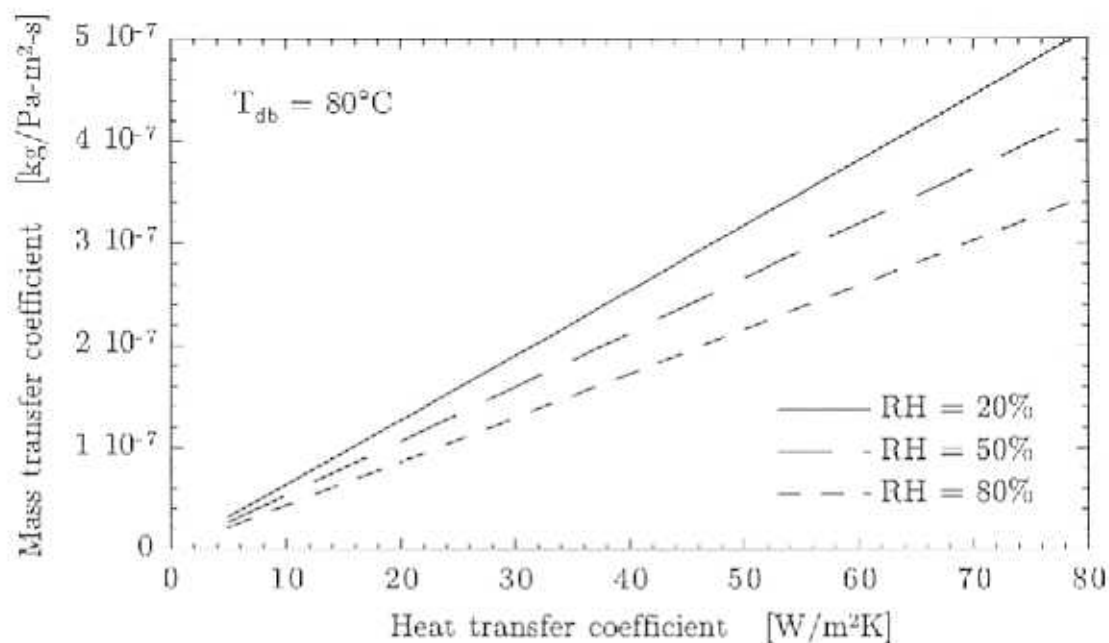
Figure 5.23: Mass transfer coefficients calculated from heat transfer coefficients using the analogy between heat and mass transfer at low mass transfer rates for three different humidities and one temperature.

Assuming that the driving force for mass transfer is the difference between the vapor pressure of water at the casing surface and the partial pressure of water in the approaching moist air, the mass transfer coefficient was calculated from the equation

$$\dot{m} = k_p \, A \, (p_{w,s} - p_{w,\infty}) \tag{5.21}$$

where A denotes the exposed surface area of the casing, k_p the mass transfer coefficient based on a partial pressure driving force and $\dot{m}$ the mass of water evaporated at the casing surface per time. Since the casing surface was assumed to be wet, the experimental setup was equivalent to that of a wet bulb temperature determination and a pseudo steady state developed where the temperature of the water inside the casing equaled the wet bulb temperature of the approaching air. In this case, the vapor pressure of water at the casing surface $p_{w,s}$ could be directly determined from the known relationship between temperature and pressure of a saturated vapor. It was

Table 5.5: Determination of the mass transfer coefficient k_p from the weight loss of water-filled standard moisture-permeable cellulose casings suspended in a stream of unsaturated air in a smokehouse [1].

Experiment	Number of samples (filled casings)	k_p, mean value $[\text{kg/Pa m}^2\text{ s}] \times 10^7$	k_p, standard deviation $[\text{kg/Pa m}^2\text{ s}] \times 10^7$
in batch type smokehouse [2]	6	4.1	1.1
free convection [3]	3	0.50	0.35

[1] a heat transfer coefficient of $h = 66$ W/m^{2}K was measured for the same air velocity
[2] $T_{db} = 20^\circ$C, $T_{wb} = 11^\circ$C ($RH = 31\%$), medium air velocity
[3] same ambient temperature and humidity but no air velocity

assumed that the time needed to reach this pseudo steady state was small compared to the time at which the loss of water caused a dimensional change of the filled casing. The batch type pilot plant smokehouse described earlier in this section was used to provide the air flow for these experiments. The same setting of the air velocity used for the determination of the heat transfer coefficient (Section 5.4) was used in these experiments. Using psychrometric relations to obtain $p_{u,\infty}$ from the total pressure and the dry and wet bulb temperatures of the approaching air, the mass transfer coefficient was calculated from Equation (5.21). Results of the experiments are shown in Table 5.5. The measured mass transfer coefficients compare well with those calculated by using the heat and mass transfer analogy from measured heat transfer coefficients as shown in Figure (5.23).

5.5 Moisture Loss of Emulsion Products during Processing

The moisture loss of meat emulsion products during processing was monitored for two different processing environments, a batch operated forced air pilot plant smokehouse and the test section of the laboratory apparatus described in Section 5.1. In addition to these experiments, the initial and final masses of the samples used in the deter-
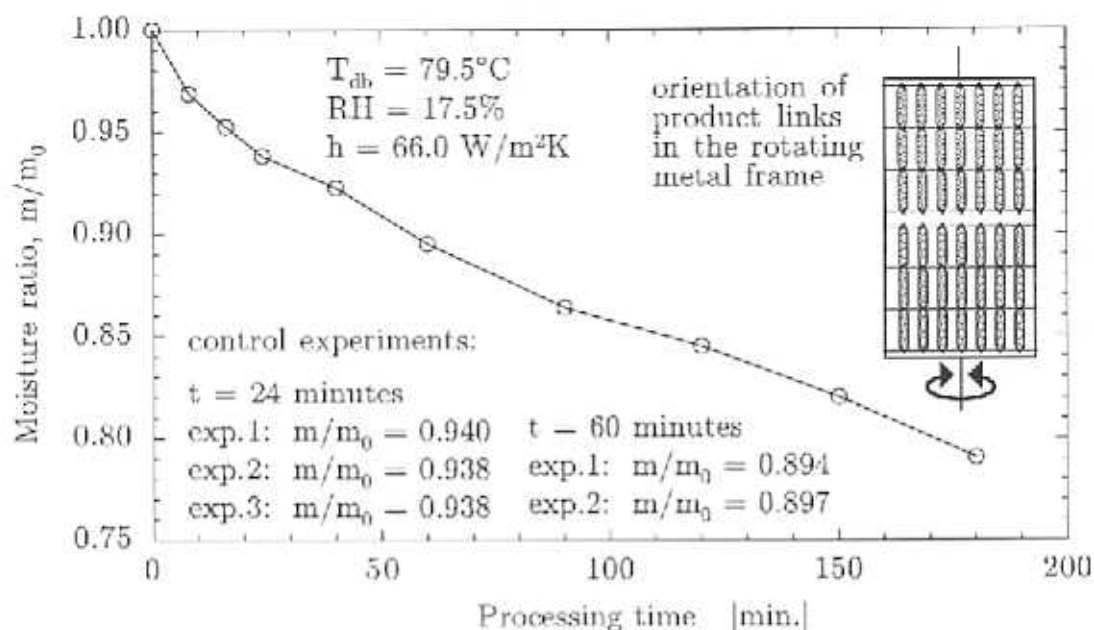
Figure 5.24: Weight loss of full-fat products stuffed in standard moisture-permeable cellulose casings and processed in a batch type smokehouse. The products were removed at various times of processing. The precision of the measurements was tested at two times. The data of these control experiments are provided at the bottom of the plot.

mination of the temperature profiles (Section 5.2) were recorded and are reported in Table 5.1.

The weight loss of products during processing in the forced air pilot plant smokehouse was recorded by removing products at specific processing times. Thirteen strands consisting of three products each were prepared by stuffing a standard moisture-permeable cellulose casing ($D = 23$ mm) with a full-fat meat emulsion. The ends of the stuffed strands were closed with a knot. The strands were then weighed and placed into a metal frame with rubber nicks. When pushed into these nicks, the individual product links formed from the stuffed strands. One of the product strands in the middle of the frame was removed at this time and weighed again. No decrease in the weight was observed. The prepared metal frame was then placed vertically into

the center of the preheated smokehouse and connected to a rotating device. During processing, this device rotated the metal frame by approximately 340 degrees back and forth, with one turn lasting approximately 5 seconds and no delay between individual turns. The processing conditions were $T_{db} = 79.5°C$, $RH = 17.5\%$ and $h = 66.0$ W/m^{2}K. This value of the heat transfer coefficient was measured for the same setting of the air velocity in a separate experiment (Section 5.4). In order to monitor the weight loss during processing, the product strands were removed from a randomly selected position in the frame at times ranging from 8 to 180 minutes and weighed. At two times (24 minutes and 60 minutes), more than one strand was removed from the smokehouse to test the reproducibility of the experiment. The measured moisture losses, plotted as a fraction of the initial weight, are shown in Figure 5.24. The individual values measured at the times when several product strands were removed to test the reproducibility of the experiment, and a sketch of the product arrangement in the metal frame, are also given in Figure 5.24.

The weight loss of products during processing in the test section of the laboratory apparatus described in Section 5.1 was measured by recording their weight every 10 minutes. The samples were removed from the test section, weighed and immediately returned to their original position. The removal, weighing and return took approximately 45 seconds. It was assumed that this time period was short enough to have negligible influence on the measured weight loss. Full-fat and no-fat emulsions, both stuffed in moisture permeable standard cellulose casings ($D = 23$ mm), were investigated for this experiment. Two runs under the same conditions, $T_{db} = 78°C$, $RH = 6.1\%$ and $h = 33.3$ W/m^{2}K, were conducted for each sample. The value of the heat transfer coefficient was measured in a separate experiment for the same flowrate through the apparatus (Section 5.4). Results are shown in Figure 5.25. The no-fat product lost significantly more moisture than the full-fat product (about 25% after
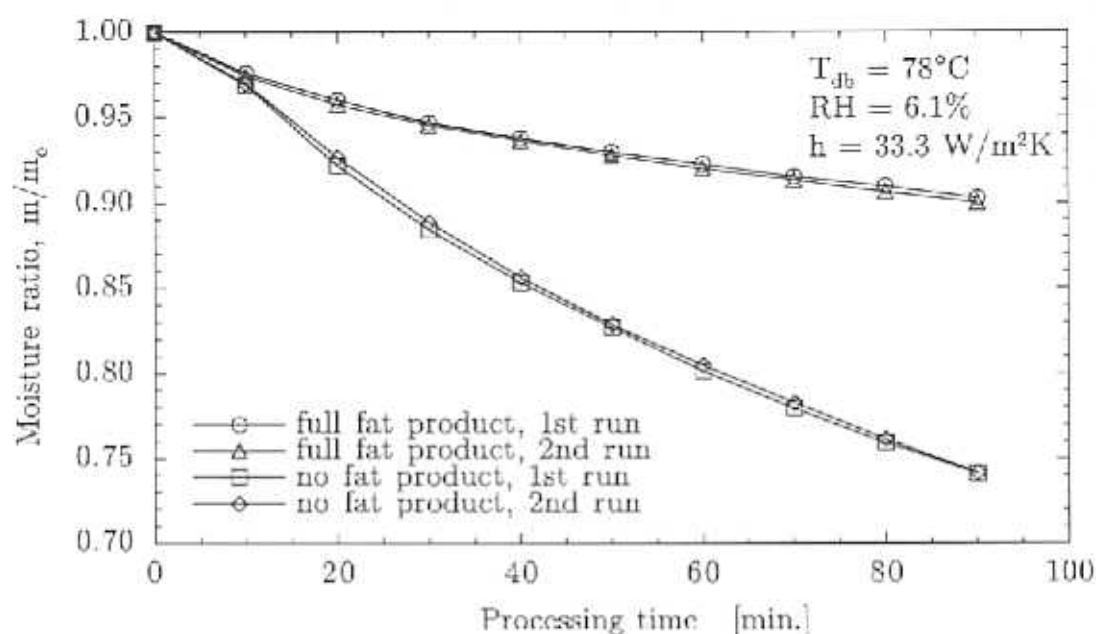
Figure 5.25: Measured weight losses of full-fat and no-fat products stuffed in standard moisture-permeable cellulose casings and processed in the test section of the laboratory apparatus.

90 minutes compared to approximately 10%). This result confirms that the moisture loss is limited by internal diffusion of moisture to the product surface. Consequently, the no-fat emulsion with its higher effective moisture diffusion coefficient can supply more moisture from the inner regions of the product to the surface. These findings are in agreement with the results from the temperature profile measurements (Section 5.2).

5.6 Dry Density of Meat Emulsion

The *dry density* describes the ratio of the bone dry mass (i.e. protein, fat, carbohydrates and inorganic materials) and the volume of the meat emulsion. One assumption employed in the simulation model developed in Chapter 3 was that the volume of the meat emulsion remains constant during the relatively small moisture losses encoun-

Table 5.6: Results from the determination of the dry density of full-fat and no-fat meat emulsions based on the total density and the moisture content. The dry density is a parameter needed for the simulation model.

Sample	Mass [g]	Volume [ml]	Total density [kg_t/m^3]	Moisture content [kg_m/kg_t]	Dry density [kg_d/m^3]
full-fat product	119.8	117	1024	0.576	434
no-fat product	138.8	134	1036	0.870	135

tered during commercial processing. Therefore, the dry density can be viewed as a somewhat artificial parameter needed for the simulation model to relate the moisture concentration (in terms of mass of water per mass of dry material) to the moisture density (in terms of mass of water per volume).

The dry densities of a full-fat and a no-fat emulsion were determined experimentally. A stuffing machine and standard cellulose casings were used to produce some links of each emulsion type. The twisted casing connections of two links were then secured with a thin string and the links remaining on each end of the strand were cut away and discarded. The two products obtained by this procedure were then weighed and submersed into a graduated cylinder (total volume of 500 ml) initially half-filled with water. It was assumed that the error introduced through the presence of the thin casing was negligible. The time needed to take the readings was also very short compared to the time needed for any moisture diffusion into the product to affect the reading. The initial moisture content (per wet basis) was known from the preparation of the two emulsion types. The dry density for each emulsion was then obtained from the equation

$$\rho_d = \frac{m\,(1 - \omega_m)}{V} \tag{5.22}$$

where m, V and ω_m are the measured (wet) mass, the measured volume and the known moisture content per wet basis, respectively. The results of these dry density

experiments are summarized in Table 5.6. The higher dry density of the full fat emulsion corresponds to its lower moisture content. The slightly higher total density of the no-fat product can be explained by the density differences of water, fat and protein.

5.7 Nuclear Magnetic Resonance (NMR) Experiments

Several experiments with magnetic resonance imaging (MRI) and pulsed field-gradient (PFG-NMR) methods were conducted in an attempt to measure moisture concentration profiles and effective moisture diffusion coefficients, respectively. First, the basic principles of all nuclear magnetic resonance techniques are introduced. This part is followed by a description of the individual MRI and PFG-NMR experiments.

5.7.1 Some Basic Principles

Not all important aspects of NMR are introduced here. This would be a formidable task well outside the scope of this section. However, some basic principles that will aid in the understanding of the experiments described in Sections 5.7.2 and 5.7.3 are covered here. Atoms of interest in NMR have nuclei possessing magnetic dipole moments arising from spin-like motions. These atoms have nuclei with an odd number of protons or neutrons. The spin-like motion generates a magnetic moment, μ, which is collinear with the angular momentum, J, also called spin, and related by the equation

$$\mu = \gamma J \tag{5.23}$$

where γ is the gyromagnetic ratio, a constant for a given isotope. If such a nucleus is placed in a magnetic field, the magnetic moment will experience a torque, resulting in a precession of the magnetic moment about the magnetic field, analogous to a top

precessing about the earth's gravitational field. The frequency of this precessional motion is given by the *Larmor equation*

$$\omega = \gamma\, B_0 \tag{5.24}$$

where ω, γ and B_0 are the *Larmor precession frequency*, the *gyromagnetic ratio* and the *magnetic field strength*, respectively. Equation (5.24) is sometimes also called the *fundamental equation* of Nuclear Magnetic Resonance.

The fundamental principle of all nuclear magnetic resonance techniques is the absorption of resonant radiation by an ensemble of nuclei with magnetic moments. The absorption of radiation by a molecule involves an energy level transition from its stable ground state to an excited state of higher energy. For the transition to take place, the energy of the radiation must match the energy difference ΔE between the two states. Planck's law

$$\Delta E = h\,\nu \tag{5.25}$$

relates this energy difference to the energy of the radiation quantum, where ν is the frequency of the radiation and h a Planck's constant. Consequently, the spectrum of frequencies at the which a substance has strong absorptions gives a map of the energies of the excited states of the molecules in the substance.

Two views of this fundamental mechanism exist, the *classical mechanics* viewpoint and the *quantum mechanical* view. Both ways of thinking about the nuclear magnetic resonance phenomenon are useful and complement each other. For example, if one could measure the components of the magnetization vector of a single proton, only two discrete values would be observed. This is because atomic phenomena do not behave classically, i.e. they do not obey Newtonian mechanics. However, the signal observed in an NMR experiment is derived from a large ensemble of spins and behaves

in a classical manner, i.e. the bulk magnetization from all of the spins in the sample can be represented by a single vector.

A detailed discussion of the physical principles leading to the use of magnetic resonance imaging (MRI) and pulsed field-gradient nuclear magnetic resonance methods can be found in a number of sources, including Abragam [1961], Stilbs [1987], Smith and Ranallo [1989] and Callaghan [1991]. A summary of the applications of MRI in the food industry is given by Schrader *et al.* [1992].

5.7.2 Moisture Profiles from Magnetic Resonance Imaging

Measurements of moisture profiles in meat emulsion products were conducted at the National Magnetic Resonance Facility at Madison (NMRFAM). The laboratory apparatus described in Section 5.1 was moved to that location. The goal was to process meat emulsion products under the same conditions as those used in the temperature profile experiments and to subject them to the imaging process. It was planned to remove the samples from the test section at different processing times in order to obtain moisture profiles at different stages of the processing.

A Bruker Instruments DMX-400 WB (9.4 Tesla) magnetic resonance spectrometer operating at 400 MHz for proton detection was used. Images were acquired in a probe equipped with self-shielded gradients and a 25 or 30 mm probehead. Both standard gradient-refocused echo (GRE) techniques with a $3°$ tip angle from a low power 2 ms pulse and line spin-echo (SE) experiments were used. In the GRE measurements, the echo time (time between the $3°$ pulse and the mid-point of the echo) was 3.2 ms and the repetition time (time between pulse sequences) was 14.5 ms. The resonance from fat protons was suppressed by the use of a frequency selective pulse followed by a strong gradient along the direction of the slice axis. The field of view for imaging was 30 mm. The echoes were acquired in 256 points with 128 phase-encoding steps.

Two data sets were collected per image and the slice thickness was 8 mm. The line spin-echo (SE) experiments were performed with an echo time of 9.75 ms and a repetition time of 8 seconds. Selection was achieved using a slice gradient during the $90°$, 2 ms pulse and a phase gradient during the $180°$, 2 ms pulse. Suppression of the fat resonance was achieved by use of a frequency selective pulse before the spin-echo sequence. Eight scans were acquired in each experiment. The slice thickness in the spin-echo experiments was also 8 mm.

Shimming (i.e. the use of external magnetic fields to compensate for magnetic field gradients generated by the presence of the sample in the magnet) was done initially on a tube of tap water filled to a level similar to what a meat emulsion product occupied. Final shimming was done on an uncooked meat product. Water linewidths were on the order of 200 Hz. The signal to noise ratio (S/N) was about 8:1 for the GRE experiments and about 16:1 for the SE experiments.

Despite various attempts at different parameter settings, no reproducible moisture profiles could be obtained with either the GRE or the SE method. In the GRE experiments, the magnetic susceptibility gradients present in the meat products caused extreme variations in the signal intensity across the sample. In the case of the non-fat products, the signal intensity variation was too great to consider acquiring any usable data. This variation eventually led to the use of the SE experiment. However, even in these experiments, the signal intensity varied more than the ambient noise. It was postulated that the inhomogeneities were caused by variations in the water content of the products on the 50-100 μm range, i.e. the resolution limits of the experiment. In addition, it was thought that inadequate shimming was responsible for the experimental difficulties. Even though the samples were relatively homogeneous, their large size and minor variations in shape interfered with the stringent requirements for reproducible sample orientations in the magnet. The necessity for acquiring images
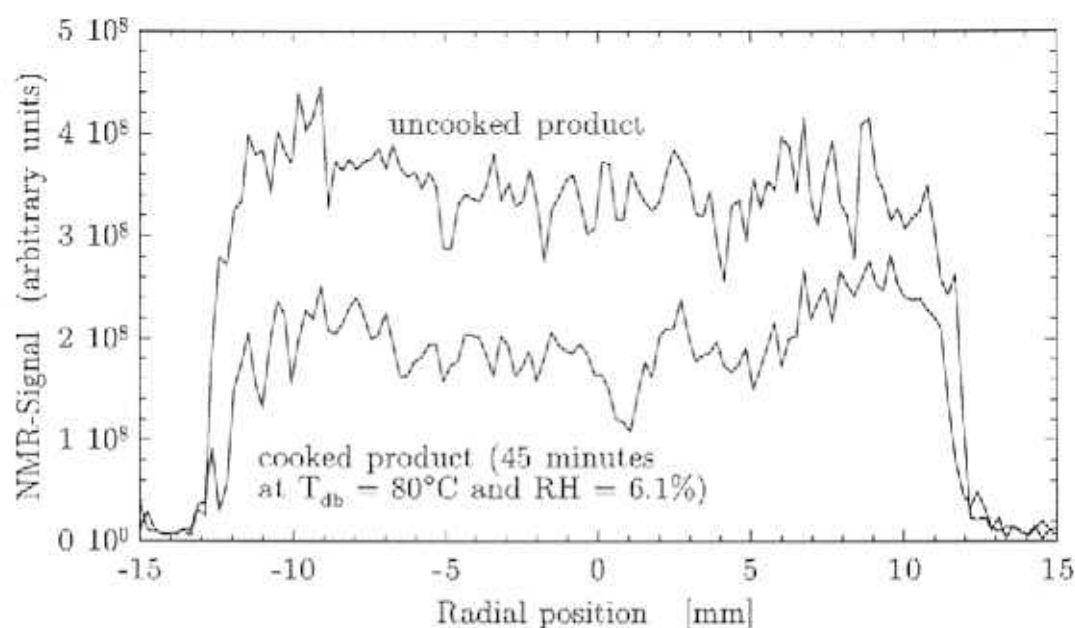
Figure 5.26: NMR-signals from line spin-echo experiments for a full-fat meat emulsion in a cellulose casing before thermal processing (top line) and after processing at 80°C for 45 minutes (bottom line). The measured weight loss between the uncooked and the cooked sample was 7.2%

as rapidly as possible in order to prevent distortions of the moisture profiles limited the available time for shimming between the removal of products from the test section of the processing apparatus and the insertion into the imaging probe. The relatively high salt content of the meat products was also thought to cause imaging problems. Upon cooking, the loading of the radiofrequency coil was outside of the compensation range for the coil. This led to an uncertainty in the absolute signal intensity and a loss in the signal to noise ratio.

In general, the signal to noise limits of the experiment may have made any gradients undetectable. Since the emulsion products were losing only 5 to 10% of the initial water content, the noise across the sample may have hidden this intensity loss even though it was concentrated as a gradient near the edge of the sample. Fewer problems were encountered with the spin-echo experiments but it was still not pos-

sible to obtain reproducible results. Typical magnetic resonance signals from the spin-echo experiments for a full-fat product before and after thermal processing are shown in Figure 5.26. The moisture loss, as measured with a balance after 45 minutes of processing, was 7.2%. However, the obtained magnetic resonance signals indicate a significantly higher moisture loss.

5.7.3 Self-Diffusivities with a PFG-NMR Technique

Several experimental techniques can be used to measure the mutual diffusion coefficients found in Fick's law for binary or multicomponent mixtures. The common starting point for these methods is a non-equilibrium state of a macroscopic system, for example caused by a step change in external species concentrations. Because of the relatively small magnitude of diffusion coefficients in many materials, these methods tend to be very time consuming. In recent years, nuclear magnetic resonance has been used to measure self-diffusion coefficients, also called tracer diffusion or intradiffusion coefficients (Coffman [1994]). These techniques examine systems that are at equilibrium and yield results in a matter of minutes. Although mutual diffusion and self-diffusion describe different phenomena, the two coefficients have been said to be closely related. Different notation schemes for diffusion coefficients can be found in the literature. In the present study, the self-diffusion coefficients are denoted by D' (or D_1^* and D_2^* to indicate the self-diffusion coefficients of different species).

Self-diffusion characterizes the random walk process experienced by molecules in a solution or solid as a result of thermal motion. The mean square displacement, r^2, in an isotropic system without thermal or concentration gradients is given by the Einstein equation

$$\langle r^2 \rangle = 6 D^* t \qquad (5.26)$$

where the angular brackets symbolize a time average. Typical self-diffusion coeffi-

cients for food systems range from about 10^{-9} m^2/s to 10^{-12} m^2/s. The larger figure corresponds to a root mean square displacement of 0.077 mm during one second.

Stejskal and Tanner [1965] reported a method to measure self-diffusion coefficients with a pulsed field-gradient spin-echo nuclear magnetic resonance technique (PFG-NMR). In the PFG-NMR experiment, the application of a magnetic field which varies with position makes it possible to label the molecules by the Larmor precession frequency (Section 5.7.1) and monitors the root mean squared distance the molecule travels during the course of the experiment. The magnetic field is homogeneous throughout the experiment and the effective dispersion and refocussing of the spins occurs in two identical field-gradient pulses. The system is initially at thermodynamic equilibrium in a static magnetic field of strength B_0. The effective observation time Δ over which the self-diffusion coefficient is determined corresponds to the delay time between the two magnetic field-gradient pulses of duration δ.

For unrestricted Brownian diffusion, the ratio of the echo attenuation with and without applied magnetic field gradients is related to the diffusion coefficient and experimental parameters. Stejskal and Tanner [1965] derived the equation

$$S/S_0 = \exp[-(\gamma \, \delta \, g_c \, I)^2 \, D^* \, (\Delta - \frac{\delta}{3})] \tag{5.27}$$

where S is the echo amplitude, S_0 is the echo amplitude in the absence of the field-gradient pulses, γ is the gyromagnetic ratio of the observed nucleus (for the hydrogen nucleus, or proton, $\gamma/2\pi = 42.58$ MHz/T), δ is the duration of the field gradient pulses, g_c is the field gradient produced by the gradient coil per unit current, and I is the current through the gradient coil. If the natural logarithm of the signal of a one-component solution is plotted against the time of the experiments, expressed as $(\gamma \, \delta \, g_c \, I)^2 \, (\Delta - \delta/3)$, a straight line is observed. Equation (5.27) can be extended to the case of two diffusing species with different diffusion coefficients. Assuming that

the two species diffuse independently, one obtains

$$S = S_1 \exp[-(\gamma\,\delta\,g_c\,I)^2\,D_1^*\,(\Delta - \frac{\delta}{3})] + S_2 \exp[-(\gamma\,\delta\,g_c\,I)^2\,D_2^*\,(\Delta - \frac{\delta}{3})] \quad (5.28)$$

where D_1^* and D_2^* are the diffusion coefficients for two species, respectively. If the natural logarithm of the signal of a two-component solution is plotted against the time of the experiments, two distinct slopes are observed if the self-diffusion coefficients of the individual species differ significantly.

When a molecule cannot diffuse freely, for example because it is trapped inside of a small particle within a heterogeneous system, the diffusion coefficient extracted from the PFG-NMR experiment will differ from the diffusivity of the molecule in an unbounded region. As the molecule diffuses for a longer period of time, there is a higher probability that it will encounter the walls of the particle. It can be expected that the echo attenuation at long observation times will be determined by the dimensions of the particle. Several researchers (e.g. Callaghan et al. [1983], Van Den Enden et al. [1990], Lönnqvist et al. [1991], Balinov et al. [1993] Fourel et al. [1994]) have used this phenomenon to relate self-diffusion coefficients measured with a PFG-NMR method for different observation times Δ to the structures of emulsion systems. The appropriate expressions for the spin-echo intensity for restricted diffusion have been derived for various geometries, including parallel barriers and spherical cavities. For restricted diffusion in a spherical cavity, the self-diffusion coefficient is related to the cavity radius R by

$$D^* = \frac{R^2}{5\,\Delta}. \quad (5.29)$$

Experiments with meat emulsions were conducted on a Chemagnetics CMC-300 spectrometer operating at 300 MHz with a 9.8 cm bore superconducting magnet. A glass tube of 5 mm internal diameter was used to introduce the samples into the center of the magnet. Details of the apparatus are described by Gibbs [1989] and in a related
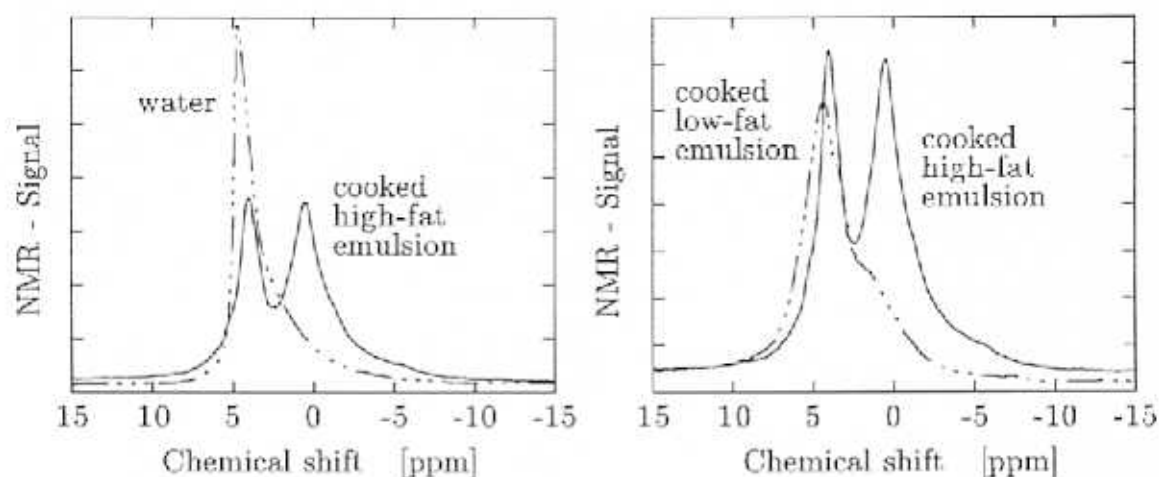
Figure 5.27: One-dimensional NMR spectra for high-fat and low-fat meat emulsion samples. The comparison with water (left plot) allowed the assignment of one of the emulsion peaks to the water protons. The data was collected on a Chemagnetics CMC-300 spectrometer operating at 300 MHz.

paper [Gibbs *et al.*, 1991]. Both uncooked and cooked emulsions were investigated at two temperatures, 25°C and 50°C. The higher temperature was considered too low to cook the uncooked emulsion. The uncooked samples were obtained from a commercial processing operation. The cooked, i.e. processed, products were purchased from a local store. The moisture content of the samples was determined with the A.O.A.C. [1990] oven drying method described in Section 5.3. The uncooked emulsions were filled by means of a syringe into the sample tube. A sharp knife was used to cut sections from the center of the processed products. Two observation times Δ were used in the experiments. The two times ($\Delta = 16.6$ ms and $\Delta = 133$ ms) correspond to one and eight periods of the 60 Hz alternating current used in the experiments. Because of limits in the signal to noise ratio, it is not possible to conduct PFG-NMR experiments with significantly longer observation times. The duration of the field gradient pulses δ and the current through the gradient coil I were varied from 2 to 9 ms and from 0 to 3 A, respectively.

Some of the measured one-dimensional Fourier transformed free induction decays
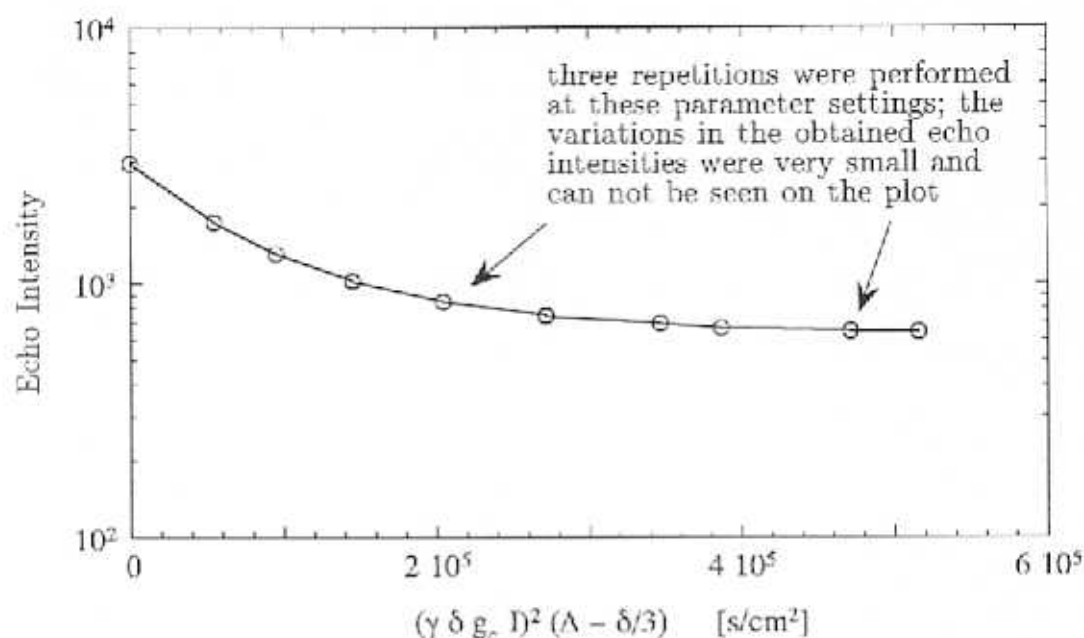
Figure 5.28: Echo intensity for a low-fat cooked meat emulsion at 25°C. Each entry was obtained from the Fourier transformed free induction decay at the corresponding value of the expression $(\gamma \, \delta \, g_c \, I)^2 \, (\Delta - \delta/3)$.

(spectra) of the emulsions are shown in Figure 5.27. The comparison with the spectrum for pure water allowed the assignment of one of the emulsion peaks to the water protons (Figure 5.27-a). The comparison of full-fat and no-fat samples was used to assign the second peak to the lipid protons (Figure 5.27-b). This method of identifying the peaks is similar to the technique reported by Callaghan et al. [1983] for different cheese products. As an example, the measured signal attenuation data at 25°C for the low-fat cooked emulsion is shown in Figure 5.28. The resulting self-diffusion coefficients are summarized in Table 5.7. The diffusivities were obtained from a nonlinear least-squares fit with Equation (5.28) to the data plotted in the form of Figure 5.28. The 95% confidence intervals shown with the diffusivity data in Table 5.7 give the uncertainty associated with the fit, and are not replicate samples or measurements. However, some measurements of echo intensities were conducted three times in order to test the reproducibility of the experimental setup. A very

Table 5.7: Proton self-diffusion coefficients for low-fat and high-fat meat emulsions measured with a pulsed field-gradient nuclear magnetic resonance (PFG-NMR) method[1]. The self-diffusion coefficients D_1^* (for the diffusion of water protons) and D_2^* (for the diffusion of fat protons) were calculated from Equation (5.28). No experiments were conducted at $T = 50°C$ for $\Delta = 133$ ms.

Temperature, sample	Moist. content[2] u, [kg$_m$/kg$_d$]	$\Delta = 16.6$ ms		$\Delta = 133$ ms	
		$D_1^* \times 10^9$ [m^2/s]	$D_2^* \times 10^{11}$ [m^2/s]	$D_1^* \times 10^9$ [m^2/s]	$D_2^* \times 10^{11}$ [m^2/s]
$T = 25°C$					
low-fat, cooked	1.75 (64%)	1.45 ± .03	4.51 ± .72	1.32 ± .02	9.60 ± .41
high-fat, cooked	0.99 (50%)	1.44 ± .06	2.39 ± .50	1.14 ± .02	4.01 ± .25
low-fat, uncooked	3.56 (78%)	1.67 ± .05	28.4 ± 1.8	1.40 ± .02	32.8 ± 2.9
high-fat, uncooked	1.27 (56%)	1.54 ± .14	3.88 ± 1.5	1.34 ± .04	6.75 ± .61
$T = 50°C$					
low-fat, cooked	1.75 (64%)	2.29 ± .16	3.42 ± .89	–	–
high-fat, cooked	0.99 (50%)	2.35 ± .19	2.16 ± .57	–	–
low-fat, uncooked	3.56 (78%)	2.77 ± .07	22.3 ± 6.9	–	–
high-fat, uncooked	1.27 (56%)	2.39 ± .54	2.94 ± .88	–	–

[1] for pure water at 26.5°C, a self-diffusion coefficient of $D^* = 2.33 \times 10^{-9}$ m^2/s was measured
[2] the values in parentheses are the moisture fractions in percent

close agreement was found between the individual results (Figure 5.28). For pure water at 26.5°C, a self-diffusivity of $D^* = 2.33 \times 10^{-9}$ m^2/s was measured with the same experimental setup.

The values obtained for the water self-diffusivities in meat emulsions are somewhat smaller than the self-diffusivity for pure water and indicate that the water molecules cannot diffuse as unrestricted as in free solution. However, the values obtained for the self-diffusion coefficients of water are in general one order of magnitude larger than the values for effective moisture diffusivities reported by Agrawal [1976], who found that values of D_{eff} between 0.6 and 1.3×10^{-10} m^2/s best described the moisture concentration profiles and moisture losses during the processing of meat emulsion products. The decrease of the obtained water self-diffusion coefficients with increasing

time Δ at $T = 25°C$ indicates that the water molecules are restricted at a length scale that corresponds to this time span (16.6 to 133 ms), for example at the interfaces of protein matrix and fat particles. In general, the short times Δ during which the self-diffusion is monitored in the PFG-NMR experiment seems to prevent conclusions about its magnitude at longer times, i.e. the times during which moisture diffusion occurs in the processing of meat emulsion products (minutes to hours).

Equation (5.29) can be used to estimate the size of the fat droplets in the meat emulsion. Using an observation time of $\Delta = 133$ ms and the range of self-diffusion coefficients for the fat protons listed in Table 5.7 ($D^* = 4 \times 10^{-11}$ to $D^* = 30 \times 10^{-11}$ m^2/s) yields cavity radii of 5.2 μm to 14.1 μm. These values agree with the findings reported by Carrol and Lee [1981] who investigated meat emulsions with a light microscope and found the lipid droplets to range in size from 100 μm down to the resolution of the microscope (Section 2.8).

Chapter 6

Parameter Estimation and Simulation Results

In this chapter, a nonlinear parameter estimation program, together with the simulation model developed in Chapter 3, is used to determine the effective moisture diffusion coefficient of the meat emulsion from experimentally determined data. These data include the temperature, moisture loss and moisture profile measurements conducted in this study (described in Chapter 5) and the temperature data for the processing of large diameter emulsion products reported by Hanson [1988]. Several functional forms of the effective moisture diffusion coefficient are investigated for their potential of minimizing the deviations between measured and simulated data.

Most of the input parameters of the simulation model developed in Chapter 3 were taken from data reported in previous work, for example the specific heat and the thermal conductivity of meat emulsions (Chapter 2), or were determined experimentally, for example the average heat transfer coefficients in various processing environments (Chapter 5). Very little reliable data for the moisture diffusion coefficient were found in the literature. Since this parameter is believed to have a large influence on the simulation results, measurements were attempted with a pulsed field-gradient nuclear

magnetic resonance method (Section 5.7.3). However, the self-diffusivities obtained with this technique showed a dependence on the relatively short times of observation during the magnetic resonance experiments (16.6 ms and 133 ms) and could therefore not be related to the effective moisture diffusion coefficients found during the processing of meat emulsion products. Hence, the effective moisture diffusion coefficient was determined indirectly from the measured dependent variables, i.e. the temperature profiles, moisture profiles and moisture losses (Chapter 5). For this purpose, a nonlinear parameter estimation program, in conjunction with the simulation model developed in Chapter 3, was used to compute the effective moisture diffusion coefficients that provided the best fit of measured and simulated data. In addition to the dependent variables measured in this study, the effective moisture diffusion coefficient was estimated from the temperature data for the processing of bologna products as reported by Hanson [1988] (Section 2.4). However, since the values of the average heat transfer coefficients were not reported in Hanson's study, the nonlinear parameter estimation program was used to determine both the moisture diffusion coefficient and the heat transfer coefficient from the reported data.

6.1 The Parameter Estimation Program

In principle, the parameter vector of the simulation model that minimizes the deviations between measured data and modeled results could be obtained from a systematic investigation of all possible parameter values. In practice, however, this approach is too time consuming and a methodology that selects the parameters based on the responses of the previous parameter choice is necessary. This task is accomplished by parameter estimation programs. The computer program GREG (Stewart *et al.* [1993]), written in FORTRAN, was used for the parameter estimation calculations in this study. The parameters providing the best fit between measured and simulated
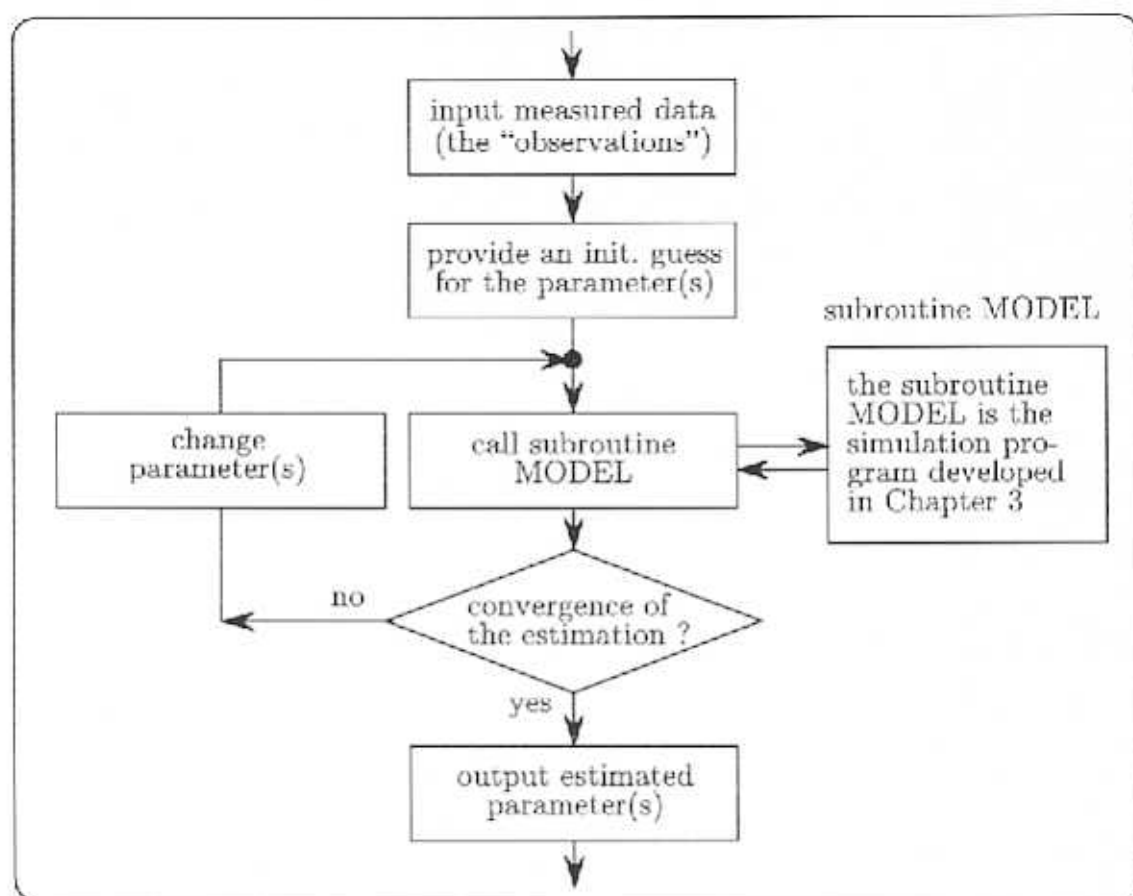
Figure 6.1: Procedure used by the nonlinear parameter estimation program to find the values of the effective moisture diffusion coefficient and the heat transfer coefficient that minimize the deviations between measured and simulated data. The subroutine MODEL, i.e. the simulation program provided by the user, is linked with the parameter estimation program.

data are found by calling the simulation model with different parameter values. The parameter vector can represent a single model parameter, for example the (constant) moisture diffusivity, or several model parameters, for example the coefficients in a function for the moisture diffusivity if the latter depends on the moisture concentration and/or the temperature (Table 6.1). The parameters can be estimated from the measured data (also called observations) of one or several dependent variables. The terms single-response and multiresponse are used to describe these situations. The

minimization with GREG is performed by a modified Newton method, starting from a supplied initial guess for the parameters. In each iteration, the objective function, i.e. the deviations between the measured and simulated data, is approximated by a quadratic function over a feasible region of the space given by the supplied lower and upper bounds of the parameters. The objective function for single-response estimations is the weighted sum of squares of the deviations of the observations. For multiresponse estimations, a modified objective function can be used if the relative precisions of the responses are unknown. A minimum point is then computed from the quadratic approximation and the resulting parameters are changed when a further minimization of the objective function is possible. These iterations are repeated until a convergence criterion is satisfied or a maximum allowable number of iterations is reached. A graphical representation of the described procedure is given in Figure 6.1.

6.2 Estimation Results and Residuals

In this section, the results of the parameter estimations are described. The residuals are plotted in Subsections 6.2.1 to 6.2.5. In all plots showing measured and simulated data, the former are drawn with solid lines. Values of the model parameters that did not change with parameter estimations and simulations for different experiments are summarized in Table 6.2. These values were obtained from measurements (Chapter 5) or from findings reported in the literature.

Several models for the effective moisture diffusion coefficient were investigated. In addition to a constant effective moisture diffusion coefficient, several functional forms accounting for possible concentration and temperature dependencies were examined (Table 6.1). However, the objective functions for the multiparameter models were only marginally smaller than the residuals obtained using constant moisture diffusion coefficients. The results of the parameter estimation with constant diffusion coeffi-

Table 6.1: Functional forms of the effective moisture diffusion coefficient investigated with the nonlinear parameter estimation program for their potential of minimizing the deviations between measured and simulated data.

Investigated model	Comment
$D_{eff} = \text{const.}$	simplest case
$D_{eff} = a\, u^b\, T^c$	three parameter model
$D_{eff} = a\, \exp\left(u^b\, T^c\right)$	three parameter exponential model
$D_{eff} = a\, \exp\left(b + c\, u^d + e\, T^f\right)$	six parameter exponential model

cients for all simulations described in the following subsections are summarized in Table 6.3. The last column indicates the figure where the measured data are plotted together with the simulated results, using the moisture diffusion coefficient and the heat transfer coefficient computed with the parameter estimation program.

6.2.1 Temperature data from small diameter products

Surface and center temperatures of full-fat and no-fat small and medium diameter products processed in the test section of the laboratory apparatus at different relative humidities were recorded with thin thermocouples (Section 5.2). The data acquisition system was set at a sampling interval of 5 seconds. Therefore, 1080 time/temperature observations were recorded for each thermocouple in experiments lasting 90 minutes. From these data, 32 pairs of surface and center temperatures, distributed between times of 0 and 85 minutes were selected from each experiment as the observations for the parameter estimation program. The heat transfer coefficient in the test section of the laboratory apparatus was measured with a solid aluminum probe using the lumped capacitance method (Section 5.4) and a value of 33.3 W/m^{2}K was obtained. The analogy of heat and mass transfer (Section 5.4) was then used to calculate a

Table 6.2: Values of the model parameters that did not change with simulations or parameter estimations for different processing conditions.

Simulation parameter and value or model	Comments	Defined/described in Section/on page
dry density, kg_d/m^3		
$\rho_d = 434$	for full-fat emulsion	5.6/117
$\rho_d = 135$	for no-fat emulsion	5.6/117
heat of evaporation of water, kJ/kg		
$\Delta \hat{H}_v = 3165 - 2.426\, T$ [K]	curve fit to tabulated data	
specific heat, kJ/kg K		
$c_d = 1.58$	for the dry emulsion components	2.1/13
$c_w = \sum_0^5 a_i T^i$	for water, the a_i's are given below	
$c = \omega_d c_d + \omega_w c_w$	ideal solution model for emulsion	3.2.1/45
thermal conductivity, W/m K		
$k = 0.080 + 0.52\,\omega_m$	for all meats, as reported by Swent [1975]	2.1/13
equilibrium moisture content, kg_m/kg_d		
$u = \sum_1^5 b_i\, RH^i$	curve fit to data reported by Igbeka and Blaisdell [1982], the b_i's are given below	2.5/23

$a_0 = 757.1$, $a_1 = -11.56$, $a_2 = 7.0838 \times 10^{-2}$, $a_3 = -2.1655 \times 10^{-4}$, $a_4 = 3.3019 \times 10^{-7}$
$a_5 = -2.0088 \times 10^{-10}$, $b_1 = 1.0802$, $b_2 = -8.3266$, $b_3 = 30.65$, $b_4 = -48.919$, $b_5 = 28.408$

mass transfer coefficient of 1.8×10^{-7} kg/Pa m^2 s. The initial temperature of the meat products was 6°C. Initial moisture concentrations of $u = 1.358$ kg$_m$/kg$_d$ for the full-fat emulsions and $u = 6.692$ kg$_m$/kg$_d$ for the no-fat samples, corresponding to moisture mass fractions of 0.576 and 0.870, respectively, were measured and used in the simulations. The values of the effective moisture diffusion coefficients computed with the parameter estimation program ranged from 1.13×10^{-10} to 2.24×10^{-10} m^3/s for the full-fat emulsion and from 1.77×10^{-10} to 3.55×10^{-10} m^2/s for the no-fat samples (Table 6.3). Since all full-fat emulsions used in these small diameter temperature experiments came from the same batch, an average value of $D_{eff} = 1.48 \times 10^{-10}$ m^3/s was calculated for this emulsion type. The variations in the estimated results are caused by limitations of the experimental data and/or the simulation model. Similarly, all

Table 6.3: Results from the nonlinear parameter estimation. The given values of the effective moisture diffusivity and the heat transfer coefficient provide the best fit of measured and simulated data. The values in parentheses give the 95% probability interval of the corresponding parameter.

Values of the effective moisture diffusion coefficient in $[m^2/s]$ and the heat transfer coefficient in $[W/m^2\,K]$			Figure/ on page
temperature profiles from small diameter products in cellulose casings			
	full-fat product	no-fat product	
$RH = 6.1\%$	$D_{eff} = 2.24\,(\pm0.135)\times10^{-10}$	$D_{eff} = 3.55\,(\pm0.341)\times10^{-10}$	6.2/139
$RH = 15.6\%$	$D_{eff} = 1.07\,(\pm0.098)\times10^{-10}$	$D_{eff} = 2.52\,(\pm0.155)\times10^{-10}$	6.2/139
$RH = 32.4\%$	$D_{eff} = 1.13\,(\pm0.185)\times10^{-10}$	$D_{eff} = 1.77\,(\pm0.109)\times10^{-10}$	6.2/139
average value	$D_{eff} = 1.48\times10^{-10}$	$D_{eff} = 2.61\times10^{-10}$	
temperature profiles from full-fat medium diameter products in fibrous casings			
$T_{db} = 77°C,\ RH = 7.1\%$		$D_{eff} = 1.63\,(\pm0.203)\times10^{-10}$	6.3/141
$T_{db} = 77°C,\ RH = 18.0\%$		$D_{eff} = 0.910\,(\pm0.201)\times10^{-10}$	6.3/141
$T_{db} = 77°C,\ RH = 37.4\%$		$-^1$	6.3/141
average value		$D_{eff} = 1.27\times10^{-10}$	
moisture loss experiments			
full-fat product in batch smokehouse		$D_{eff} = 0.913\,(\pm0.151)\times10^{-10}$	6.4/143
full-fat product in the laboratory app.		$D_{eff} = 0.987\,(\pm0.121)\times10^{-10}$	6.5/143
no-fat product in the laboratory app.		$D_{eff} = 3.73\,(\pm0.247)\times10^{-10}$	6.6/144
moisture profile experiments			
small diameter product (full-fat)		$D_{eff} = 2.52\,(\pm1.95)\times10^{-10}$	6.7/146
large diameter product (low-fat)		$D_{eff} = 2.36\,(\pm0.182)\times10^{-10}$	6.8/146
temperature data reported by Hanson			
$T_{db} = 91°C,\ RH = 40\%$	$h = 40.4\,(\pm3.6)$	$D_{eff} = 5.10\,(\pm1.20)\times10^{-10}$	6.9/149
$T_{db} = 82°C,\ RH = 60\%$	$h = 48.2\,(\pm8.6)$	$-^1$	6.10/149
$T_{db} = 75°C,\ RH = 80\%$	$h = 65.4\,(\pm17.2)$	$-^1$	6.11/150
average value	$h = 51.3$		

[1] the uncertainties associated with these parameter estimations were too large to extract useful information

no-fat emulsions were taken from one batch. The average moisture diffusivity in this case was $D_{eff} = 2.61\times10^{-10}$ m^2/s. These values were used in the final plots of the residuals which are shown in Figure 6.2. In order to facilitate an easy comparison be-

tween the different levels of the relative humidity and the emulsion type (full-fat and no-fat), the individual plots are arranged on a single page. Overall, a good agreement between the measured and simulated data can be observed. The relative humidity has only a small influence on the measured temperatures. The simulated results are more affected by the humidity level. At low humidities (6.1%), the simulation model tends to overestimate the measured surface and center temperatures for both full-fat and no-fat products. At the higher relative humidities, the simulated temperatures at some processing times are smaller than the measured data.

6.2.2 Temperature data from medium diameter products

The surface and center temperatures of a full-fat medium diameter meat emulsion product processed in the test section of the laboratory apparatus were measured for two types of casings, a moisture-impermeable polyamide material and moisture-permeable cellulose casings. The selection of a subset of data from all the temperatures recorded with the data acquisition system was described in the previous subsection. The heat transfer coefficients for the medium diameter products were calculated from Equation (5.13), using the measured heat transfer coefficients for the small diameter products and the known air velocities for the experiments with small and medium diameter samples. Values of $h = 39.4$ W/m^{2}K for $D_{pr} = 43$ mm and $h = 45.2$ W/m^{2}K for $D_{pr} = 45$ mm were calculated (Table 5.4). For the products contained in moisture-permeable fibrous casings, mass transfer coefficients of 2.0×10^{-7} kg/Pa m^2 s were obtained from the analogy of heat and mass transfer (Section 5.4). The initial temperature and moisture concentration of the medium diameter products was 6°C and 1.358 kg$_m$/kg$_d$ ($\omega_m = 0.576$), respectively. For the products in moisture-permeable fibrous casings, the effective moisture diffusion coefficients calculated with the parameter estimation program were $D_{eff} = 1.63 \times 10^{-10}$ m^2/s for the
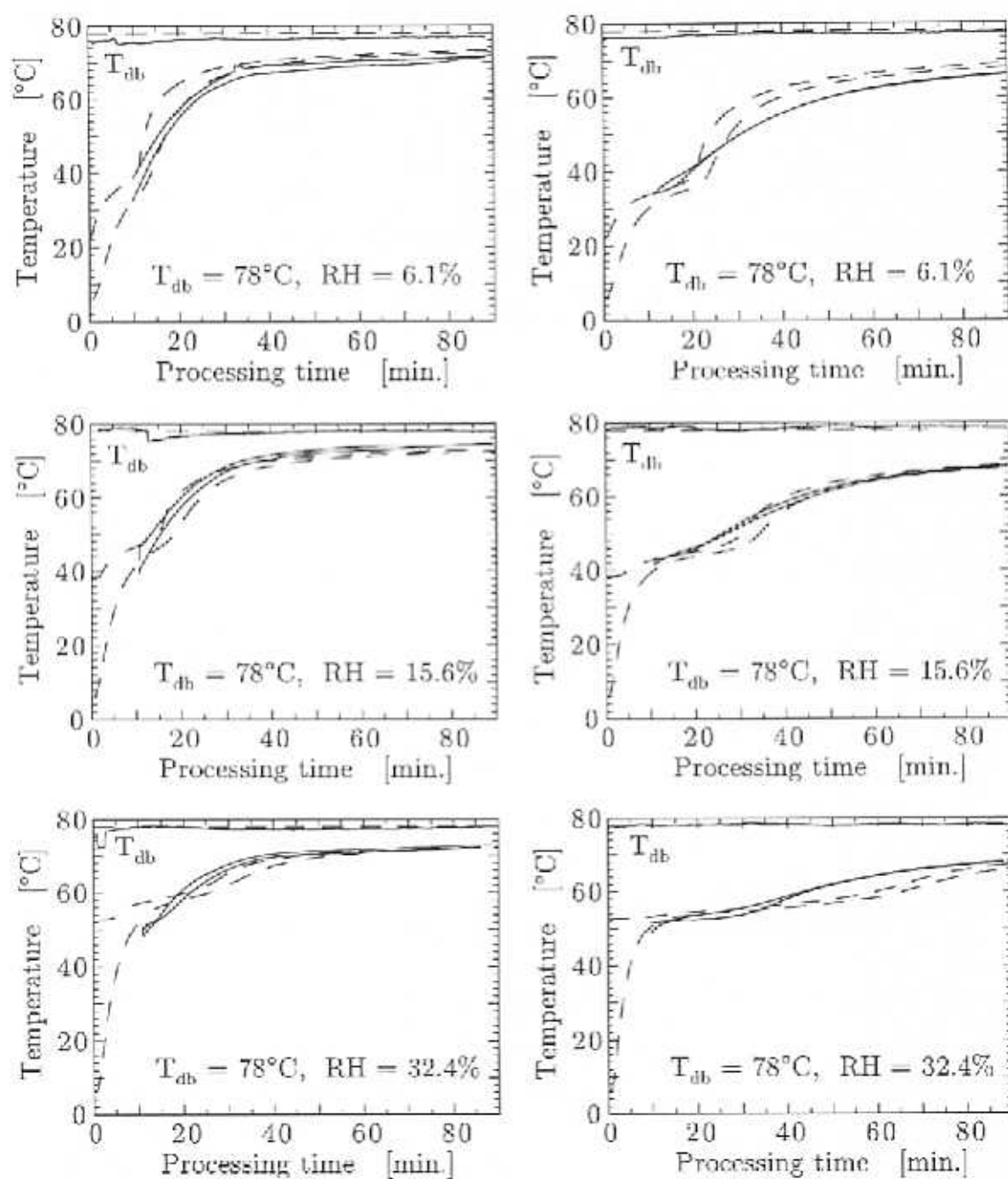
Figure 6.2: Comparison of measured and simulated surface and center temperatures for full-fat (left plots) and no-fat (right plots) small diameter meat emulsion products processed in moisture-permeable cellulose casings at three relative humidities. The measured and simulated data are plotted with solid and dashed lines, respectively. The settings of the simulation parameters not given in the plots are described in the text.

lowest investigated relative humidity (7.1%) and $D_{eff} = 0.91 \times 10^{-10}$ m^2/s for medium humidity (18.0%). The uncertainty associated with the parameter estimation for the higher humidity case was too large to allow for the extraction of useful information. An average effective moisture diffusivity of 1.27×10^{-10} m^2/s was calculated for medium diameter products and was used in the final plots of the residuals which are shown in Figure 6.3. As in the presentation of the data in the previous subsection, all plots are arranged on one page. A good agreement between the measured and simulated data can be observed for the products processed in the moisture-impermeable polyamide casings (left plots). However, the simulated surface temperature tends to overestimate the measured data. For the higher humidity case ($RH = 37.4\%$), the measured surface temperature at early processing times ($t < 10$ minutes) is approximately 7°C below the dew point temperature of 54.9°C that is used as the constant temperature boundary condition in the simulation model. However, the qualitative behavior of the measured and simulated surface temperatures, i.e. a period of relatively constant temperatures followed by an increase after processing times of 10 to 15 minutes, agrees well for this higher humidity case. At the lower investigated humidities ($RH = 7.1\%$ and $RH = 18.0\%$), this distinct behavior cannot be seen for either the measured or the simulated data. The measured and simulated center temperatures for all three investigated relative humidities are in very good agreement. For the products processed in the moisture-permeable fibrous casings, the agreement between experiments and simulation is less pronounced. For all three levels of the relative humidity, the simulated surface temperatures at early processing times tend to plateau at the wet bulb temperatures of the processing air, followed by a distinct increase at later processing times. For the two lower relative humidity cases, this behavior is not seen with the measured data. At the higher humidity ($RH = 37.4\%$), the measured surface temperature displays a similar behavior at early processing
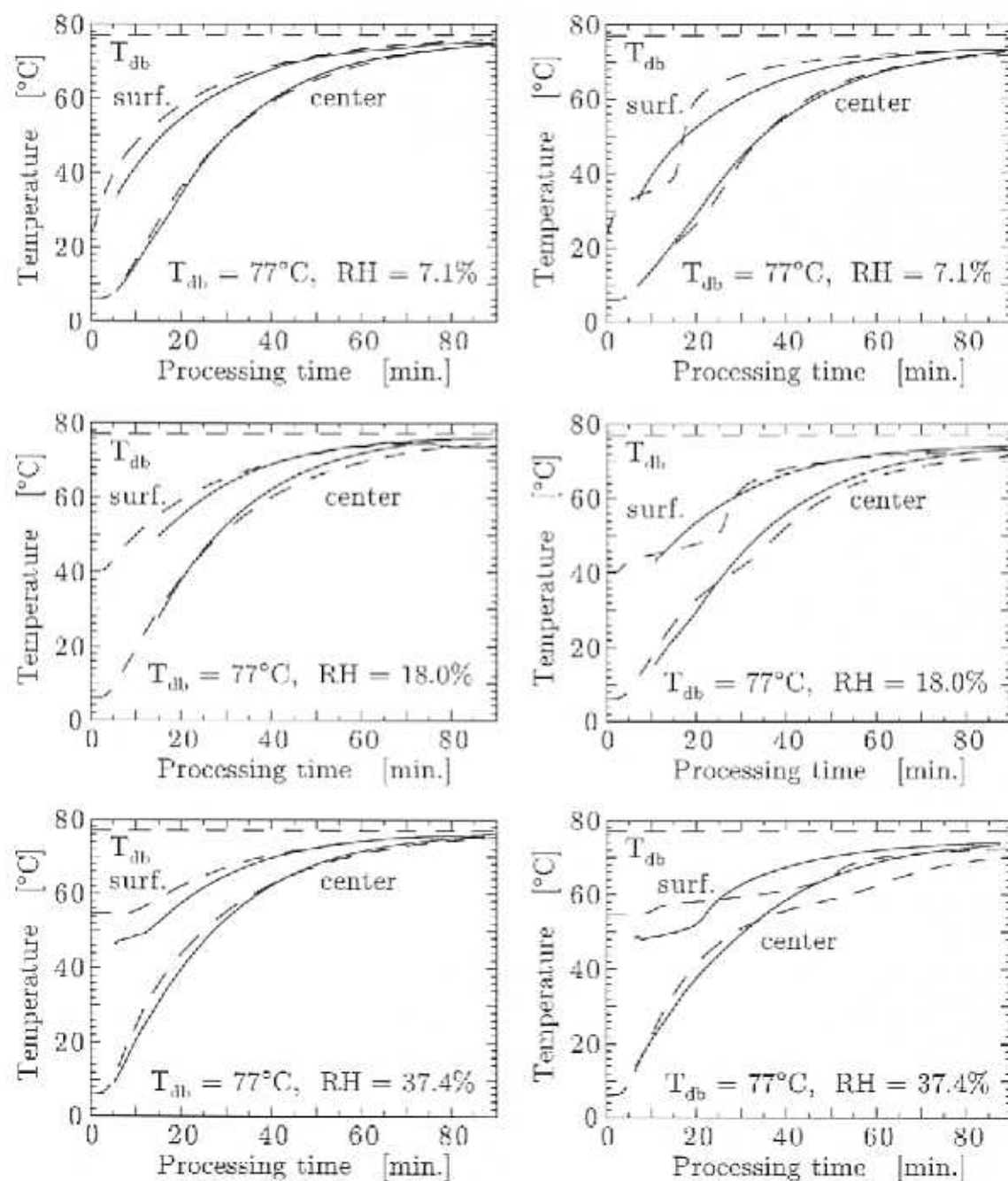
Figure 6.3: Comparison of measured and simulated surface and center temperatures for full-fat medium diameter meat emulsion products processed in moisture-impermeable polyamide casings (left plots) and moisture-permeable fibrous casings (right plots). The measured and simulated data are plotted with solid and dashed lines, respectively. The values of simulation parameters not given in the plots are described in the text.

times with temperatures approximately 5°C below the wet bulb and dew point temperatures of the processing air. Dry bulb, wet bulb and dew point temperatures for all temperature profile experiments with small and medium diameter products conducted in this study are summarized in Table 5.1. A somewhat better agreement between measured and simulated data is observed for the center temperatures. For the higher humidity ($RH = 37.4\%$), the difference between measured and simulated surface temperature translates into a proportional difference for the two center temperatures. For the two lower humidities, the difference between the measured and simulated center temperatures is relatively small.

6.2.3 Moisture loss data

The moisture loss of small diameter meat emulsion products in water-permeable cellulose casings during processing was monitored for full-fat emulsions in a commercial batch type smokehouse and for both full-fat and no-fat emulsions in the test section of the laboratory apparatus (Section 5.5). Two experiments under the same conditions were conducted for the full-fat and no-fat products in the test section of the laboratory apparatus. The measured data from both experimental runs were in very close agreement (Figure 5.25) and the results from the first experiments were used as the input for the parameter estimation program. In both processing environments, the heat transfer coefficients were measured with the lumped capacitance method using a small solid aluminum probe (Section 5.4). Values of $h = 66.0$ W/m^{2}K and $h = 33.3$ W/m^{2}K were obtained in the batch type smokehouse and the test section of the laboratory apparatus, respectively. Mass transfer coefficients of 4.0×10^{-7} kg/Pa m^2 s and 1.8×10^{-7} kg/Pa m^2 s, respectively, were calculated from the analogy of heat and mass transfer (Section 5.4). The initial moisture contents were $u = 1.358$ kg$_m$/kg$_d$ for the full-fat emulsions and $u = 6.692$ kg$_m$/kg$_d$ for

Figure 6.4: Comparison of measured and simulated moisture losses for a full-fat emulsion contained in moisture-permeable cellulose casings and processed in a commercial batch type smokehouse.

Figure 6.5: Comparison of measured and simulated moisture losses for a full-fat emulsion contained in a moisture-permeable cellulose casing and processed in the test section of the laboratory apparatus.
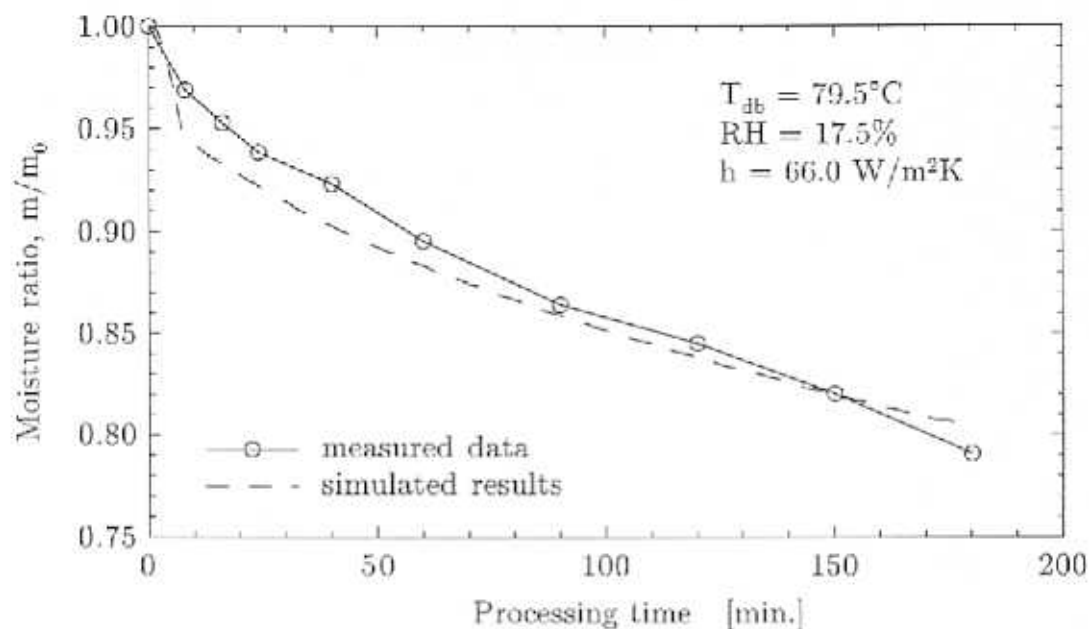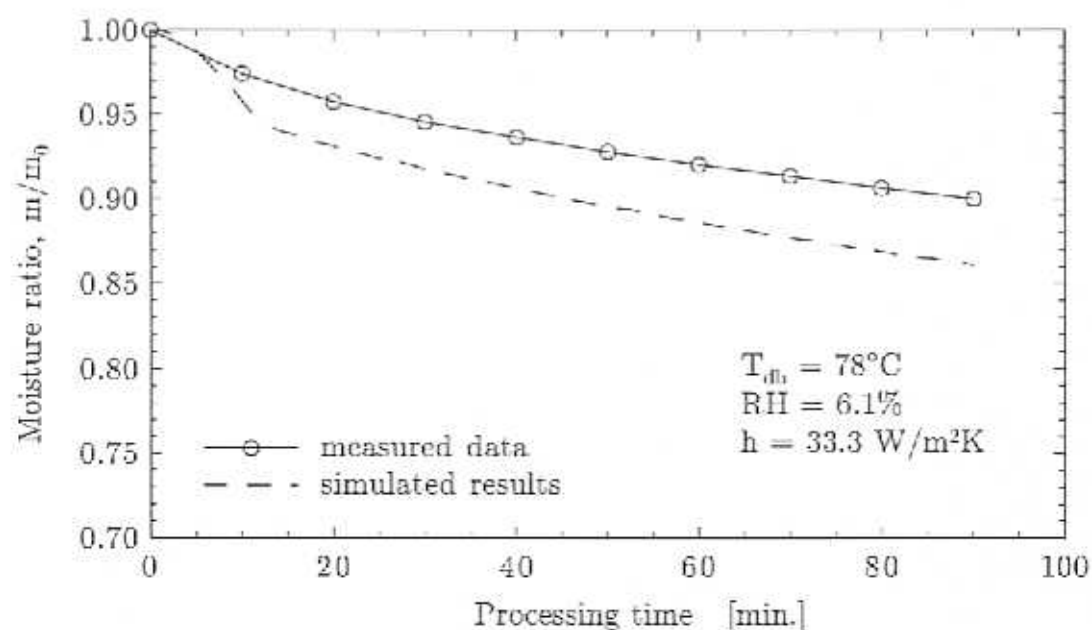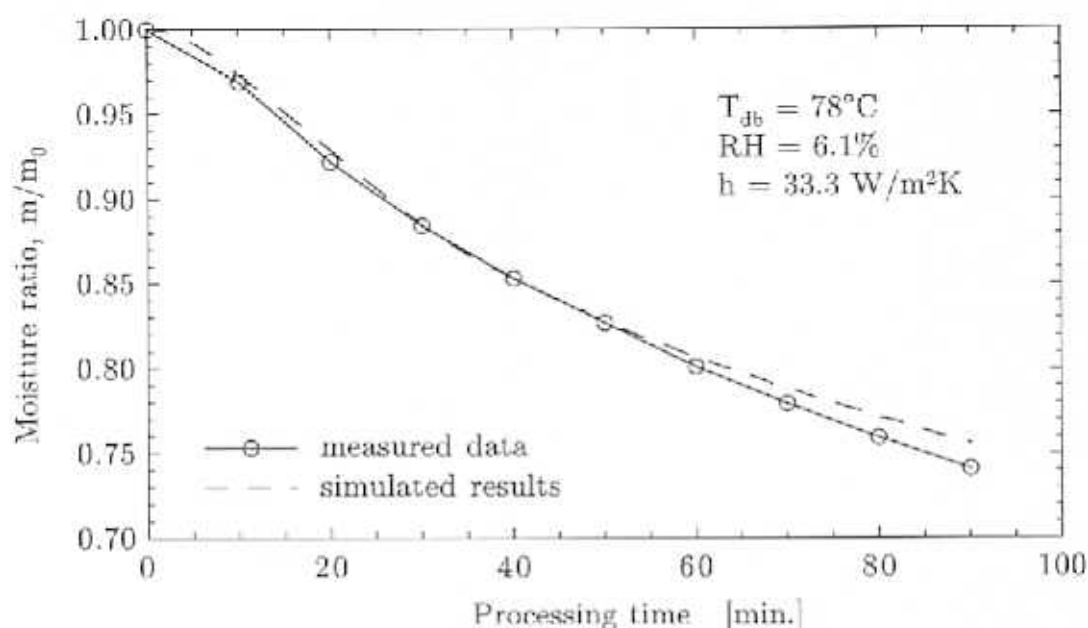
Figure 6.6: Comparison of measured and simulated moisture losses for a no-fat emulsion contained in a moisture-permeable cellulose casing and processed in the test section of the laboratory apparatus.

the no-fat samples, corresponding to moisture mass fractions of 0.576 and 0.870, respectively. The effective moisture diffusion coefficients computed with the parameter estimation program were 0.913×10^{-10} m^2/s for the full-fat product processed in the smokehouse and 0.987×10^{-10} m^2/s for the full-fat product in the test section. A value of 3.73×10^{-10} m^2/s was obtained for the no-fat product. The values for the two full-fat products are in close agreement and are similar to the values determined from the temperature data described in the two previous subsections. However, the full-fat emulsions were obtained from different batches and it was concluded that the small variations in the estimated values for the diffusion coefficients could be caused by differences in the composition of the emulsions. Therefore, no average values were formed and the residual plots for the two full-fat moisture loss experiments were computed using the individual diffusion coefficients given in Table 6.3. The effective diffusivity for the no-fat emulsion is higher than those obtained for the full-fat

products. This difference was attributed to the higher moisture content of the no-fat emulsion. The comparison of measured and simulated data for the full-fat product investigated in the batch type smokehouse is shown in Figure 6.4. A good agreement between experiments and computed results can be seen. The simulation model accurately describes the relatively large moisture loss during the first 10 minutes of the experiment, followed by a period of a relatively constant decrease in the mass of the product. The comparisons of measured and simulated data for the full-fat and no-fat products processed in the test section of the laboratory apparatus are shown in Figure 6.5 and 6.6, respectively. The results computed with the simulation model overestimate the moisture loss for the full-fat product. At the end of the experiment, a difference of approximately four percent in the moisture ratio is observed. A much better agreement of measured and simulated data exists for the no-fat product (Figure 6.6). Here, the simulation model accurately predicts the moisture loss during the whole course of the experiment.

6.2.4 Moisture profile data

Values of the moisture concentration of processed products at different radial positions were measured with invasive methods for large ($D_{pr} = 10.8$ cm (4.25 inch)) and small ($D_{pr} = 23$ mm (0.87 inch)) diameter samples after emerging from the final thermal processing zones of commercial smokehouses (Section 5.3). The thermal schedules used in the processing operations were summarized in Table 5.2. The data for the large diameter product were obtained from three different circumferential positions of a slice cut from the center of the product (Figure 5.15). An average moisture concentration was calculated for each radial position and was used as the observation input for the parameter estimation program. The moisture profile data from the small diameter product were obtained from four samples processed under identical

Figure 6.7: Comparison of measured and simulated moisture profiles for a small diameter product processed in a commercial smokehouse. The processing conditions in the individual smokehouse zones are given in Table 5.2.
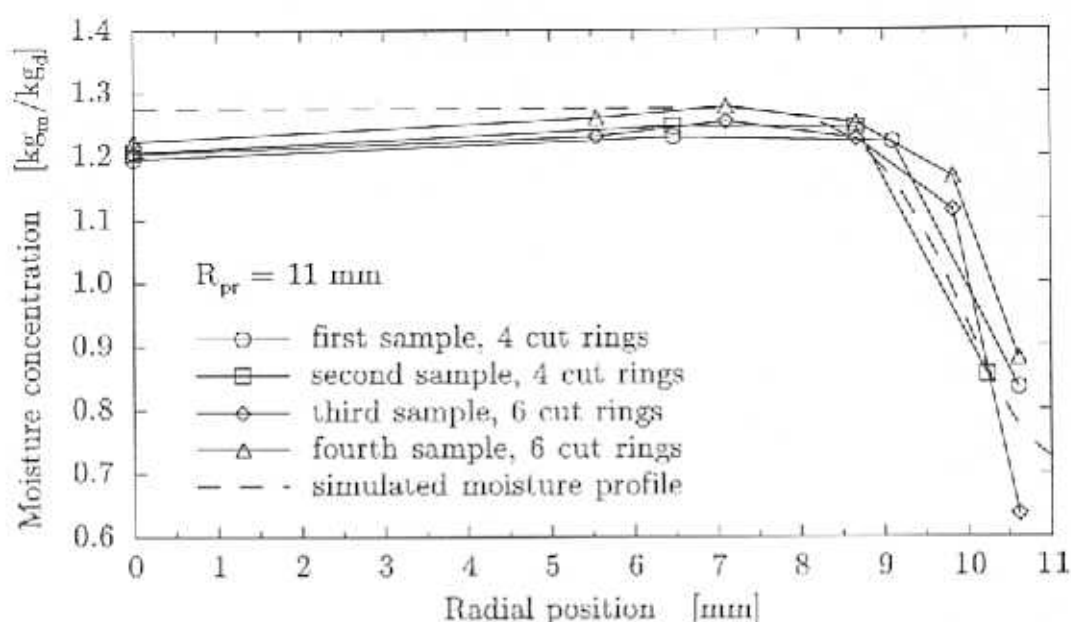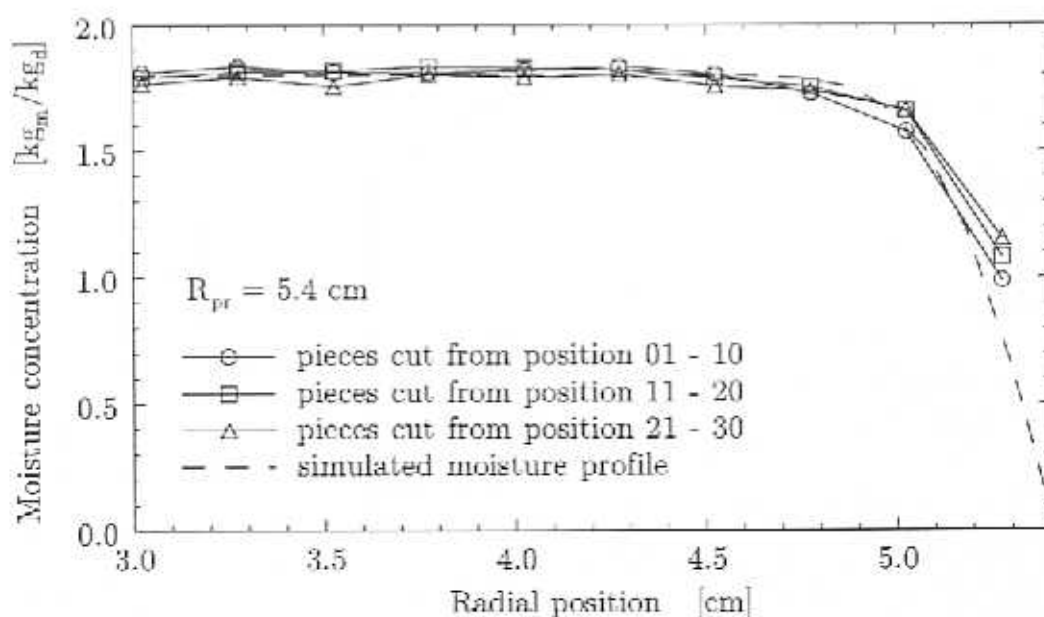

Figure 6.8: Comparison of measured and simulated moisture profiles for a large diameter product processed in a commercial smokehouse. The processing conditions in the individual smokehouse zones are given in Table 5.2.

conditions (Figure 5.16). An average moisture concentration profile was calculated from all four samples and was used with the parameter estimation program. The average heat transfer coefficients were measured with a lumped capacitance method. A solid aluminum probe and a brine-filled aluminum vessel were used for the small and the large diameter processes, respectively. The measured heat transfer coefficients in the individual processing zones are summarized in Table 5.4. The analogy of heat and mass transfer (Section 5.4) was used to calculate the corresponding mass transfer coefficients. After processing, the moisture concentration in the center of the products remained at their initial value. For the small diameter product, an initial moisture content of $u = 1.275$ kg$_m$/kg$_d$ was determined. This value translates into a moisture mass fraction of 0.560 and is therefore very close to the target value of 0.576 used in the manufacturing of the full-fat meat emulsion. An initial moisture content of $u = 1.8$ kg$_m$/kg$_d$, corresponding to a moisture mass fraction of 0.643, was used with the simulations of the large diameter product. Effective moisture diffusivities of 2.52×10^{-10} m^2/s and 2.36×10^{-10} m^2/s were found for the small and large diameter products, respectively. However, the uncertainty associated with the parameter estimation for the small diameter product is relatively large and the actual value could be closer to the diffusion coefficients found in the previous simulations for full-fat emulsions. The diffusion coefficient estimated from the low-fat large diameter product falls between the values for the full-fat and no-fat emulsions and hence indicates a connection between moisture content and effective moisture diffusivity. The comparison of measured and simulated data for the small diameter product is shown in Figure 6.7 and a very good agreement can be observed. The decrease of the measured moisture concentration towards the center of the product is thought to be the result of the procedure used to cut the individual sample pieces (Section 5.3). The moisture concentration at the product surface is very well represented by the simulation

model. The simulated data show a point of inflection near the product surface. This behavior is caused by the settings of the dry bulb temperature and relative humidity in the individual processing zones (Table 5.2). A low relative humidity in the second processing zone is followed by larger values in the final two zones. Hence, a large potential for mass transfer at the beginning of the processing causes relatively large internal moisture concentration gradients. When the potential for mass transfer decreases in the last two processing zones, the steep gradients relax and cause the point of inflection. Because of the relatively few experimental data points, this behavior cannot be seen in the measured data. Overall, there is no evidence that the Fickian approach is not an accurate predictor for mass transfer as suggested by Ruan et al. [1991] and Schrader et al. [1992] for somewhat different systems. The comparison of measured and simulated data for the large diameter product is shown in Figure 6.8. Similar to the simulation for the small diameter product, a very good agreement between the experiments and the computed data can be observed. The calculated moisture gradients at the product surface agree very well with the measured data. Since the driving force for mass transfer was high throughout the thermal processing, no inflection point in the moisture concentration near the product surface is observed. The overall good agreement of measured and simulated data reiterates the successful use of the Fickian approach for mass transfer within the product.

6.2.5 Temperature data for bologna processing

Hanson [1988] investigated the effects of various processing conditions on the heat and mass transfer in large diameter (10.4 cm (4.1 inch)) meat emulsion products. Two types of casings were used in this study, moisture-permeable standard fibrous casing and moisture-impermeable fibrous casing. The product temperature at four different locations (surface, 1/4 and 1/2 of the distance to the center and center),

Figure 6.9: Simulated and measured (as reported by Hanson [1988]) surface and center temperatures for the processing of bologna at a humidity of 40%.

Figure 6.10: Simulated and measured (as reported by Hanson [1988]) surface and center temperatures for the processing of bologna at a humidity of 60%.
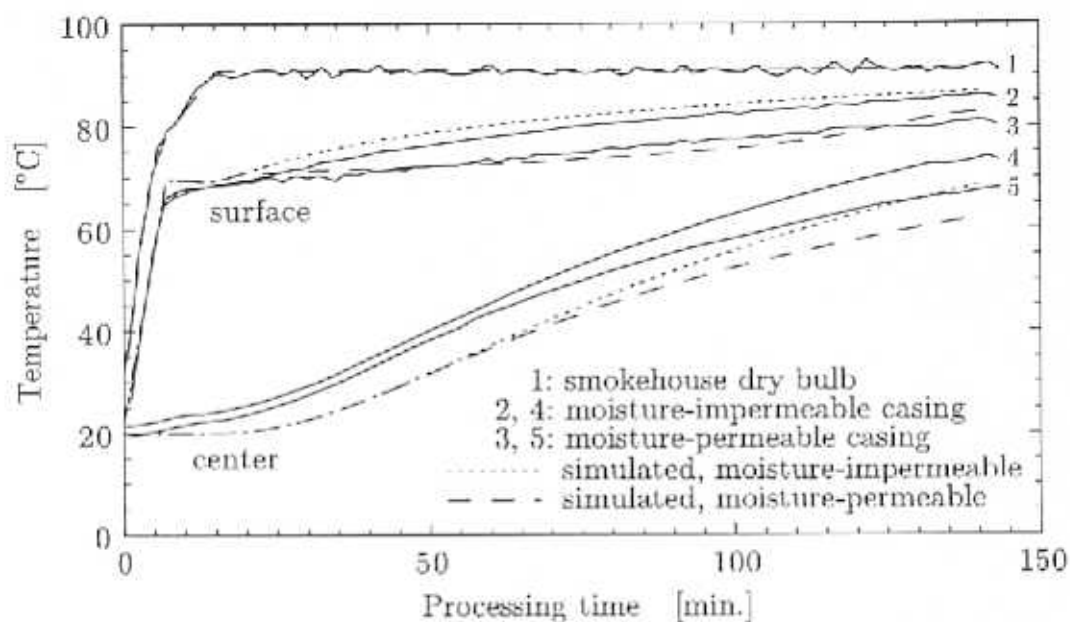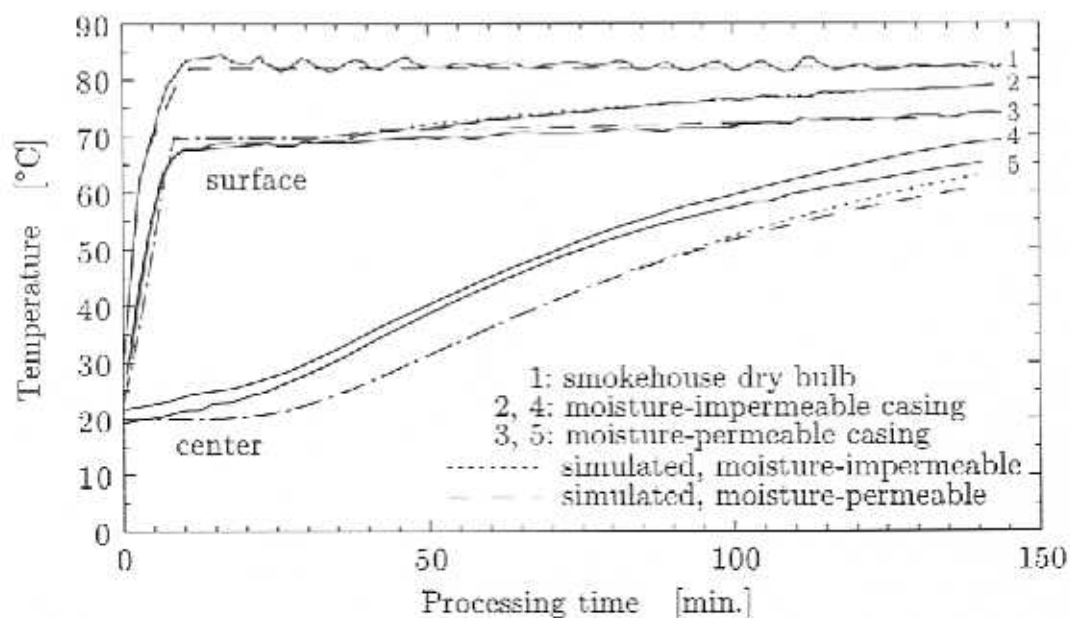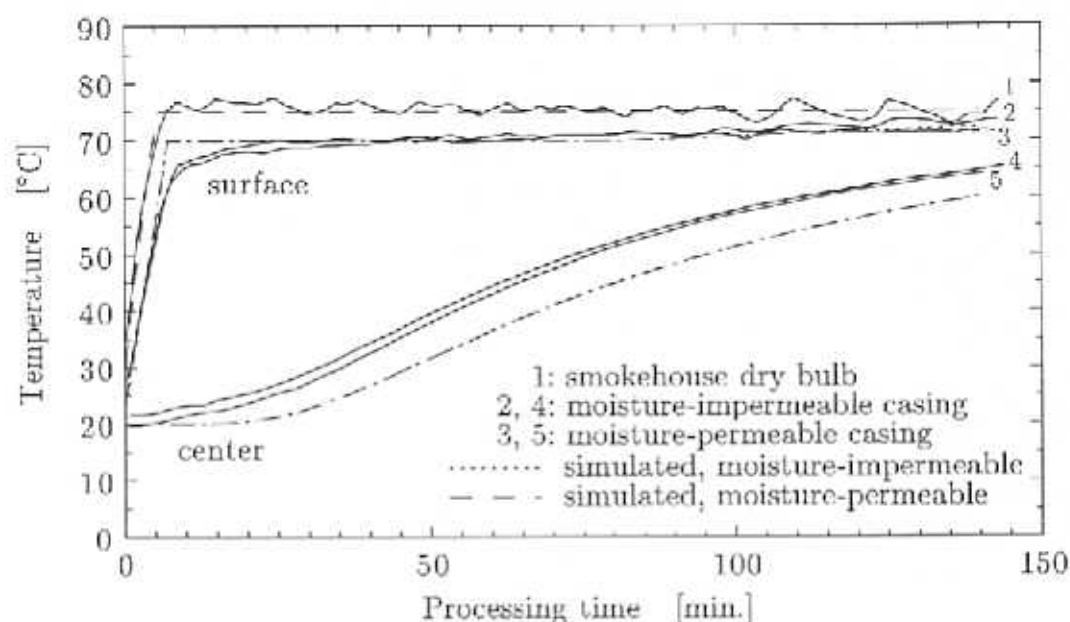
Figure 6.11: Simulated and measured (as reported by Hanson [1988]) surface and center temperatures for the processing of bologna at a humidity of 80%.

the oven dry-bulb and wet-bulb temperatures and the moisture losses were recorded during processing. For three different processing conditions, direct comparisons of the product surface and center temperatures for the two casing types were reported in graphical form. The data reported in these plots were used to test the simulation model developed in this study. The original data used to generate the graphs were not available. Hence, the corresponding plots were scanned and digitized (DigiGraf, Symantec Corporation). Twenty-four pairs from the resulting temperature versus time data were selected as the observation input for the parameter estimation program. The average heat transfer coefficients in the smokehouse used for the processing were not determined in Hanson's study. Therefore, before estimating the effective moisture diffusion coefficients, the nonlinear parameter estimation program was used to determine the average heat transfer coefficients from the reported temperature data. In order to reduce the uncertainty associated with the parameter estimation,

the data reported for the moisture-impermeable casings were used for this purpose. When using the parameter estimation program in the multiresponse mode, i.e. using both the surface and center temperature as the observation input, unreasonably high heat transfer coefficients (above 200 W/m²K) were computed for all three processing conditions. These results were caused by a systematic offset in the reported center temperatures (Figures 6.9 to 6.11), probably caused by an error in the thermocouple measurements. In theory, the slope of the center temperatures at the beginning of the experiments should be zero. This requirement follows from the solution of the conduction equation and has to be satisfied even for infinitely high heat transfer coefficients. In practice, this behavior can hardly be verified for small diameter products in which the center temperature will increase rapidly. However, the center temperature of larger diameter products with their increased thermal mass has to remain constant for some period of time. The data reported by Hanson [1988] show an increase with time from the beginning of the experiment. Because of these restrictions on the reported data, only the surface temperatures were chosen as the observation input for the parameter estimation program. For the three processing conditions, heat transfer coefficients of 40.4(±3.6), 48.2(±8.6) and 65.4(+17.2) W/m²K, respectively, were computed. These values seem very reasonable when compared with heat transfer coefficients measured in this study for batch type smokehouses (Section 5.4). An average value of 51.3 W/m²K was computed and used in the subsequent estimation of the effective moisture diffusion coefficient from the data reported for the moisture-permeable casings. A diffusion coefficient of 5.1×10^{-10} m²/s was computed for the processing conditions with the lowest humidity. The driving force for mass transfer during processing with the higher humidities was very low. Hence, the effective moisture diffusivity had little influence on the simulated surface temperature data and the uncertainties associated with the estimated diffusion coefficients were too high to

permit the extraction of useful information. The value of $D_{eff} = 5.1 \times 10^{-10}$ m^2/s was therefore used for all three humidities. A very good agreement between the measured and simulated surface temperatures for all humidities and both types of casings can be observed. The difference between the surface and center temperatures of the products in the moisture-impermeable and the moisture-permeable casings decreases with increasing humidity, i.e. with a decreasing driving force for mass transfer. The simulation model accurately captures this behavior. A systematic error was detected in the measured center temperatures and the simulation model is believed to be a more accurate predictor of the actual center temperatures.

The overall results for the effective moisture diffusion coefficient validate the simulation model and the method of determining the effective moisture diffusivity with a parameter estimation program from measured data. The estimated effective moisture diffusion coefficients compare very well with the range of diffusivities reported by Agrawal [1976]. In that study, values of D_{eff} between 0.6×10^{-10} and 1.3×10^{-10} m^2/s best described the moisture concentration profiles and moisture losses during the processing of meat emulsion products. The value of the dry-weight moisture content of the emulsions used in Agrawal's study was $u = 1.85$ kg$_m$/kg$_d$, corresponding to a moisture mass fraction of 0.65, and is therefore located between the values for the full-fat and no-fat emulsions used in this study.

In this chapter, measured data from several experiments were compared with simulation results and a good agreement was observed in most cases. The remaining differences are caused by the limitations of the simulation model. The transport phenomena during the thermal processing of meat emulsion products are influenced by many product and process parameters. It is possible that the use of a more accurate simulation model reduces the remaining deviations between measured and simulated data.

Chapter 7

Summary and Recommendations for Future Work

This chapter is divided into two parts. First, the work presented in the previous chapters is summarized. Special emphasis is given to the comparison of simulated and experimentally determined data. Next, recommendations for future investigations are outlined. These extensions of the current research include refinements to both the experimental studies and the simulation model.

7.1 Summary

A simulation model for heat and mass transfer during the thermal processing of cylindrical meat emulsion products was developed. The model assumed that the moisture diffuses in liquid form from the interior of the product to the surface where it evaporates. Other assumptions included negligible shrinkage of the product during processing, temperature and moisture concentration gradients only in the radial direction, mass transfer caused by a moisture concentration gradient and a negligible resistance of the casing to heat and mass transfer. Two sets of boundary conditions were introduced for the simulation model. The first set considered mass transfer to

the product when the water vapor pressure over the product surface was lower than the water vapor pressure in the processing air. In this case, the released latent heat of the condensing moisture raised the surface temperature of the product until the surface vapor pressure exceeded that of the processing air and mass transfer from the product to the processing air began. In the second set of boundary conditions, the mass transfer coefficient was set to zero if the water vapor pressure over the product surface was lower than the corresponding value in the processing air. Hence, mass transfer to the product during the early stages of processing was not considered and the surface temperature was set to the dew point temperature of the processing air. Both sets of boundary conditions employed the equilibrium moisture content of the meat emulsion, i.e. the isotherm, as the coupling condition between the moisture concentration at the product surface and the water vapor pressure of the air in contact with the product.

An explicit finite difference scheme was used to solve the differential equations of the simulation model. Several important aspects of this method, including different discretization approaches at the boundaries, were introduced. The error associated with various assumptions of the simulation model was also investigated. Since the local heat transfer coefficients for the flow over a cylinder vary with the circumferential position, the internal product temperatures for typical processing conditions and no mass transfer were calculated for both one-dimensional and two-dimensional situations. The results for both scenarios were in close agreement and it was concluded that the error introduced by the assumption of a one-dimensional process was small. The influence of the choice of the boundary condition, i.e. allowing or neglecting mass transfer to the product, on the computed simulation results was tested by simulating the temperature and moisture concentration in a small diameter product during processing at typical smokehouse conditions. The product temperatures for

both sets of boundary conditions were in good agreement. Because of the differences with respect to mass transfer to the product, the surface moisture concentrations at early processing times were significantly different. Since the boundary conditions allowing mass transfer to the product included the additional assumption that no condensing moisture dripped off the product, the set of boundary conditions that did not allow mass transfer to the product was selected for the subsequent simulations. The energy equation in the developed simulation model accounts for the enthalpy of the diffusing moisture. Since many publications in the literature dealing with the thermal processing of food products neglect this contribution, the importance of the corresponding term was investigated. For this purpose, the temperature and moisture concentration response of a small diameter product processed with typical conditions was simulated without considering the enthalpy term in the energy equation. The computed values were compared with simulation results based on the complete energy equation. For both the surface and center temperatures, a maximum difference of approximately 5°C was observed for the two cases. Because of the difference in the center temperatures, the processing times needed to reach the specified cooking temperature of 68.3°C differed by approximately 10 minutes. It was concluded that the error introduced by neglecting the enthalpy term was significant. The influence of the equilibrium moisture content, the thermal conductivity and effective moisture diffusivity of the meat emulsion and the average heat and mass transfer coefficients on the simulation results was investigated in a parametric study. The magnitude of the effective moisture diffusion coefficient had a large influence on the computed cooking time. On the other hand, the influence of the mass transfer coefficient was rather small. It was concluded that the moisture transport was limited by internal diffusion.

A laboratory apparatus was constructed and used for the processing of small and

medium diameter meat emulsion products. The temperature, humidity and velocity of the processing air could be controlled. Compressed air was humidified in a bubble column and subsequently heated with an electrical resistance element. The pressure loss between the bubble column and the test section containing the meat products was found to exhibit a relatively strong influence on the humidities in the test section. Surface and center temperatures of the meat products were measured with thermocouples. An analog to digital converter board was used to log the data to a personal computer. Because of heat conduction along the length of the thermocouples, the measured temperatures deviated from the real values. In order to estimate the magnitude of this error with a mathematical analysis, the thermocouples were treated as needle fins. The error for the worst case was found to be less than 2°C. However, the exact value depended on the unknown heat transfer coefficient between thermocouple and meat emulsion.

Moisture concentration profiles of small and large diameter processed products were measured. The samples were removed from the last thermal processing zones of commercial continuous smokehouses. A slice was cut from the center section of the large diameter product and small rectangular pieces were cut with a razor blade from three circumferential positions. Concentric cork borers were used to cut sample rings from the small diameter products. The moisture contents of the sample pieces were determined with a standard oven drying method. The moisture concentration within the large diameter sample was constant in the center of the product and decreased towards the surface. In addition to the decrease towards the product surface, the moisture profile within the small diameter sample displayed a small decrease towards the product center. This behavior was attributed to the different surface to volume ratios of the cut concentric rings that were thought to influence the moisture concentrations measured with the oven drying method. The accuracy of the oven drying

method for small uniform sample pieces was tested with the Karl Fischer titration method. The results from both techniques were in close agreement.

The use of magnetic resonance imaging methods for the determination of moisture profiles within meat emulsion products was not successful. Low signal to noise ratios prevented the extraction of useful information from the experiments.

The average heat transfer coefficients in the processing environments under investigation in this research were measured with the lumped capacitance method. A small solid aluminum probe of 23 mm diameter, closely resembling a real small diameter meat emulsion product, was used to measure the heat transfer coefficient in a commercial continuously operated smokehouse, in a batch operated pilot plant smokehouse and in the test section of the laboratory apparatus. A brine-filled aluminum vessel of 10.2 cm diameter was employed to determine the heat transfer coefficient in a commercial smokehouse used for the processing of large diameter meat products. The temperature response of the lumped systems and the corresponding dry bulb temperatures were recorded with temperature data traces, which are wireless programmable temperature sensors. The obtained heat transfer coefficients in the processing environments used for small and large diameter products ranged from 14 to 66 W/m^2K and from 25 to 41 W/m^2K, respectively. The analogy of heat and mass transfer for small mass transfer rates was used to compute average mass transfer coefficients from the measured heat transfer coefficients. The computed values ranged from 1.8×10^{-7} to 4.0×10^{-7} $kg/Pa\,m^2\,s$.

The moisture losses of small diameter full-fat and no-fat emulsion products contained in moisture-permeable cellulose casings were measured in the test section of the laboratory apparatus. Two experiments were conducted for each emulsion type. The obtained moisture ratios, i.e. the fractions of the initial weight, after 90 minutes of processing at low relative humidities were 0.90 and 0.75 for the full-fat and no-fat

products, respectively. The agreement between the results from the individual runs was very good. A batch type commercial smokehouse was used to monitor the weight loss of small diameter full-fat products. The moisture ratios after 90 and 180 minutes of processing were 0.86 and 0.79, respectively. The heat and mass transfer coefficients in this batch type smokehouse were approximately twice as large as those measured in the test section of the laboratory apparatus. In addition to these separate moisture loss experiments, the initial and final masses of the products used in the temperature profile experiments were recorded. The transfer of moisture between the product and the processing air was not limited by the mass transfer resistance of the casing. The moisture losses during the thermal processing of no-fat products were significantly larger than those of full-fat product processed in identical moisture-permeable cellulose casings and with the same processing conditions. These results, together with the higher moisture content and effective moisture diffusion coefficient of the no-fat products, indicate that the internal movement of moisture is the limiting factor to mass transfer. This finding is supported by the results of the experiments measuring the mass transfer coefficients from the weight loss of water-filled moisture-permeable cellulose casings in an unsaturated processing environment in which the heat transfer coefficient was known. The permeability of the casings was low enough to prevent water from dripping off the outside of the material. At the same time, the resistance to mass transfer was small enough to maintain a fully wetted outer casing surface. The measured mass transfer coefficients compared favorably with those calculated from the analogy of heat and mass transfer using the known heat transfer coefficient. If the casing had limited the diffusion of moisture, the measured mass transfer coefficients would have been smaller than those obtained from the analogy of heat and mass transfer.

The dry densities of full-fat and no-fat emulsions were determined by submerging

the corresponding products into a graduated cylinder filled with water. The initial moisture contents of the samples were known from the preparation of the two emulsion types. The measured dry densities for the full-fat and no-fat emulsions were 434 and 135 kg_d/m^3.

Measurements of the effective moisture diffusion coefficient were attempted with a pulsed field-gradient nuclear magnetic resonance method. The self-diffusion coefficients obtained with this method have been said to be related to the mutual diffusion coefficients, and hence the effective diffusion coefficients. However, the observed self-diffusivities showed a dependence on the relatively short times of observation during the magnetic resonance experiments (16.6 ms and 133 ms) and could therefore not be related to the effective moisture diffusion coefficients found during the processing of meat emulsion products.

A nonlinear parameter estimation program was used in conjunction with the simulation model to find the values of the effective moisture diffusion coefficient and the heat transfer coefficient that provided the best fit of measured and simulated data. Average effective moisture diffusion coefficients were calculated for those experiments that used meat emulsions coming from the same batch, i.e. it was argued that the variations in the estimated results were caused by limitations in the experimental data and/or the simulation model. The effective moisture diffusion coefficients estimated for the no-fat emulsions were larger than those obtained for the full-fat products. From the small diameter temperature profile experiments, an average effective diffusivity of $D_{eff} = 2.61 \times 10^{-10}$ m^2/s was found for the no-fat products, compared to a value of $D_{eff} = 1.48 \times 10^{-10}$ m^2/s for the full-fat samples. For the moisture loss experiments in the test section of the laboratory apparatus, an effective diffusivity of $D_{eff} = 3.73 \times 10^{-10}$ m^2/s for the no-fat product was estimated. The estimated effective moisture diffusion coefficients compare very well with the range of diffusivities

reported by Agrawal [1976]. The experimental results used with the parameter estimation program comprised several dependent variables (temperature profiles, moisture losses and moisture profiles) and were recorded in different processing environments (i.e. the test section of the laboratory apparatus, batch type and continuously operated smokehouses) for different emulsion compositions (full-fat, low-fat and no-fat). In addition, the data were obtained from experiments conducted in this research and from findings reported in the literature.

Overall, the experimentally determined heat and mass transfer during the processing of cylindrical meat emulsion products was in good agreement with the results predicted by the simulation model developed in this research. In particular, the measured moisture concentration profiles in small and large diameter products agreed very well with the simulated values. The differences between measured and simulated data in the temperature profile and moisture loss experiments were thought to be caused by the limitations of the simulation model. Many parameters influence the heat and mass transfer during the thermal processing of meat emulsion products. The simulation model considered many of these complicating effects, for example the changing boundary conditions during the initial processing stages and the dependence of the product density and thermal conductivity on the moisture concentration. However, it is possible that other parameters which were not considered in the simulation model influence the heat and mass transfer during processing. The identification of these variables and their incorporation into the simulation model is a possible area of research for future investigations.

7.2 Recommendations for Future Work

Possible extensions of the research presented in this study include modifications to the laboratory apparatus used for the processing of small and medium diameter meat

emulsion products and refinements of the simulation model.

The laboratory apparatus used to investigate the heat and mass transfer during the processing of cylindrical meat emulsion products was described in Section 5.1. Varying relative humidities in the test section of the apparatus were obtained by saturating an air stream in a bubble column at temperatures below the desired processing dry bulb temperature, followed by a sensible heat input. Therefore, the humidification of the processing air was accomplished without steam injection and the apparatus could be moved to the location of the magnetic resonance machine used in the moisture profile experiments (Section 5.7). The relative humidity in the test section was a function of the water temperature in the bubble column, the dry bulb temperature in the test section and the pressure difference between the bubble column and the test section. The bubble column was made from a polyvinylchloride tube. At higher temperatures, the material became soft and leakages occurred at the various pipe and hose connections. Hence, the temperatures of the water inside the column were restricted to values below approximately 60°C (140°F). Therefore, the humidities in the test section with dry bulb temperatures of approximately 80°C were constrained to values below 40%. If the bubble column were made from a different material, for example steel or aluminum, higher relative humidities could be obtained in the test section and used in the processing of meat emulsion products.

Measurements of product surface and center temperatures in the test section were conducted with preassembled subminiature type T (copper/constantan) thermocouples of 0.508 mm (0.020 inch) diameter (Section 5.1). Because of conduction along the length of the thermocouple, the measured temperatures were affected by a bias error. The magnitude of this error was investigated with a mathematical analysis, treating the thermocouples as needle fins (Section 5.2). It was found that the error was a strong function of the contact resistance between the thermocouple and the

meat emulsion, the thermal conductivity of the thermocouples and their lengths. For reasonable values of the contact resistance, the bias error for both thermocouples in the medium diameter products and the surface thermocouple in the small diameter products was negligible. The error associated with the thermocouple in the center of the small diameter products was estimated to be as large as $2°C$ ($3.6°F$). This error could be reduced by the use of a thermocouple assembly with a lower average thermal conductivity. For example, the voltage signal in type J couples is generated by the joining of iron and constantan wires. Hence, the relatively high thermal conductivity of the copper wire in the type T thermocouples could be avoided. Type J thermocouples can be used to measure temperatures ranging from $0°C$ to $760°C$ ($32°F$ to $1400°F$) and would therefore be suitable for the temperatures under investigation in this study.

The moisture profile experiments (Section 5.3) were conducted on samples that were obtained from commercial processing equipment. Hence, the processing schedule included a smoking operation (Chapter 1). The thermal processing in all other experiments conducted in this research consisted of the application of hot humid air without added smoke. The results from the parameter estimation studies (Chapter 6) indicated that the smoke has no detectable influence on the transfer of heat and mass. To verify this finding, the transport phenomena in meat emulsion products processed with and without the application of smoke under otherwise identical conditions could be investigated. The batch type smokehouse used for the moisture loss experiments would be suitable processing environment for these measurements.

Some of the variations between the measured and simulated moisture losses for the full-fat products in the test section of the laboratory apparatus were thought to be caused by the weighing procedure used in the experiments. In intervals of 10 minutes, the products were removed from the test section, weighed and returned to their

original position. One weighing operation took approximately 45 seconds. A continuous recording of the mass of the meat emulsion product during processing would eliminate the possibility that the periodic removal from the test section significantly influences the measured moisture ratios. This continuous weighing could be accomplished by using a wire attached to an electronic balance which would suspend the meat emulsion product into the test section.

An explicit finite difference method was used to solve the differential equations of the simulation model. At each timestep, the system of equations describing the boundary conditions for heat and mass transfer was solved with a nonlinear equation solver subroutine. However, due to the explicit scheme used at the interior gridpoints, relatively small timesteps had to be used in order to avoid numerical instabilities. When using the nonlinear parameter estimation program, the simulation model is called many times with different parameter settings. The time needed to find the optimal set of parameters could be decreased by using an implicit finite difference scheme with larger time steps as a means of solving the simulation model.

In the current configuration, the computer code used to solve the simulation model consists of several program subroutines in addition to data input and output files. The incorporation of all program modules into one unit with a user-friendly interface would greatly increase the usability for researchers who want to employ the developed model for further parameter studies without the need of frequent recompiling and linking of the various program subroutines.

Several applications for the simulation model developed in this research exist, for example the design of new processing equipment and the optimization of existing thermal processing schedules. This optimization can reduce the manufacturing costs by identifying those processing conditions that process a product with the least amount of energy in the shortest possible time.